Regulatory mechanisms of the calcium selective ion channels

TRPV6 and ORAI1

Dissertation

zur Erlangung des Grades eines Doktors

der Naturwissenschaften der Mathematisch-
Naturwissenschaftlichen Fakultät

der Universität des Saarlandes

vorgelegt von

Dalia Al-Ansary

Homburg 2009

To my parents, brother and sister without whose unconditional love, support and patience I would have not been who or where I am today.

Acknowledgement

I would like to express my sincere gratitude to my advisor, Dr. Barbara Niemeyer, for sparing no effort throughout the PhD program for teaching and training me to variable techniques in molecular biology and electrophysiology. I am also indebted by the time she dedicated for guiding me to an optimized planning and conductance of experiments as well as for discussing results and above all I am grateful for her ideas and stimulating suggestions that enriched this work, for her encouragement and patience.

I am also grateful to Prof. Veit Flockerzi in whose laboratory most of the experimental work for this dissertation was done. During this time Prof. Flockerzi provided me with help and valuable ideas and discussions. I wish to thank Dr. Ulrich Wissenbach for making the TRPV6 stable cell lines that were used in this work and Dr. Marcel Meissner for providing us with mouse TRPV6 fusion proteins used in the initial binding experiments. I wish to thank Heidi Löhr for taking care of cell culture work and for teaching me how to do it. For their technical help, I would like to thank Ute Soltek and Karin Wolske. To my former colleagues in the Department of Experimental Pharmacology and Toxicology I would like to express special thanks for their help and support.

I would like to express my gratitude to Dr. Ute Becherer for the several trials she performed to address TRPV6 trafficking issues using TIRF microscopy. Also, I would like to thank her for the time she dedicated during the PhD term to discuss data and for her valuable input and discussions as well as for critically reading this manuscript.

I am extremely grateful to Prof. Markus Hoth, Dr. Ivan Bogeski and Dr. Carsten Kummerow for giving me the opportunity to take part in their interesting project about regulation of ORAI channels which was a fruitful addition to my original PhD project. I am also thankful to Dr. Eva Schwarz for performing the Orai1/Orai3 qRT-PCR experiments. In the Department of Biophysics, I would like to thank Anja Ludes, Bettina Strauß and Andrea Armbrüster for their technical assistance and the lab members for their critical input.

My sincere thanks go to Barbara Disteldorf who devoted a lot of work during her diploma to clone and purify TRPV6 fusion proteins under native conditions to be used for further ATP-binding experiments.

I would also like to thank Prof. Peter Lipp and Prof. Yusuf Hannun for providing us with cDNA for GFP-PKCα and GFP-PKC$_{\text{ßII}}$

I wish to thank the graduate research school Calcium-signaling and cellular nanodomains at the University of Saarland for providing the opportunity to join the program and for funding the project.

Last but not least I wish to thank my dear friends Mathias Pasche, Anna Drews, Melanie Flick and Ashraf Hussein for their continuous help and support.

1   Table of Contents

2   Zusammenfassung

Kalziumionen sind eines der wichtigsten intrazellulären Botenstoffe der Zelle. Kleinste Veränderungen ihrer zytosolischen Konzentration triggern eine Vielzahl von zellbiologischen Prozessen, u.a. Exozytose, Kontraktion und Veränderungen von Enzymaktivität. Eine genaue und enge Kontrolle ihrer Konzentration durch Regulation ihres Einstroms, z.B. durch Ionenkanäle, aber auch ihrer Speicherung und des Transports aus der Zelle heraus ist deshalb essentiell. TRPV5 und TRPV6 sind die einzigen Mitglieder der TRP Kationenkanal Familie die eine hohen Selektvität für Kalzium aufweisen und sind an der Aufrecherhaltung der Kalziumhomeöstase im Körper beteiligt. Eine weitere Familie von Ionenkanälen mit hoher Selektivität für Kalziumionen wird von den Orai Genen kodiert. Hierbei gibt es drei homologe menschliche Gene, von denen das ORAI1 Protein der wesentliche ionenleitende Bestandteil des Speicherentleerungs-aktivierten Kalzium Einstroms (CRAC) in Lymphozyten ist. Das Ziel dieser Arbeit war es, Regulationsmechanismen der Ca^{2+} selektive Ionenkanäle TRPV6 und ORAI1 zu untersuchen.

Um die intrazelluläre Kalziumkonzentration konstant zu halten, müssen Zellen dynamisch auf Änderungen ihres metabolischen Zustandes, z.B. durch Änderungen der zellulären ATP Konzentration, reagieren. Ein erstes Ziel dieser Arbeit war es zu untersuchen, ob und wie der von TRPV6 getragenen Kalziumstroms durch ATP reguliert werden kann. Hierzu wurden zunächst elektrophysiologische Messungen in der sog. „whole-cell patch-clamp" Konfiguration durchgeführt. ATP bewirkte eine signifikante Veränderung sowohl im Zeitverlauf der Entwicklung als auch in dem „rundown" Verhalten der TRPV6 getragenen Ströme. Diese Effekte zeigten eine Spezifität für das verwendete Nukleotid und waren nicht abhängig von der Hydrolyse von ATP. Da bereits eine Regulation der kalziumabhängigen Inaktivierung von TRPV6 durch PIP_2 in der Literatur beschrieben war (Rohacs et al., 2005), wurde die Unabhängigkeit des ATP Effektes vom PIP_2 Effekt mittels Mutagenese einer putativen PIP_2 Bindungsstelle (R606Q) und durch die fehlende Wirkung eines wasserlöslichen PIP_2 Derivats bestätigt.

Die Konzentrationsabhängigkeit des ATP-Efffektes ergab eine halbmaximale ATP konzentration (EC_{50}) von ~380 µM mit einem apparenten Hill-Koeffizient von 4.8. Der EC_{50} Wert des ATP Effektes liegt nahe am Bereich der freien intrazellulären ATP Konzentration (Gajewski et al., 2003) und ermöglicht den Kanälen sensitiv auf geringe Schwankungen der ATP Konzentration zu reagieren. Um zu untersuchen ob ATP direkt an den Kanal bindet, wurden zunächst Versuche mit *in-vitro* translatierten TRPV6 an ATP-Agarose durchgeführt. Zur weiteren Eingrenzung von Bindungstellen wurden mehrere Fusionproteine der intrazellulären Proteindomänen hergestellt und in Bakterien exprimiert. Aufgrund eines integrierten Histidin-tags konnten die Fusionsproteine unter verschiedenen Bedingungen (nativ oder denaturiert) aufgereinigt werden und anschliessend im ATP-Agarose „pull-down" auf Bindung untersucht werden. Da die Aktivierung von Proteinkinase C (PKC) durch PMA die Effekte von ATP auf den Kalziumeinstrom von TRPV6 zu einem grossen Teil verhindern kann, wurden zunächst potentielle ATP Bindungsstelle in unmittelbarer Nähe der putativen Phosphorylierungsstellen von TRPV6 untersucht. Durch Mutagenese eines doppelten Arginin Motifs innerhalb der N-terminalen Ankyrin-repeat Domäne (R153Q/R154P) konnte der funktionellen ATP

4

Generated by Foxit PDF Creator © Foxit Software
http://www.foxitsoftware.com   For evaluation only.

Effekt aufgehoben werden und so eine spezifische Bindungstelle charakterisiert werden. Um die Spezifität des PMA Effektes weiter zu untersuchen wurde das inaktive Analogon von PMA (αPDD) und verschiedene PKC Inhibitoren getestet. Hierbei konnte eine Spezifität des Effektes auf einen Subtypus der klassischen PKC's, PKC$_{ßII}$, eingegrenzt werden. Diese Isoform war auch in *in-vitro* Phosphorylierungsversuchen in der Lage rekombinantes TRPV6 Protein schwach zu phosphorylieren. Eine zusätzliche Analyse durch Mutagenese der putativen Phosphorylierungsstellen innerhalb des TRPV6 Proteins ergab dass sowohl eine N-terminale PKC Erkennungsstelle, S144, als auch eine C-terminale Stelle, T688, an der Vermittllung des PMA Effektes beteiligt ist.

Zusammenfassend postulieren wir ein Model, indem ATP durch Bindung sowohl an den N- als auch an den C-terminus von TRPV6 den Kalziumeinstrom limitiert und dadurch den sog. „rundown" verhindert. Aktivierung von PKC$_{ßII}$ kann diesen Effekt durch Phosphorylierung spezifischer Aminosäuren verhindern und stellt somit einen Gegenregulationsmechanismus dar.

Ein weiterer Aspekt dieser Arbeit beschäftigte sich mit der Regulation der ORAI1 Kanäle durch Änderungen des extrazellulären Redoxzustandes. In entzündetem Gewebe sind differenzierte Immunzellen (Effektor T$_h$-Zellen) einer relativ hohen Konzentration von reaktiven Sauerstoffspezies (ROS) ausgesetzt. Da die Lymphozytenfunktion von der Aktivität der ORAI Kanäle gesteuert wird, wurde der Einfluss von reaktiven Sauerstoffspezies, in diesem Fall H_2O_2, auf ORAI1 untersucht. Messungen der intrazellulären Kalziumkonzentration und des Speicheraktivierten Einstroms zeigen, dass H_2O_2 den ORAI1 vermittelten Einstrom mit einem IC$_{50}$ Wert von $\sim$ 40 µM blockiert. Interessanterweise wurde der homologe ORAI3 Kanal nicht durch H_2O_2 inhibiert. Gerichtete Mutagenese einzelner reaktiver Cysteine mit anschliessender biochemischer und funktioneller Analyse ergab, dass Cystein 195 der wesentliche Redoxsensor von ORAI1 ist. Da die homologe Stelle in ORAI3 ein Glycin ist, haben wir durch Mutagenese dieses Glycins in ein Cystein H_2O_2 sensitive ORAI3 Kanäle generiert, also eine sogenannte „gain-of-function" Mutation hergestellt. Um zu untersuchen, wieso menschliche Effektor-T-Zellen weniger sensitiv auf H_2O_2 reagieren als naïve T-Zellen haben wir RT-PCR Versuche durchgeführt um die relativen Mengen an ORAI1 bzw. ORAI3 Transkripten zu erfassen. In der Tat wurde in Effektor Zellen mehr ORAI3 exprimiert. Eine heterologe Ko-transfektion von ORAI1 mit ORAI3 zeigte eine Reduktion der H_2O_2 Sensitivität. Diese Ergebnisse könnten also eine mögliche Erklärung für reduzierte ROS Sensitivität der Effektor T$_h$-Zellen darstellen und es wäre möglich durch eine Regulation der ORAI1/3 Expression die Aktivität der T$_h$-Zellen in entzündetem Gewebe zu steuern.

3   **Summary**

Since recognition of Ca^{2+} as a second messenger, considerable research has been directed towards understanding the tight Ca^{2+} homeostatic mechanisms that keep the intracellular free calcium concentration in a very tight range. Controlling the activity of Ca^{2+} selective ion channels is one critical component of these homeostatic mechanisms. TRPV6 and TRPV5, as members of the non-voltage gated family of TRP ion channels, have an exceptional Ca^{2+} selectivity and are considered gate keepers for Ca^{2+} homeostasis. An additional Ca^{2+} selective family of ion channels is the ORAI family that includes three homologous channels in humans with ORAI1 being the main component mediating Ca^{2+}-release activated calcium (CRAC) current in lymphocytes. The present work aimed at understanding regulation of the Ca^{2+} selective ion channels TRPV6 and ORAI1.

To understand how cells adapt their Ca^{2+} uptake to changes in cellular metabolic state, regulation of Ca^{2+} influx by ATP was characterized. ATP dramatically alters both the kinetics of current development and completely prevents rundown of TRPV6-mediated currents. These effects are nucleotide specific and do not require hydrolysis of ATP. Furthermore, the ATP effect is independent of regulation by PIP_2, which has previously been shown to regulate TRPV6 (Rohacs et al., 2005).

Using a range of ATP concentrations a dose response curve was constructed and the EC_{50} of the ATP effect was calculated to be ~380 μM with a Hill coefficient of 4.8. This value corresponds well to cellular free ATP concentrations (Gajewski et al., 2003) and renders the channels sensitive to small fluctuations within cellular ATP. To identify whether ATP directly binds to the channel protein, the binding of *in vitro* translated TRPV6 protein to ATP-agarose was investigated. To narrow down specific binding site(s), different histidine tagged fusion proteins covering different intracellular domains were generated. Fusion proteins were purified under two different experimental conditions (denaturing and native). Subsequent ATP-agarose pull-down experiments identified several potential binding domains. Because activation of protein kinase C (PKC) by PMA prevented the effects of ATP both on kinetics and run-down of TRPV6 currents, potential ATP complexing residues in vicinity of phosphorylation sites were analyzed. Mutational analyses (R153Q/R154P) identified specific residues within the ankyrin repeat domain critical for conferring the functional ATP effect. To address the specificity of the PMA effect, an inactive analogue of PMA (4αPDD) and a range of PKC inhibitors were applied. Analyses of PKC modification indicates that the effects of PMA are mediated by a specific PKC isoform $PKC_{ßII}$. This specific isoform can weakly phosphorylate TRPV6 as shown by *in vitro* phosphorylation experiments. Moreover, mutational analyses of potential phosphorylation sites identified two sites (S144, T688) as being of particular importance in mediating the effects of PMA.

Altogether, the results suggest a model in which ATP binds to both C- and N-termini of TRPV6 limiting Ca^{2+} influx and preventing rundown, an effect that can be prevented if the channel is phosphorylated at PKC consensus sites within the N- or a C-terminus (S144, T688).

Regulation of ORAI1 by changes in the extracellular environment was also subject of the present work. Because differentiated lymphocytes (effector T_h-cells) are exposed to substantial concentrations of reactive oxygen species (ROS) within inflamed tissues, regulation of ORAI1 channels by ROS was investigated. Measurements of Ca^{2+} signals and whole cell currents show that H_2O_2 inhibits ORAI1-

mediated Ca^{2+} influx with an $IC_{50} \sim 40$ µM. In contrast, ORAI3 channels are not inhibited by H_2O_2. Site directed mutagenesis followed by functional and biochemical investigation identifies C195 to be the redox sensor of ORAI1. This finding is confirmed by introducing a potential "gain-of-function" mutation that renders ORAI3 sensitive to H_2O_2 regulation. RT-PCR performed using RNA purified from naïve and effector T_h cells showed that the relative expression of ORAI1/ORAI3 is shifted to a higher ORAI3 ratio in effector compared to naïve T_h cells. Cells co-transfected with ORAI1/ORAI3 in a ratio similar to upregulated ORAI3 showed less H_2O_2 inhibition than ORAI1 alone. These results provide a possible explanation of the observation that effector T T_h cells are more tolerant to H_2O_2 than naïve T_h cells. In addition, the data suggests that ROS regulation of ORAI channels fine tunes the activity of T_h cells.

4   Glossary

Units and measurements

% (v/v)	Percent volume/volume
% (w/v)	Percent weight/volume
×g	Multiples of force of gravity
μg	microgram
μl	Microlitre
bp	Base pairs
cfu	Colony forming unit
Ci	Curi
cm	Centimeter
Da	Dalton
g	Gram
h	Hour
kb	Kilo base
kD	Kilo Dalton
kV	Kilo volt
l	Litre
M	Molar
mA	Milliampere
min	Minute
ml	Millilitre
mM	Millimolar
mV	Milli Volt
ng	Nanogram
pA	Pico Ampere
pF	Pico Farad
PKC	Protein kinase C
pS	Pico Siemens
rpm	Revolution per minute
RT	Room temperature
s	Second
U	Unit (of enzymatic activity)
V	Volt

Miscellaneous abbreviations

Δ	Delta, deletion
Ab	Antibody
ADP	Adenosine-5'-diphosphate
AEBSF	4-(2-Aminoethyl)-benzenesulfonylfluorid

AMP	Adenosine-5'-monophosphate
ANK	Ankyrin repeat domain
APS	Ammonium persulfate
ATP	Adenosine-5'-triphosphate
BCA	Bicinchoninic acid
BSA	Bovine serum albumin
cAMP	Cyclic adenosine monophosphate
cDNA	Copy DNA
CIP	Calf intestine phosphatase (alkaline phosphatase)
Co-IP	Co-immunoprecipitation
DMSO	Dimethyl sulfoxide
DNA	Deoxyribonucleic acid
dNTP	Desoxynucleotide-5'-triphosphate
DTT	Dithiothreitol
E.coli	*Escherichia coli*
EDTA	Ethylendiamin-N, N, N`,N`-tetraacetic acid
EGFP	Enhanced green fluorescent protein
EGTA	Ethylene glycol tetraacetic acid
FCS	Fetal calf serum
G-418	Geneticin
GPCR	G-protein coupled receptor
GTP	Guanoosine-5'-triphosphate
HEK293	Human embryonic kidney cells
IMP	Inosine monophosphate
IPTG	Isopropyl-β-D-thiogalaktosid
IRES	Internal ribosome entry site
LB	Luria Bertani Nutritive medium
NMDA	N-methyl-D-aspartic acid
OD_{600}	Optical density at wave length 600 nm
PBS	Phosphate buffered saline
PEG	Poly ethylene glycol
PKC	Protein kinase C
PMSF	Phenylmethylsulfonylfluoride
Primer	Oligodesoxynukleotide
PS	Phosphatidylserine
SDS	Sodiumdodecylsulfate
TBE	Tris-Borat-EDTA-Buffer
TBS	Tris buffered saline
TBST	Tris buffered saline with 0.1% tween 20

TCA	Trichloroacetic acid
TEMED	N,N,N`,N`-Tetramethylethylendiamin
T_m	Melting temperature
Tris	Tris-(hydroxymethyl)-aminomethan-hydrochlorid
TRP	Transient receptor potential
Tween	Polyoxyethylensorbitanmonolaureate
UTP	Uridine-5'-triphosphate
UV	Ultraviolet
WB	Western blot
WT	wildtype
X-Gal	5-Brom-4-Chlor-3-indolyl-β-D-galactoside

5   Introduction

For a cell to preserve its integrity and perform its functions it has to fulfil its needs from the available surrounding resources, respond to the perceived stimuli and adapt to changes. Communication between different intracellular components, signalling, is therefore a crucial requirement for cellular survival and efficiency. Calcium ions (Ca^{2+}) are ubiquitous second messengers that trigger a plethora of biological processes. An array of Ca^{2+} "on" and "off" switches act in concert to tightly regulate intracellular Ca^{2+} levels. While different calcium permeable ion channels in the plasma membrane allow Ca^{2+} influx and endoplasmic and sarcoplasmic reticula allow Ca^{2+} release form internal stores both sources leading to subsequent increase in cytoplasmic levels ($[Ca^{2+}]_i$), a diversity of intracellular Ca^{2+} distribution systems, Ca^{2+} ATPases and ion exchangers work on extrusion of Ca^{2+} whenever in excess.

The scope of our work are regulatory mechanisms governing the activity of two plasma membrane Ca^{2+}-selective channels. On the basis of their activation mechanisms, Ca^{2+} channels are classified into four main groups. First the voltage operated Ca^{2+} channels (VOCC) that mediate heart action potential and fusion of vesicles of many excitable cells. VOCCs are activated by depolarization of the plasma membrane. Second, the ligand-gated calcium channels which comprise a range of structurally and functionally diverse channels that are particularly prevalent in secretory cells and at nerve terminals. They are activated by the binding of an agonist (e.g ATP, serotonin, glutamate and acetylcholine) to the extracellular domain of the channel. Depletion of Ca^{2+} stores is the mechanism activating the third subset of channels, store operated calcium channels (SOCC). This depletion can be induced by a Ca^{2+}–mobilizing messenger or a pharmacological agent. Less prevalent are the mechanically activated Ca^{2+} channels which respond to deformation and thereby convey information concerning stress and shape changes that a cell is experiencing such as those occurring with stretched tracheal or heart cells or in auditory hair cells. In addition to these well established mechanisms of activation, there is growing evidence that some Ca^{2+} channels are activated by lipid second messengers though these are not classified as an independent group.

5.1   TRP Ion Channels

The transient receptor potential superfamily entails a diverse family of cation channels. This superfamily is distinct in displaying a remarkable diversity of ion selectivities, modes of activation and physiological functions. A prevalent property of TRP members is being of particular importance in sensory physiology ranging from vision to gustation, olfaction, audition, mechanosensation and thermosensation. TRP channels also allow individual cells to sense changes in the local environment such as alteration in fluid flow, pH, temperature and mechanical stress. *Trp* gene was first identified as a *Drosophila melanogaster* phototransduction defective mutant. While calcium stores in wildtype photoreceptors resond to a prolonged light stimulation with an initial and an adaptive phase response, the *trp*-carrying photoreceptors show a transient response that decays to a basal line (Cosens and Manning, 1969). Montell and Rubin (Montell and Rubin, 1989) first cloned the gene underlying the *trp* phenotype, although the physiological role of the protein was unknown. The firm role of calcium as a

second messenger involved in adaptation and excitation led Minke and Selinger (Minke and Selinger, 1992) to suggest that *trp* gene may code for a plasma membrane calcium transporter essential for replenishment of stores and Hardie and Minke demonstrated in the same year that the TRP protein indeed functions as a calcium permeable ion channel (Hardie and Minke, 1992). Also in 1992, a closely related channel was identified from photoreceptors and termed TRPL (Phillips et al., 1992). The photoreceptor response in Drosphila requires both channels as mutants lacking both TRP and TRPL are completely unresponsive to light (Niemeyer et al., 1996).

Since then, TRP channels have been identified in various multicellular organisms from worms to humans. According to their sequence and topological similarities, the TRP channels are divided into two main groups that together include the seven TRP subfamilies. Group 1 includes the five subfamilies that bear the strongest sequence homology to the founding member Drosophila TRP. These subfamilies are the ankyrin (TRPA), canonical (TRPC), melastatin (TRPM), and vanilloid (TRPV) in addition to TRPN (no mechanopotential, NOMPC) which is not found in mammals although expressed in some vertebrates such as zebrafish. The subfamilies acquire their names from the initially described member, which in most cases is named after the channel activator. Mucolipin (TRPML) and polycystin (TRPP) channels constitute group 2 because they are distantly related to group one. The founding TRPP ant TRPML proteins were discovered as gene products mutated in autosomal dominant polycystic kidney disease (ADPKD) and mucolipidosis type IV (MLIV), respectively. TRPY is a group of ancient proteins expressed in fungi (founding member is the yeast vacuolar protein, Yvc1). These proteins are weakly related to TRP proteins and thus not classified along either Group 1 or 2 TRPs (Montell, 2005). An overview on the classification of TRP channels subfamilies is depicted in figure 1
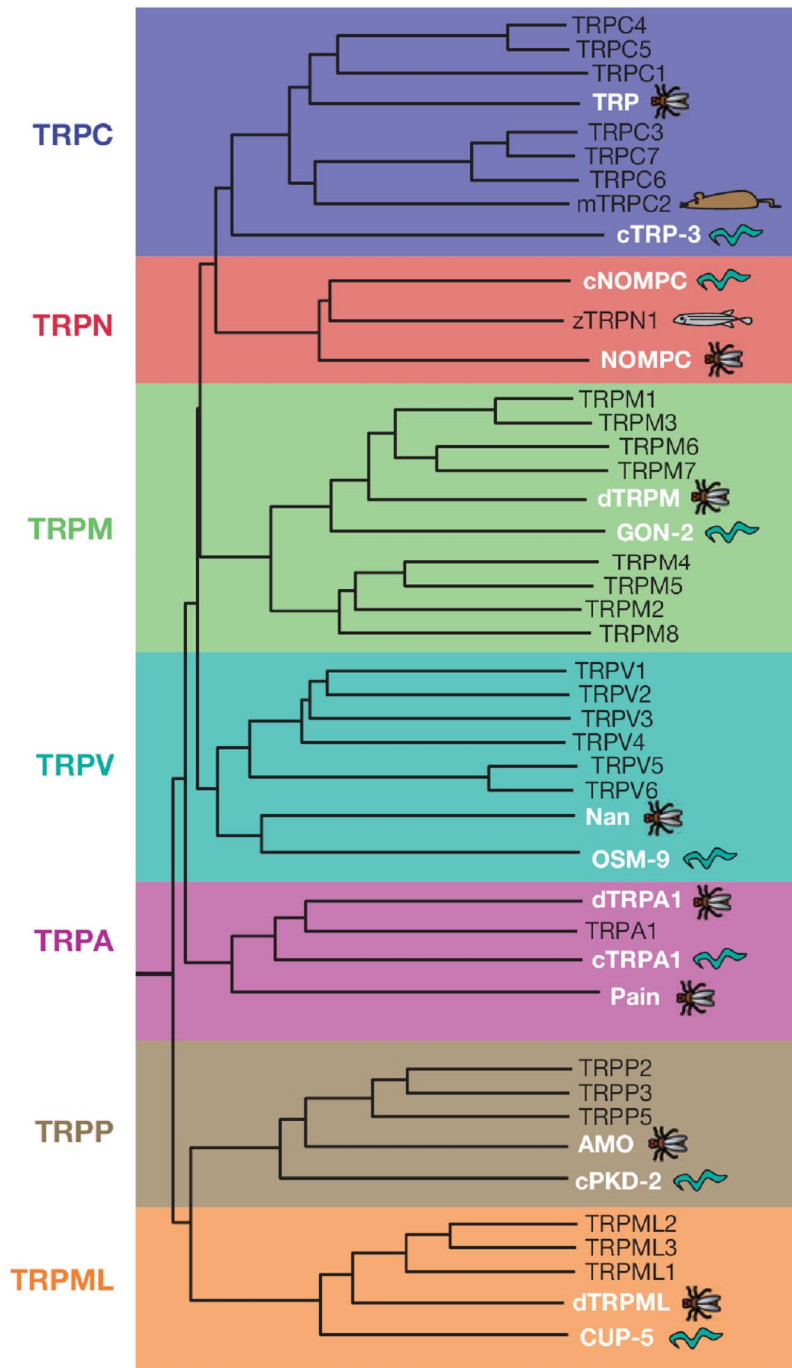
Figure 1: Phylogenetic tree showing the relatedness of TRP proteins. The dendrogram of vertebrate TRPs includes mostly human TRPs, except for mouse TRPC2 and zebrafish TRPN1. White text and cartoons highlight the TRP proteins from worms and flies. One *C.elegans* and one *Drosophila* member of each subfamily are included (Venkatachalam and Montell, 2007)

The core of a TRP channel structure has N- and a C- termini located intracellularly and 6 domains spanning the plasma membrane with a pore region flanked between the fifth and sixth. Hydropathy analyses predict a seventh N-terminal hydrophobic domain in many TRPC, V, M, P and ML family members. TRPP and TRPML have an extended extracellular loop between S1and S2. TRP proteins

13

like many other 6 transmembrane domain channels form a tetrameric quaternary structure where each subunit contributes to a shared selectivity filter and ion-conducting pore (Venkatachalam and Montell, 2007).

The N-terminus of TRPC, V, A and N contain a number of ANK repeat domains. While the canonical and the vanilloid subfamilies have few repeats (up to 4 and 6, respectively), the ankyrin (TRPA) and no mechanopotential (TRPN) subfamilies have many conserved repeats (up to 18 and 29, respectively). By definition, an ANK repeat domain is a ~ 33 residue motif found in tandem arrays ranging from 3 to more than 30 repeats (Mosavi et al., 2004). However, an ANK repeat is not a tightly conserved sequence but rather a conserved secondary and tertiary structure: helix-turn-helix or a hairpin of two short α–helices, followed by a hairpin loop that projects perpendicular to the helical axes (Gaudet, 2008). Poor conservation of the ANK sequence hampers an accurate definition of the number of ANK repeats in a given protein. TRPM channels are different from other group 1 TRP. They are longer proteins and lack ANK repeats. Instead they contain TRPM homology domains (MHD) of unkown function. For ANK repeats several functional aspects have been proposed that include self-interacting motifs, necessary for tetramerization of TRPV6, TRPV5 and TRPV4 (Arniges et al., 2006; Chang et al., 2004; Erler et al., 2004), the formation of a gating spring of the putative mechanosensory channels TRPN and TRPA1 (Corey et al., 2004; Howard and Bechstedt, 2004) as well as binding to regulatory molecules like calmodulin and ATP (Lishko et al., 2007). However, although necessary for overall function of the channels containing them, the detailed function ANK repeats remain elusive.

C-terminal to the sixth transmembrane domain a loosely conserved homologous block of ~25 residues appears in all TRP channels, and is termed the TRP domain. The TRP domain encompasses two TRP boxes; the first is a highly conserved 6-amino acid sequence (e.g EWKFAR in TRPC channels) that is separated from the second proline-rich TRP box by ~12 residues. TRP domains are shown to be required for PIP_2 binding and regulation of channel gating in TRPM8 and TRPV5 (Voets and Nilius, 2007). TRP channels also contain partial pleckstrin homology (PH) domain that forms functional PH holodomain only when associated with cognate sequences in other proteins (Lee et al., 2003).

Several subgroups and some single members also contain a very well described structural domain known as coiled coil domain. These heptad repeat $(abcdefg)_n$ structures are some of the best defined protein-protein interaction domains with a conserved alpha-helical structure where hydrophobic amino acids at the (a) and (d) positions form the core of the domain. Coiled coils are suggested to play a role in TRP channel subunit-subunit interactions to mediating heteromultimerization [TRPγ and TRPL, (Xu et al., 2000)] and homomultimerization of TRPM channels (Tsuruda et al., 2006). An interesting property of some TRP members, namely TRPM channels is the possession of an unusual C-terminal domain with atypical protein kinase enzyme activity. These channels are thus termed chanzymes (Venkatachalam and Montell, 2007). Main structural domains of TRP channels are shown in figure 2
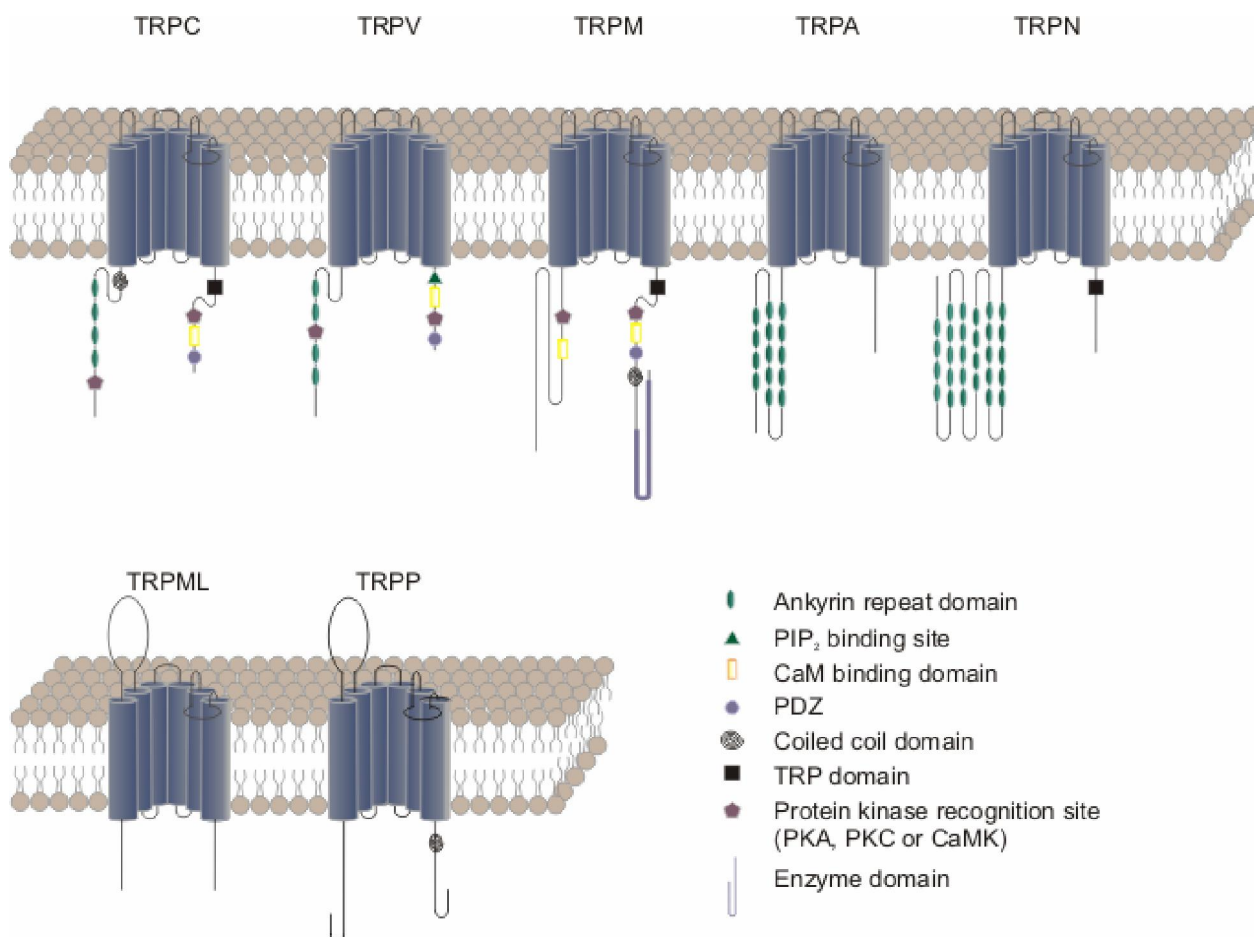
Figure 2: Structural features of TRP superfamily. A schematic representative of each subfamily belonging to group 1 (upper panel) or group 2 (lower panel). Domains indicated depicted in the index panel. Reproduced from (Venkatachalam and Montell, 2007) and (Pedersen et al., 2005)

TRP channels mediate transmembrane flux of cations down their electrochemical gradients. With the exception of TRPM4 and TRPM5, all TRP channels are permeable to Ca^{2+}. TRPV5 and TRPV6 are highly Ca^{2+} selective unlike other TRP channels. There are several established modes for activation of TRP channels. While some TRP channels are indirectly modulated via a GPCR-mediated pathway, others are activate by ligand binding. Ligands can be exogenous molecules like capsaicin or icilin, endogenous lipids or lipid metabolites, purine nucleotides or inorganic ions. Direct physical activation can also evoke a TRP response. Putative direct activators include acute temperature changes, mechanical stimuli, cell swelling, conformational coupling to IP_3 and channel phosphorylation [activation mechanisms reviewed in (Ramsey et al., 2006)].

5.2   TRPV subfamily and TRPV6

The founding members of TRPV subfamily are OSM-9 in *C.elegans* and TRPV1 in mammals. OSM-9 was identified during genetic screening for defects in osmotic avoidance (Colbert et al., 1997) while an elegant expression cloning strategy was able to identify TRPV1 among channels activated by vanilloid compounds (Caterina et al., 1997). The TRPV channels can be subgrouped into four branches by

15

sequence homology (Fig.3) Two branches constitute the mammalian TRPVs: the thermosensitive TRPV1-4 and the Ca^{2+} selective TRPV5-6. The other two branches are invertebrate branches including the *C.elegans* OSM-9 and the *Drosophila* Inactive (Iav) and Nanchung (Nan) proteins. Osmo-9 functions in osmotic avoidance, olfaction, mechanosensation and social feeding (de Bono, 2003), while *Drosophila* Iav and Nan participate in auditory response (Kim et al., 2003); (Gong et al., 2004).

In addition to the vanilloid compound capsaicin, TRPV1 is shown to be activated by other substances including resiniferatoxin, endocannabinoid lipids such as anandamide, eicosanoids, and 2-APB. Heat ≥ 43°C activates TRPV1 and this threshold is shifted to room temperature by injury-induced tissue acidosis and inflammatory cytokines (Zhang et al., 2005) which underlie the nociceptive function of TRPV1. TRPV2, as well, is activated by noxious heat (≥ 52°C) and is, together with TRPV1, expressed in small to medium-diameter dorsal root ganglia (DRG) neurons maintaining the fidelity of signalling in response to painful heating (Caterina et al., 1999). Warmer temperature are, on the other hand, enough to activate TRPV3 (33-39°C) and TRPV4 (27-34°C) (Montell, 2005). Besides heat, thermosensitive TRPVs can integrate several other stimuli [reviewed in (Vennekens et al., 2008)].

While TRPV1-4 are Ca^{2+} permeable with little selectivity to divalent over monovalent cations (P_{Ca}/P_{Na} between 1 and 10), TRPV5 and TRPV6 are explicitly classified in the second subset of TRPV channels because they show strikingly high Ca^{2+} selectivity (P_{Ca}/P_{Na} >100) that makes them virtually impermeable to monovalent ions except in absence of divalent cations (Vennekens et al., 2000; Yue et al., 2001).

Figure 3: Phylogenetic tree showing the four branches of TRPV family. The mammalian TRPVs: subgroups into TRPV1-4 and TRPV5, 6; *Drosophila* TRPVs: Nanchung and Inactive; *C. elegans* TRPVs:OSM-9 and OCR1-3. Distance scale is expressed as the number of substitutions per amino acid (Liedtke and Kim, 2005)

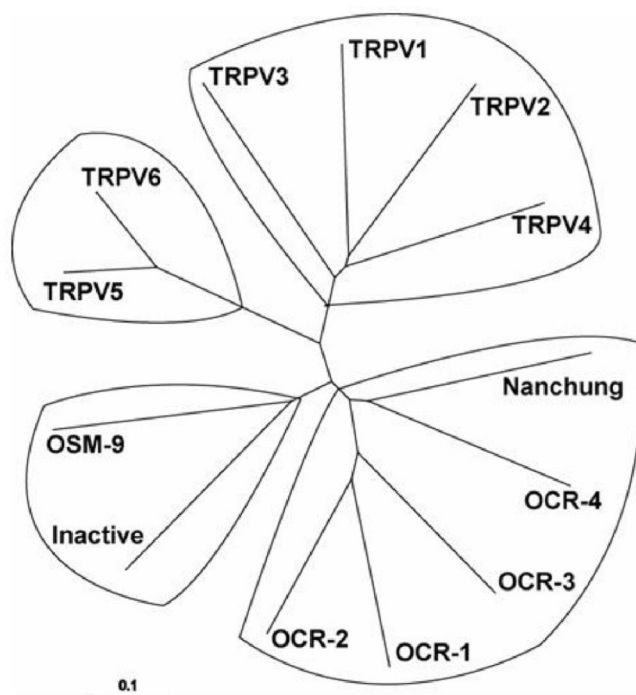TRPV6 was first identified as the calcium transport protein responsible for calcium uptake and thus named (CaT1) (Peng et al., 1999). The completion of the genome sequencing project declared CaT1 and CaT-L, identified by Wissenbach and co-workers in 2001(Wissenbach et al., 2001), to be orthologous proteins that were, together with ECaC2 (Hoenderop et al., 2001), named as TRPV6. TRPV5 and 6 are only 22-24% identical to thermosensitive TRPVs but they share 74% amino acid identity (Ramsey et al., 2006) and are located in close proximity on the human genome where TRPV6 is located on chromosome 7q33-q34 and TRPV5 on 7q35. The fact that these human chromosomal locations correspond to murine chromosome 6 and to chromosome 4 in rat suggest that TRPV5 and TPRV6 have arisen by gene duplication from an ancestral gene, the pufferfish Takifugu rubripes, for example, has only one gene which is slightly more similar to TRPV6 than to TRPV5 (Qiu and Hogstrand, 2004). The chromosomal organization of TRPV6 is conserved among several species. Depending on the species, the deduced amino acid sequence results in 719, 725, and 727 amino acid-proteins in pufferfish, humans and rodents, respectively. The calculated molecular weight of human TRPV6 is 83.21 kDa, with a pI of 7.56. Due to posttranslational glycosylation, heterologously expressed TRPV6 protein can be detected at molecular weights ranging between 75-100 in a denaturing SDS-PAGE gel (Wissenbach and Niemeyer, 2007).

TRPV6 was initially cloned from rat duodenum and Northern blot analysis showed that it is expressed chiefly in the small intestine and rat colon (Peng et al., 1999). Trials to detect TRPV6 in murine and human intestinal tissues were divergent. In two independent studies, TRPV6 could not be detected in human (Wissenbach et al., 2001); or mouse (Hirnet et al., 2003) intestinal tissue while two other groups were able to detect TRPV6 transcripts in human patients' duodena (Barley et al., 2001; Peng et al., 2000). Expression of TRPV6 is, however, prevalent in placenta, pancreas (human and murine), testis, epithelial cells of salivary glands (Hirnet et al., 2003; Hoenderop et al., 2001; Muller et al., 2000; Peng et al., 2000; Wissenbach et al., 2001; Xu et al., 2009). In addition, it has been shown that Ca^{2+}-transporting epithelia can coexpress TRPV5 and TRPV6 generating in theory a pleiotropic set of functional heterotetrameric channels with different Ca^{2+} transport kinetics (Hoenderop et al., 2003). Expression of TRPV6 associates with prostate cancer progression (Fixemer et al., 2003) and is shown to underlie Ca^{2+}-mediated cell proliferation believed to be essential for tumour progression (Schwarz et al., 2006).

TRPV5/6 display a selectivity for monovalent cations corresponding to Eisenman sequence X or XI ($Na^+ \sim Li^+ > K^+ > Cs^+$) and for divalent cations $Ca^{2+} > Ba^{2+} > Sr^{2+} > Mn^{2+}$. In absence of divalent cations, TRPV6 has single channel monovalent cation conductance of 27-73 pS measured over a range of -10 to -80 mV (Semenova et al., 2009; Vassilev et al., 2001). A positively charged aspartate residue in the pore region of TRPV6 (D541) and TRPV5 (D542) are shown to play a pivotal role commanding the conductive properties of the two channels (Nilius et al., 2001; Voets et al., 2004). Mutating the aspartate to alanine abolishes Ca^{2+} permeation, and to lysine renders the channel non functional. By binding to this aspartate Mg^{2+} blocks TRPV6 pore, as Voets and colleagues have shown (Voets et al., 2004; Voets and Nilius, 2003; Voets et al., 2001).

Structurally, TRPV6 is a typical TRPV channel. The N-terminal end encompasses six ANK repeat domains with the third domain being of prevalent importance for homotetramerization of TRPV6 as

well as for the dominant negative effect of a pore mutant on native channel subunits (Erler et al., 2004). A potential PIP_2 binding residue is located within the TRP box at the C-terminal end of TRPV6 protein. Depletion of PIP_2 is shown to mediate Ca^{2+}-dependent inactivation (Rohacs et al., 2008). In heterologous expression systems, TRPV6 shows constitutive activity at low intracellular Ca^{2+} concentrations and negative voltage. Hyperpolarizing cells expressing TRPV6 increases the electrical driving force and thus lets more Ca^{2+} through the channel. TRPV6 shows distinct inward rectification with minimal outward currents with highly buffered pipette solutions. Calcium selectivity is also manifested by the channel's impermeability to monovalent cations except in absence of divalent cations (Wissenbach et al., 2001; Hoenderop et al., 2001).

TRPV6 regulatory mechanisms: Because TRPV6 channels could be constitutively active in native systems, regulating the number of channels at the plasma membrane is critical. The auxiliary protein S11A10 associates with the conserved VATTV motif in the C-terminal end of TRPV6 and is found to be crucial for TRPV6 targeting to the plasma membrane (van de Graaf et al., 2003). Furthermore, surface expression is driven by interaction with the calcium binding protein 80K-H to the MLERK motif downstream of the S11A10 binding site (Gkika et al., 2004). The same motif has been shown to bind preferentially to the GDP-bound form of Rab11a prior to routing of TRPV5/6 to the plasma membrane (van de Graaf et al., 2006). This regulatory mechanism was later confirmed for TRPV5 which was shown to be internalized in a clathrin-dependent manner into vesicular structures then localizes to perinuclear structures positive for Rab11a (van de Graaf et al., 2008). TRPV5/6 have a conserved glycosylation site at the extracellular loop between transmembrane domains 1 and 2 (Hirnet et al., 2003). Hydrolysis of the complex carbohydrate residues at this site by klotho, a ß-glucuronidase with sialidase activity (Kuro, 2009), keeps the channels anchored at the plasma membrane enhancing their currents (Chang et al., 2005).

Besides the control of surface expression, TRPV6 is a subject of Ca^{2+} dependent and independent regulation. When TRPV6-expressinng cells are subjected to a prolonged hyperpolarizing pulse they show a multiphasic inactivation pattern. The first phase is rapid witnessed only in presence of extracellular Ca^{2+} but not Ba^{2+}. The subsequent complex slower phase is partially mediated by binding of Ca^{2+} activated calmodulin (Derler et al., 2006; Niemeyer et al., 2001). Calmodulin binding is prevented by *in vitro* PKC phosphorylation at threonine 702 (Niemeyer et al., 2001). As a Ca^{2+} sensor, calmodulin was also shown to regulate activity of mouse TRPV6 where consensus motifs were identified within the N-terminal end, the transmembrane domain and at the C-terminal end (Lambers et al., 2004). However, N-terminal binding could not be confirmed for murine TRPV6 by two independent groups (Derler et al., 2006; Phelps et al., 2008).

A distinguished property of the human TRPV6 gene is that it exhibits non-synonymous substitutions at three loci, namely amino acid 157, 378 and 681, resulting in two different alleles with a coupled polymorphism: the ancestral allele (TRPV6a: RVT) and the derived allele (TRPV6b: CMM). A unique attribute of the two alleles is the confinement of the ancestral allele to a distinct geographical distribution as it is predominant in African populations and the derived allele in other tested populations thus also termed new world allele (Akey et al., 2006). The geographical confinement suggests that the ancestral allele of *TRPV6* must have been subjected to selection of a pre-existing

mutation in the ancestral African population which subsequently became advantageous in a new environment and rose to high frequency represented by the derived allele in the new world (Hughes et al., 2008). However, if and how selection conferred functional advantage remain elusive. Trying to reveal potential functional differences between the two alleles, Huges et al compared the electrophysiological properties of both alleles in patch clamp experiments but could not spot significant differences (Hughes et al., 2008). Clinically, a higher occurrence of renal stones was observed in individuals heterozygous for the ancestral allele (Suzuki et al., 2008a), however, only one patient homozygous for the ancestral allele was part of the study. Because the expression of TRPV6 is shown to correlate with developmental stage and invasiveness of some cancers like prostate cancer (Fixemer et al., 2003), it is interesting to find out whether *TRPV6* polymorphism is involved in the higher occurrence of prostate cancer among African Americans (Abdalla et al., 1998). Our study attempts to contribute to uncovering possible differences between the two alleles in heterologous systems.

5.3   Regulation of ion channels by ATP

ATP is a multifunctional nucleotide representing the molecular unit of intracellular energy. ATP tunes the electrical activity of excitable and nonexcitable cells through direct or indirect modulation of several ion transporters and channels. The already identified mechanisms underlying this modulation are variable: while some require ATP hydrolysis and involve protein kinases, others are mainly carried out by intermediary regulatory proteins that are not for all cases well identified. The structural motifs regulating ATP binding and hydrolysis have been elucidated by the resolution of numerous crystal structures, both of isolated domains and of complete proteins (Hollenstein et al., 2007)

ATP-mediated regulation of many ion exchangers is well described. For example, ATP increases the activity of Na^+/Ca^{2+}-exchanger (NCX) by direct PKA- and PKC-mediated phosphorylation (Caroni and Carafoli, 1983), increasing PIP_2 production (Hilgemann and Ball, 1996) and via a GPCR-mediated stimulation (DiPolo and Beauge, 1998). Other exchangers regulated by ATP include Ca^{2+}- , H^+-, Na^+/K^+-ATPases and Na^+/H^+ exchanger [reviewed in: (Annunziato et al., 2004)].
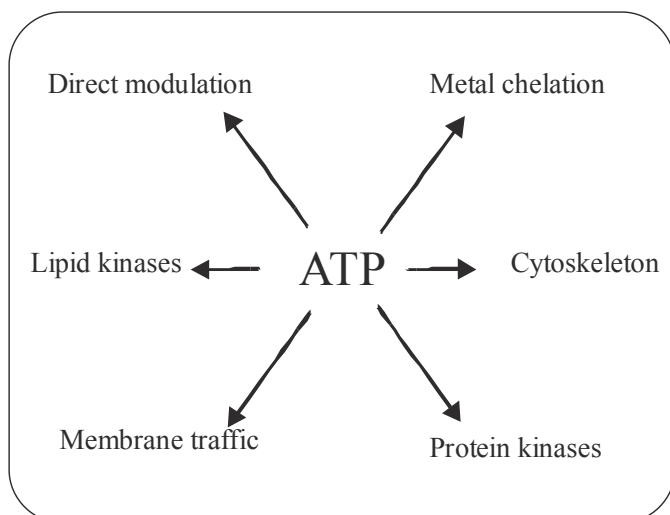
Figure 4: Mechanisms by which ATP modulates ion transporter and channel function (Hilgemann, 1997)

Figure 4 summerizes the ATP-dependent mechanisms regulating ion transporters. By activation of lipid kinases, ATP increases the production of PIP_2 that modulates activity of several ion channels (Huang, 2007). ATP also stimulates the outward chloride current by chelating Ca^{2+}. A drop in intracellular ATP level induces pronounced changes of cytoskeletal organization, often appearing as depolymerisation of F-actin (Golenhofen et al., 1995). This effect conceivably disturbs interaction of ATP with the actin filaments and anchoring of ion transporters to the plasma membrane. Compartmentalized ATP i.e. ATP bound to the plasma membrane is another way of modulation channels. Availability of membrane-bound ATP determines how well the different pumps are fuelled.

While the molecular evidence for the aforementioned mechanisms is still in most cases unclear, mechanisms regulating the ATP-sensitive K^+ (K_{ATP}) channels are extensively described. Single-channel studies showed that direct binding of ATP to Kir6.2 decreases channel activity by decreasing the mean open time, reducing the mean burst duration and increasing the frequency and duration of the interburst closed states (Craig et al., 2008). Besides direct binding to a classical or unique motif, ATP-dependent modulation of channel activity could be mediated by changing intrinsic channel properties, for example increasing the open channel probability of InsP3R TypeI (Betzenhauser et al., 2009). Contrary to the inhibitory effect of ATP on K_{ATP} channels, ATP was shown to reduce rundown of L-type Ca^{2+} channels with a dual mechanism with only one mechanism involving phosphorylation and not requiring ATP hydrolysis (Yazawa et al., 1997).

Many TRP channels are regulated by ATP. In rat cardiac myocytes ATP is shown to activate TRPC3/7 (Alvarez et al., 2008) and TRPM4 (Scamps and Vassort, 1990). ATP is also shown to be essential for activation of TRPC6 in a calmodulin kinaseII (CamKinaseII)-dependent manner (Shi et al., 2004). TRPM7 is activated by reducing intracellular level of magnesium ATP (Penner and Fleig, 2007). By replenishment of PIP_2, ATP is able to prevent desensitization of TRPA1 (Karashima et al., 2008). On the contrary, Dattilo and coworkers reported that intracellular ATP inhibits TRPC5 currents in a phosphorylation independent effect that does not require hydrolysis of ATP (Dattilo et al., 2008).

Compared to other TRP channels, interaction of ATP with TRPV1 is probably the most intensively investigated. The crystal structure of the ankyrin repeat domain of TRPV1 revealed an ATP binding site that overlaps with a calmodulin binding domain. Competitive interaction of both ligands at this site regulates TRPV1 activity in a Ca^{2+}-dependent manner. Sufficient intracellular ATP prevents capsaicin-induced tachyphylaxis that would otherwise be induced by calmodulin binding (Lishko et al., 2007). Interestingly Phelps et al reported that TRPV6-ARD, though containing a similar number and a related structure of ankyrin repeats as TRPV1, neither binds calmodulin within its ankyrin repeat sequence nor is the ATP binding pocket of TRPV1 conserved (Lishko et al., 2007; Phelps et al., 2008). For TRPV6 and TRPV5, however, ATP was shown to prevent run-down in divalent-free conditions (Hoenderop et al., 2001). To unravel the underlying mechanism was one goal of the current work.

5.4   Regulation of ion channels by phosphorylation

Protein phosphorylation and dephosphorylation are common reversible posttranslational modifications resulting in changes in conformation, cellular location or association with other proteins with an ultimate regulatory effect on the function of ion channels. Protein kinases constitute a family of divergent enzymes responsible for addition of phosphate groups on definite consensus sites within proteins. This family of enzymes classically comprises tyrosine kinases and serine/threonine kinases. The next section presents few examples of regulatory effects of different kinases on ion channels.

Tyrosine kinase (TK)-mediated regulation is described for several ion channels. TK phosphorylates the alpha-subunit of large conductance Ca^{2+}-dependent K^+ channels (BKCa) shifting the Ca^{2+} sensitivity of the channel and producing hyperpolarisation (Fukao et al., 1999). In addition, tyrosine kinase enhances single-channel gating of NMDA receptors and consequently increases the NMDA receptor-mediated synaptic currents in neurons (Salter and Kalia, 2004). Tyrosine kinase was also shown to enhance activities of TRPC3 (Vazquez et al., 2004) and TRPM7 channels (Gwanyanya et al., 2006)

Similarly, the diverse subfamily of serine/threonine kinases is shown to modulate the activity of an array of ion channels including several TRP channels. PKC stimulation by PMA is shown to potentiate TRPM4 (Guinamard et al., 2004), TRPV1 when phosphorylated at S-502 and S-800 (Bhave et al., 2003; Numazaki et al., 2002; Premkumar and Ahern, 2000; Vellani et al., 2001) and TRPV4 (Xu et al., 2003). Furthermore, activation of PKC was shown to inhibit caveolai-mediated endocytosis thereby increasing current density and surface abundance of TRPV5 (Cha et al., 2008). Likewise, a recent study using mutational analysis of the putative phosphorylation sites S-299 and S-654 in TRPV5 shows that activation of the Ca^{2+} receptor CaR stimulates TRPV5-mediated Ca^{2+} influx via a PMA-insensitive PKC isoform pathway (Topala et al., 2009). On the other hand, inhibition of PKC-mediated phosphorylation favours cytosolic over plasma membrane distribution of TRPM7 (Yogi et al., 2009). Moreover, stimulation of PKC down regulates activities of TRPC6 (Zhang and Saffen, 2001) as well as TRPC3,4 and 5 (Venkatachalam et al., 2003). CaM-kinase is shown to enhance activities of TRPC6 (Hisatsune et al., 2004) and TRPV1 (Jung et al., 2004). Casein kinase (CK2)-phosphorylated forms of TRPP2 (Kottgen et al., 2005) and TRPP1 (Roitbak et al., 2004) are more susceptible to retrieval into the cytoplasmic compartment. PKA phosphorylation of TRPV1 at S502 leads to both heat and capsaicin-sensitization (Lopshire and Nicol, 1998; Rathee et al., 2002). On the other hand, when PKA

phosphorylates T-370 and S-116 of TRPV1, the result is a desensitized channel and modulated pain perception (Bhave et al., 2002; Mohapatra and Nau, 2003; Mohapatra and Nau, 2005). For TRPV2, channel activity is increased by PKA phosphorylation (Stokes et al., 2004).

Within TRPV6 protein putative phosphorylation sites for different kinases were identified. S142 and S144 were identified by sequence analysis as putative targets for CaM-dependent kinaseII and PKC, respectively (den Dekker et al., 2003). *In vitro* phosphorylation of TRPV6 at S702 by PKC_α prevents calmodulin binding at the C-terminus thus hindering Ca^{2+}-dependent calmodulin inactivation (Niemeyer et al., 2001). Interestingly, the derived TRPV6b allele lacks a putative PKC consensus site compared to the ancestral TPRV6a allele due to the R158C polymorphic substitution. The current work addresses how TRPV6 is regulated by PKC-mediated phosphorylation focusing on possible differential regulation of the two alleles

Because the general scope of the present work is to understand how Ca^{2+} signalling is regulated, we also investigated regulation of another family of ion channels, the ORAI family, that is not related to TRP channels but exhibits as well exquisite Ca^{2+} selectivity and will be introduced in the following chapter.

5.5   ORAI Ion Channels

In 1986, James Putney proposed the "capacitative Ca^{2+} entry hypothesis" that suggests the presence of Ca^{2+} permeable channels at the plasma membrane that are activated when IP_3 binds its receptors on ER and mediates store depletion in order to replenish these stores (Putney, 1986). Yet, he did not neither characterize the current nor the channels. The calcium release activated calcium current (I_{CRAC}) was first measured and characterized in patch-clamp recordings from mast and Jurkat T-cells and the channels were named CRAC channels (Hoth and Penner, 1992; Lewis and Cahalan, 1989; Zweifach and Lewis, 1993). I_{CRAC} measurement and the observation that thapsigargin-induced store depletion was also accompanied by Ca^{2+} influx, as seen from Ca^{2+} imaging data (Putney and Bird, 1993) strongly supported the theory. Basic biophysical features of I_{CRAC} are high selectivity for Ca^{2+}, pronounced inward rectification and an estimated single channel conductance of less than 1 pS (Hoth and Penner, 1993). Specific CRAC blockers are not yet identified. On the other hand, it is now well established that the stromal interaction protein STIM1 is a Ca^{2+} sensor that is required for CRAC activation, as revealed by RNAi screens (Liou et al., 2005; Roos et al., 2005; Soboloff et al., 2006). STIM1 was primarily identified in a library screen by its ability to confer binding of pre-B lymphocytes to stromal cells (Oritani and Kincade, 1996). *Drosophila* and *Caenorhabditis elegans* have a single STIM protein while birds and mammals have two homologues. The human *STIM2* gene shares 61% sequence identity with STIM1. Soon after identification of STIM1, the molecular identity of CRAC channels was disclosed using an unbiased genome-wide RNA interference (RNAi) screen in Drosophila S2 cells (Vig et al., 2006b; Zhang et al., 2006). Feske and coworkers identified three human homologs of CRAC channels and named them ORAI1-3. Furthermore they conducted a mutation linkage analysis using T cells isolated from patients suffering from severe combined immunodeficiency syndrome (SCID) and were able to identify a naturally occurring single point mutation (R91W) as the underlying cause of the disease(Feske et al., 2006).

Structurally (Fig. 5), STIM1 is a single transmembrane phosphoprotein with an N-terminus extending in the lumen of the ER and containing an EF-hand that binds and senses luminal $[Ca^{2+}]$ as well as a sterile-alpha motif (SAM) including two N-linked glycosylation sites. The C-terminus protrudes into the cytosol and contains two lengthy coiled-coil domains overlapping with an ezrin-radixin-moesin (ERM)-Like domain. This end of the molecule diverges substantially: the *Drosophila* protein lacks the proline-rich region and the lysine-rich tail (Liou et al., 2005).
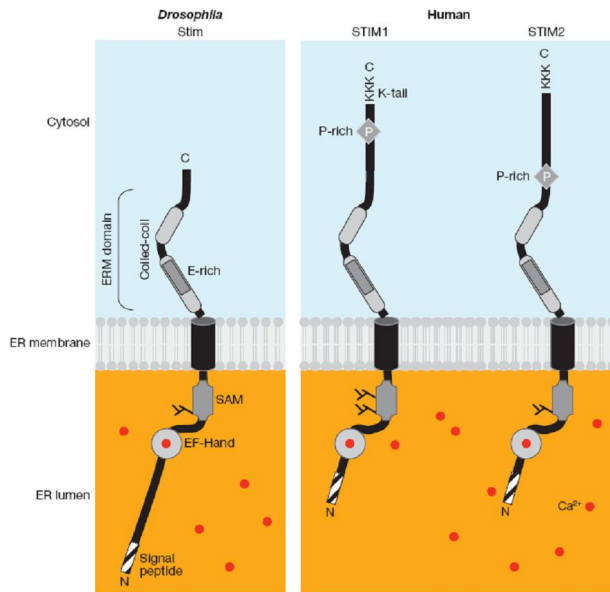
Figure 5: Domains of STIM proteins. *Drosophila* and human STIM proteins are situated in the ER membrane. Modules of STIM1, STIM2 and Stim include: the signal peptide, the predicted EF hand and SAM domains, the transmembrane region and two regions predicted to form coiled coil structures comprising the ERM domain. Proline-rich domains (P) and the lysine-rich C-terminal regions are unique to the mammalian STIM family members. *Drosophila* Stim contains an N-terminal sequence in the ER that is not present in either STIM1 or STIM2. The N-linked glycosylation sites at the SAM domain, experimentally verified for STIM1 are indicated. Background colours represent basal Ca^{2+} concentrations of ~50 nM in the cytosol and > 400 μM in the ER lumen. Ca^{2+} ions are shown as red dotst including Ca^{2+} bound to the EF hand domain. (Cahalan, 2009)

Unlike STIM1, both N- and C- termini of ORAI proteins are cytosolic and bracket four membrane spanning domains as predicted by hydropathy analysis (Fig. 6). As for many Ca^{2+} channels, a putative interaction and regulatory coiled-coil domain is found in the C-terminus of ORAI. An N-glycosylation site was identified in the extracellular loop between transmembrane domains three and four. Mutants of this site showed comparable channel activity to wildtype (Zhang et al., 2008). A part from that, ORAI channels share no other structural properties with other ion channels. The selectivity filter of ORAI pores are formed by acidic residues in transmembrane domain one and three and the first loop domain (Vig et al., 2006a).
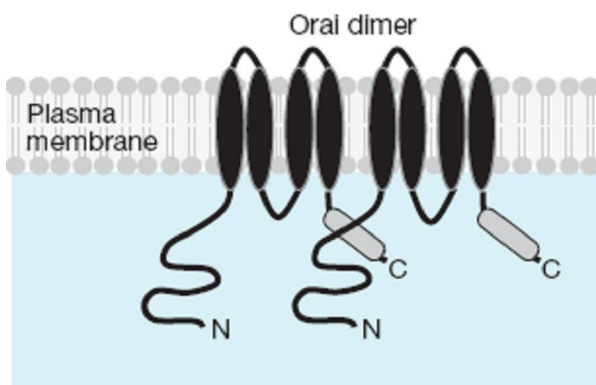
Figure 6: ORAI channel at basal state present as dimers. An ORAI channel is formed of four transmembrane domains and intracellular N- and C- termini. A coiled coil domain is indicated on the C-terminus (modified from (Cahalan, 2009))

5.5.1   Store activated operation of STIM1/ORAI

Owing to its large surface area the ER serves as an ideal intracellular Ca^{2+} capacitator, charged by SERCA pump and discharged via Ca^{2+}-permeant channels. Among the latter, are the IP3 receptors (IP_3R) that are activated by ligand (IP_3) binding leading to release of Ca^{2+} content and subsequent rise of cytosolic Ca^{2+} with a concurrent drop in ER Ca^{2+} content below resting level [300-500 µM, (Brini et al., 1999; Montero et al., 2001; Yu and Hinkle, 2000)]. At the resting state STIM exists as dimers stabilized at the ER membrane by C-terminal coiled-coil interactions and binds Ca^{2+} with low affinity. When a drop in $[Ca^{2+}]_{ER}$ <300µM is sensed the EF hand of STIM dissociates Ca^{2+} and a SAM-domain interaction is initiated leading to further Oligomerization of STIM. The formed oligomers are then redistributed from the tubular structures, where STIM dimers bind the microtubule-plus-end-tracking protein EB1 at resting state, to a punctuate cluster (puncta) close to the plasma membrane (Liou et al., 2007). At the plasma membrane STIM directly interacts with and opens ORAI channels, the effector domain being within the C-terminal end as shown by co-immunoprecipation and FRET studies [reviewed in (Cahalan, 2009)]. Expressing the C-terminal domain of STIM was adequate for constitutive activation of ORAI circumventing store depletion (Park et al., 2009). Recently, the minimal sequence essential for ORAI activation (CRAC Activating Domain, CAD) was mapped to a stretch of ~100 residues within the coiled coil region (Park et al., 2009; Yuan et al., 2009). In summary, the molecular components of CRAC current are tetramers of ORAI subunits activated by oligomers of STIM, the aggregation of which is store depletion-evoked.

5.5.2   ORAI channels and the immune response

In an immune response, variable types of immune cells are recruited to the site of immunogen contact. Professional antigen-presenting cells (APCs e.g. dendritic cells, macrophages and B-cells) process the antigen and convey the perceived immunological information, in the form of peptides bound to Class II-MHC receptors, to $CD4^+$-T_{h1} cells. Together the APCs and T_{h1} cells form the so called immunological synapse (IS). Activated T_{h1} cells will subsequently migrate into the infected tissues and in turn stimulate the locally infiltrated macrophages provoking a multiple effector pathway immune response. To eradicate an immunogen, the activated macrophages initiate an "oxidative burst" generating superoxide (O^{2-}) and hydrogen peroxide (H_2O_2) (Babior, 1984; Forman and Torres, 2001). Despite exposure to the elevated concentration of oxidants in inflamed versus normal tissues, differentiated Th-cells are still able to perform their defensive function.

The formation of an immunological synapse is accompanied by a rapid increase in the free $[Ca^{2+}]_i$, which is a prerequisite for activation, differentiation and proliferation of T-cells (Feske, 2007; Lewis, 2001; Negulescu et al., 1994; Quintana et al., 2005). The $[Ca^{2+}]_i$ rise is mediated by Ca^{2+} release from the endoplasmic reticulum (ER) through IP_3R and subsequent Ca^{2+} influx through calcium-release activated Ca^{2+} (CRAC) channels. CRAC channels in T-lymphocytes are mainly formed by homomers of ORAI1, however, heteromeric channels can also be formed with ORAI2 or ORAI3 proteins. The

ORAI-mediated Ca^{2+} influx is indispensable for an efficient immune response as indicated by the compromised immunity of SCID patients (mentioned above).

5.6   Regulation of ion channels by hydrogen peroxide

Reactive oxygen species (ROS) are typically defined as molecules or ions formed by the incomplete one-electron reduction of oxygen. Classically, ROS include free radicals such as superoxide, hydroxyl radical, and singlet oxygen as well as non-radical species such as hydrogen peroxide (H_2O_2). ROS contribute to physiological processes including microbicidal activity of phagocytes, signal transduction and gene expression and conversely they can cause oxidative damage to nucleic acids, proteins and lipids (Pan et al., 2009). In addition, many cellular processes are modulated by the redox state of proteins. Changes in structure caused by oxidation of reactive cysteine residues can change the activity of enzymes and ion transporters (Feissner et al., 2009).

In the context of ion transport, regulation of several ion transport systems and channels by ROS is well established though the mechanisms are not always understood. For example, ROS are shown to stimulate ryanodine receptors (RyR) either directly by oxidizing the redox-sensing thiols (Zima et al., 2004) or indirectly by oxidizing nitric oxide (NO) to nitrosium (NO^+) that in turn reacts with free RyR thiols and forms the RyR-stimulator, S-nitrosothiol (Stoyanovsky et al., 1997; Xu et al., 1998). The Na^+/ Ca^{2+} exchanger (NCX), SERCA and PMCA are also modulated by H_2O_2 [reviewed in (Feissner et al., 2009)]. Redox modification of sulfhydrals is thought to be responsible for a thimerosal-dependent IP_3 receptors sensitization to IP_3 (Bootman et al., 1992). Reduced glutathione/glutathione disulfide (GSH/GSSG) couple is the main cellular redox buffer and is maintained at high ratio of GSH:GSSG (Schafer and Buettner, 2001). GSSG has been shown to stimulate IP_3R channel activity by increasing the binding affinity to hepatocyte IP_3R (Missiaen et al., 1991; Renard-Rooney et al., 1995). In addition, ROS have been shown to directly stimulate IP_3R-mediated Ca^{2+} release from ER (Rooney and Thomas, 1991). Among the ion channels regulated by ROS are several K^+, Na^+ and Cl^- channels [reviewed in (Kourie, 1998)]. Likewise, many TRP channels are redox sensitive. In a PLC-dependent pathway, TRPC3 and TRPC4 are shown to form redox-sensitive cation channels that participate in Na^+ loading and membrane depolarization (Miller, 2006). Furthermore, hydrogen peroxide is shown to evoke Ca^{2+} influx through TRPM2 (Hara et al., 2002; Yamamoto et al., 2008), and cation conductance of TRPM7 (Aarts et al., 2003) and TRPM8 (Yoshida et al., 2006).

A major target of ROS-induced modification of proteins are the reactive cysteine residues. A reactive cysteine contains a thiolate group (S^-) which reacts with H_2O_2 with rates ranging from 10-10^5 $M^{-1}s^{-1}$, depending on their local environment, while the thiol groups (SH) do not react physiologically with H_2O_2 unless the reaction is catalyzed (Forman et al., 2004). The thiolate undergoes reversible (sulfenic) or irreversible (sulfinic and sulfonic acid) covalent modifications upon oxidation. Additionally, mild oxidation can induce reversible cysteine disulfide bond formation and thus prevent further irreversible cysteine modifications (Droge, 2002). The thiolate oxidation produces intermolecular cross-links that underlie ROS-induced protein oligomers (Huang et al., 1992; Jamme et al., 1995; Kako et al., 1988). The physical changes in the structure of the channel and pump proteins, like intermolecular cross

linking resulting from oxidation, modify the function of the transporting proteins and /or the availability of regulatory sites on these proteins (Kourie, 1998).

While it is clearly established that Ca^{2+}-signals in T-cells are necessary for regulation of the immune response, the role of redox status for Ca^{2+}-dependent T-cell activation is less well understood. The goal of the work presented in chapter (7.2) was to identify whether and how the main component of Ca^{2+} signal in immune response, ORAI channels, are influenced by redox status and how that affects T-cells functions at different stages of the immune response.

6   **Materials**

6.1   **Resources**

AmershamPharmacia Biotec (Freiburg, GER)

AppliChem (Darmstadt, GER)

Applied Biosystems (Foster City, USA)

BD Biosciences (Bedford, USA)

Beckman (München, GER)

Becton Dickinson Labware (Franklin Lakes, NJ, USA)

Bio-Rad Laboratories (München, GER)

Biotrend (GentaurBVBA-Bioxys) (Brussels, BEL)

Biozym (Hessisch Oldendorf, GER)

Cell signaling (Frankfurt, GER)

Dagan (Minnesota, USA)

Eppendorf (Hamburg, GER)

Fermentas (St. Leon-Rot, GER)

Fuji (Düsseldorf, GER)

Hermle (St. Leon-Rot, GER)

Hettich (Tuttlingen, GER)

Holten (Allerod, DK)

IKA (Staufen, GER)

Infors-HT (Bottmingen, Switzerland)

Integra Bioscience (Fernwald, GER)

Invitrogen (San Diego, USA)

Memmert (Schwabach, GER)

Merck (Darmstadt, GER)

Millipore (Schwalbach/Ts, D)

MWG Biotech (Ebersberg, GER)

New England Biolabs (NEB) (Frankfurt, GER)

New Brunswick Scientific (Edison NJ, USA)

Operon (Köln, GER)

Pierce (Rockford, USA)

Peqlab (Erlangen, GER)

Promega (Mannheim, GER)

Qiagen (Hilden, GER)

Roche (Basel, CH)

Roth (Karlsruhe, GER)

Sarstedt (Nürnbrecht, GER)

Sigma (Deisenhofen, GER)

Stratagene (Heidelberg, GER)

ThermoScientific (Gert-Jan Bakkenes, GER)

Uniequip (Martinsried, GER)

Wescor (Langenfeld, GER)

Whatman (Brentford, UK)

Wolf Laboratories Limited (Pocklington, UK)

Zeiss (Oberkochen, GER)

6.2   Supplies

Nitrocellulose-Membrane	Hybond N (Amersham Pharmacia)
Sterile containers for laboratory and cell culture	Falcon (BD Biosciences)
Sterile disposable pipettes	Falcon (Becton Dickinson Labware)
Filter Tip FT 20, 200 und 1000	Peqlab
	Biozyme
Sephadex ^{TM} G-50	Amersham Pharmacia
Petri dishes	Sarstedt
PVDF membrane	ImmobilonTM-P (Millipore)
Needles	Microlance 0.7, 0.55, 0.4 (BD Biosciences)

6.3   Equipment

Centrifuges	L8-60M-Ultracentrifuge (Beckman)
	OptimaTM MAX-E Ultracentrifuge (Beckman)
	Table centrifuge 5415 C (Eppendorf)
	J2-HS centrifuge (Beckman)
	96-well plate centrifuge 4-15C (Sigma)
	Universal 32R (Hettich)
	Mikro 220R (Hettich)
	Mini spin 5452 (Eppendorf)
Horizontal Gel electrophoresis apparatus	Sub-cell GT Agarose Gel Electrophoresis Systems (Bio-Rad)
Photometer	Gene quant II (Pharmacia Biotech)
	Biophotometer (Eppendorf)
Shaking water bath	WB 14 (Memmert)
Shaker	Vibrax-VXA (IKA)
Thermomixer	Vortem 56 EVC (Uniequip)
	Thriller (Peqlab)
Biological safety cabinet	HERAsafe Class II (KS12)
Electroporation machine	Nucleofector II (Amaxa bioscience)

Thermocycler	Gene Amp PCR System 9700 (Applied Biosystems)
	Master cycler, Persoanl 5332 (Eppendorf)
DNA sequencing equipment	Abi Prism 310 Genetic Analyzer (Applied Biosystems)
Fermenter	Scientific Series 25 Incubator Shaker (New Brunswick Scientific)
	Heidolph Unimax 1010 (Wolf Laboratories Limited)
	Minitron (Infors-HT)
Pipetting	Pipetboy acu (Integra Biosciences)
Vertical electrophoresis systems	Mini VE (Amersham Biosciences)
	Mini-Protean Tetra cell (Bio-Rad)
Electrophoresis power supply	Power Pac HC (Bio-Rad)
Molecular imager (gels and WB)	ChemiDocTM XRS
Rocking platform shaker	Heidolph duomax 1030
Cell culture incubator	Heraeus Function Line Incubator (Thermo Scientific)
Water bath	Lauda A100
Incubation shaker	Minitron CH-4103 (Infors HT)
Gel dryer	Gel dryer 583 (Bio-Rad)
Amplifier	EPC9 and EPC10 USB (HEK electronics)
Micromanipulater	LN Pivot Manipulator (Luigs & Neumann)
Microscope	Axio Observer A1 (Zeiss)
Puller	DMZ-Universal Puller (Dagan)
Osmometer	VAPRO ® Vapor Pressure Osmometer (Wescor)

6.4   Chemicals

Unless otherwise indicated, chemicals used for this work were purchased from one of the following suppliers Amersham Pharmacia, Boehringer Ingelheim, Invitrogen, Merck, Roth or Sigma

6.5   Reagent systems (Kits)

ABI Prism Big Dye [TM] FS Terminator Cycle Sequencing Ready Reaction Kit V 1.1 (Applied Biosystems)

BCA[TM] Protein Assay Kit (Thermo Scientific)

Hi Speed Plasmid Maxi Kit (Qiagen)

Phusion polymerase High-Fidelity PCR kit

Qiaprep spin Mini Kit (Qiagen) (27106)

QiaQuick gel extraction kit (28706)

30

Quik Change XL Kit (Stratagene)

Western Lightning™ Plus ECL (Perkin Elmer)

TNT(R) Quick Coupled Translation System (Promega)

6.6   Size standards

DNA Size standard marker: 1 kb DNA Ladder (Invitrogen)

2-Log DNA Ladder, 0.1-10 kb (NEB)

M9-Marker (Self made, Dr. U. Wissenbach)

Prestained Proteinmarker (Peqlab)

Dual Color Proteinmarker (Bio-Rad)

Kaleidoscope Proteinmarker (Bio-Rad)

6.7   Constructs

6.7.1   TRPV6 Constructs

Construct	Primer Name	Primer sequence 5'→3'	T$_m$ °C	Restriction site(s)
ARD- (C) 6×His (43-266)	BAN429	GTGGCGGCCGCGGTGTGCTTCCGCTTCTG	58	NdeI
	BAN432	GATATACATATGAAGAGGATCTGGGAGTCTCC	62	NotI
ARD (N) 10×His (43-266)	BAN375	CGGGATCCGAAGAGGATCTGGGAGTCTCC	62	BamHI
	BAN376	CGGGATCCTTAGGTGTGCTTCCGCTTCTG	58	BamHI
CT2 (C) 6×His (633-725)	BAN431	GATATACATATGGTGGAAGACAGGCAAGATC	58	NdeI
	BAN432	GTGGCGGCCGCGATCTGATATTCCCAGCTCTC	62	NotI
CT2 (N) 10×His (633-725)	BAN382	CCGCTCGAGGTGGAAGACAGGCAAGATC	58	XhoI
	BAN117	CCGCTCGAGTTAGATCTGATATTCCCAGCTC	56	XhoI
CT3 (N) 10×His (647-725)	BAN 83	CCGCTCGAGTACGCACAGGCCTTCCAC	58	XhoI
	BAN 17	CCGCTCGAGTTAGATCTGATATTCCCAGCTC	56	XhoI
NP (267-330)	BAN377	CGGGATCCGCAGTGGACGTATGGACCAC	60	BamHI
	ISE 06	CGGGATCCTTAGAAGTACGGCCGCCCG	52	BamHI
R153Q/ R154P/ EGFP/ pcDNA3	BAN190	CAGGCACTGCCTTCCAGCCTAGTCCCTGCAACCTC	114	-
	BAN191	GAGGTTGCAGGGACTAGGCTGGAAGGCAGTGCCTG	114	-
R606Q	BAN371	CACGGTGATGCTGGAGCAGAAGCTGCCTCGCTGCC	116	-
	BAN371	GGCAGCGAGGCAGCTTCTGCTCCAGCATCACCGTG	116	-
R686A	BAN380	CCTATGCCCTCAGTGTCTGCAAGTACCTCCCGCAGCAG	122	-
	BAN381	CTGCTGCGGGAGGTACTTGCAGACACTGAGGGCATAGG	122	-
S144A	BAN351	CCGCAGGGCCAGTGTCGCTGCCAGAGCCACAGGCAC	124	-
	BAN352	GTGCCTGTGGCTCTGGCAGCGACACTGGCCCTGCGG	124	-
S144D	BAN361	CCGCAGGGCCAGTGTCGATGCCAGAGCCACAGGCAC	122	-
	BAN362	GTGCCTGTGGCTCTGGCATCGACACTGGCCCTGCGG	122	-
S155A	BAN369	GCACTGCCTTCCGCCGTGCTCCCCGCAACCTCATCTAC	126	-
	BAN370	GTAGATGAGGTTGCGGGGAGCACGGCGGAAGGCAGTGC	126	-
S155D	BAN367	GCACTGCCTTCCGCCGTGACCCCCGCAACCTCATCTAC	126	-
	BAN368	GTAGATGAGGTTGCGGGGGTCACGGCGGAAGGCAGTGC	126	-
S318A	BAN357	CGGTGAAGGAGCTGGTGGCCCTCAAGTGGAAGCGGTAC	124	-
	BAN358	GTACCGCTTCCACTTGAGGGCCACCAGCTCCTTCACCG	124	-
T150A	BAN353	CTGCCAGAGCCACAGGCGCTGCCTTCCGCCGTAGTC	122	-
	BAN354	GACTACGGCGGAAGGCAGCGCCTGTGGCTCTGGCAG	122	-
T298/299A	BAN355	CCCTGCTGGAACTTATCATCGCCGCCAAGAAGCGGGAGGCTC	136	-
	BAN356	GAGCCTCCCGCTTCTTGGCGGCGATGATAAGTTCCAGCAGGG	136	-
T298/299D	BAN388	CCCTGCTGGAACTTATCATCGACGACAAGAAGCGGGAGGCTC	132	-
	BAN389	GAGCCTCCCGCTTCTTGTCGTCGATGATAAGTTCCAGCAGGG	132	-

T688A	BAN359	GCCCTCAGTGTCTCGAAGTGCCTCCCGCAGCAGTGCC	124	-
	BAN360	GGCACTGCTGCGGGAGGCACTTCGAGACACTGAGGGC	124	-
T688D	BAN365	GCCCTCAGTGTCTCGAAGTGACTCCCGCAGCAGTGCC	122	-
	BAN366	GGCACTGCTGCGGGAGTCACTTCGAGACACTGAGGGC	122	-

6.7.2   ORAI Constructs

Construct	Primer Name	Primer sequence 5'→3'	T_m °C	Restriction site(s)
ORAI1 WT pCAGGS	BAN416	GGCGATATCCTAGGCATAGTGGCTGCCGG	58	EcoRV
	BAN392	5'PHO-CGCCACCATGCATCCGGAGCCCGC	58	
ORAI2 WT pCAGGS	BAN394	5'PHO-CGCCACCATGAGTGCTGAGCTTAACGTG	64	-
	BAN402	5'PHO-TCACAAGACCTGCAGGCTGCG	60	-
ORAI3 WT pCAGGS	BAN397	5'PHO-CGCCACCATGAAGGGCGGCGAGGG	58	-
	BAN403	5'PHO-TCACACAGCCTGCAGCTCCC	58	-
ORAI1 C126S	BAN406	GCTCATCGCCTTCAGTGCCAGCACCACAGTGCTGGTGG	124	-
	BAN407	CCACCAGCACTGTGGTGCTGGCACTGAAGGCGATGAGC	124	-
ORAI1 C143S	BAN408	CGCTCATGATCAGCACCAGCATCCTGCCCAACATCG	124	-
	BAN409	CGATGTTGGGCAGGATGCTGGTGCTGATCATGAGCG	124	-
ORAI1 C195S	BAN410	GCTGAGGTGGTGCTGCTCAGCTGGGTCAAGTTCTTGCC	122	-
	BAN411	GGCAAGAACTTGACCCAGCTGAGCAGCACCACCTCAGC	122	-
ORAI3 G170C	BAN447	CTTGCTGAAGTTGTCCTGGTTTGTTGGGTCAAGTTTGTGCCC	126	-
	BAN448	GGGCACAAACTTGACCCAACAAACCAGGACAACTTCAGCAAG	126	-
ORAI1- (N)-mEGFP-pMAX	BAN412	5'PHO-ATCATGCATCCGGAGCCCGC	58	-
	BAN401	5'PHO-TCAGGCATAGTGGCTGCCGG	58	-
ORAI2 WT -(N)-mEGFP pMAX	BAN413	5'PHO-TCATGAGTGCTGAGCTTAACGTG	60	-
	BAN402	5'PHO-TCACAAGACCTGCAGGCTGCG	60	-
ORAI3 WT -(N)-mEGFP pMAX	BAN414	5'PHO-ATCATGAAGGGCGGCGAGGG	58	-
	BAN403	5'PHO-TCACACAGCCTGCAGCTCCC	58	-
ORAI1 WT -(C)-mEGFP pMAX	BAN392	5'PHO-CGCCACCATGCATCCGGAGCCCGC	58	-
	BAN425	5'PHO-GGCATAGTGGCTGCCGG	58	-
ORAI3 WT -(C)-mEGFP pMAX	BAN397	5'PHO-CGCCACCATGAAGGGCGGCGAGGG	58	-
	BAN426	5'PHO-CACAGCCTGCAGCTCCC-3'	58	-

6.7.3   Miscellaneous Constructs

Construct	Primer Name	Primer sequence 5'→3'	T_m °C	Restriction site(s)
PKC$_{βII}$	BAN 386	TGTGGGCGAAATGCTGAAAAC	62	-
	BAN 387	CTACTTAGCTCTTGACTTCGG	62	
r TRPV1	BAN 390	CGGGATCCGTCCGTCTCCGCTGGTGAG	60	BamHI
ARD	BAN 391	CGGGATCCTTAGTGTCGGCACTCGGGTTC	60	BamHI

6.7.4   Primers for sequencing vector plasmids

Vector plasmid	OligonucleotideName	Oligonucleotide sequence 5'→3'	Tm °C
pCAGGS	pCAGGS for	AACGTGCTGGTTATTGTGC	56

pCAGGS	pCAGGS rev	ACCTTCTGATAGGCAGCC	56
pcDNA3	pRC for	CTAGAGAACCCACTGCTT	54
pcDNA3	pRC rev	GCACAGTCGAGGCTGATC	58
EBFP/ECFP /EGFP/EYFP	EGFP-N-Primer	CGTCGCCGTCCAGCTCGACCA	72
EBFP/ECFP /EGFP/EYFP	EGFP-C-Primer	CATGGTCCTGCTGGAGTTCGTG	68

6.8   Plasmids

pBlueScriptII (Stratagene)

pCAGGS (J. Miyazaki)

pcDNA3 (Invitrogen)

pET21a (Novagen)

pET19b (Novagen)

pMAX (Addgene)

6.9   Restriction endonucleases and modifying enzymes

Restriction endonucleases

All restriction endonucleases were purchased from New England Biolabs (NEB).

Modifying Enzymes

Antarctic Phosphatase (Roche)

DNAse I (Calbiochem)

Pfu Turbo (Proofreading Polymerase) (Stratagene)

Phusion polymerase (Finnzymes, NEB)

RNAse A (Sigma)

T4-DNA-Polymerase (New England Biolabs)

T4-DNA-Ligase (New England Biolabs)

T4-Polynucleotide kinase (New England Biolabs)

Taq-Polymerase (Peqlab)

6.10   Antibodies

Antibodies made by Prof. Flockerzi's group:

429   Rabbit polyclonal antibody against hTRPV6, affinity purified.

26B3   Mouse monoclonal antibody against hTRPV6, affinity purified.

737   Rabbit polyclonal antibody against Histidine tag, affinity purified.

Commercial antibodies

Anti-GFP   Monoclonal 0,4 mg/ml; mixture of clones 7.1 and 13.1 (Roche)

27E8   Monoclonal anti His-tag antibody (Cell signalling)

Conjugate antibodies

Anti-Mouse IgG   Horseradish peroxidase-linked , detects mouse immunoglobulins

Anti-rabbit IgG   Horseradish peroxidase-linked, detects rabbit immunoglobulins

6.11   Antibiotics

Antibiotics were supplied by Applichem

Stock solution concentration	End concentration
50 mg/ml Ampicillin in H_2O	100 μg/ml
25 mg/ml Chloramphenicol in Ethanol	34 μg/ml
50 mg/ml Kanamycin in H_2O	50 μg/ml

6.12   Cells

XL1-Blue subcloning grade competent cells (Stratagene) were used for amplificationof plasmids.
BL21 competent cells (Novagen) were used for protein expression.

7 <u>Methods</u>

7.1 Recombinant DNA Technolgies

7.1.1 Polymerase Chain Reaction (PCR)

During a PCR a thermostable DNA polymerase, directed by a pair of specific primers and in presence of sufficient nucleotides, amplifies a desired fragment of DNA *in vitro*. After the initial round of amplification from the original template, both the starting DNA as well as the amplified fragment are used as templates in the next cycles. This sets in motion a chain reaction in which the template DNA is exponentially amplified where the amount of DNA depends on the number of cycles.

PCR is initiated by denaturing template DNA that enters then a reaction cycle repeated as often as 15-40 times. In each cycle the primers anneal to the specific recognition sequence, then, in the extension stage, the polymerase synthesizes the new strand of DNA utilizing the available nucleotides and guided by the template.

The specificity of the PCR is largely controlled by annealing temperature but also by buffer conditions. The annealing temperature should never be greater but can be 3-5 °C lower than the calculated melting temperature (Tm) of the oligonucleotides. Tm can be calculated from the empirical equation:

Tm (in °C) = 2 × count (A, T) + 4 × count (G, C)

The general PCR reaction for the Phusion polymerase was as follows:

1µl	Template DNA (30-50 ng/µl)
2.5 µl	Oligonucleotide 1 (10 pmol/ µl)
2.5 µl	Oligonucleotide 2 (10 pmol/ µl)
10 µl	5× High Fidelity Buffer
1µl	dNTPs (10mM of dATP, dCTP, dGTP, dTTP)
0.5µl	Phusion DNA polymerase
32.5 µl	H_2O

The standard program of an amplification PCR was as follows:

95°C	30 sec	1 cycle
95 °C	10 sec	
Tm (56-58°C)	30 sec	20-40 cycles
72°C	20 sec/Kb	
72°C	10 min	1 cycle
4°C	∞	

Primers can be designed to add a restriction endonuclease recognition site to the amplified DNA fragment facilitating cloning into the desired vector. In this case the specificity of the PCR can be

improved by using the two-step PCR benefiting from the increased annealing temperature due to the added bases.

The two-step PCR program was usually as follows:

95°C	30 sec	1 cycle
95 °C	10 sec	
T_m1 (56-58°C)	30 sec	6 cycles
72°C	20 sec/Kb	
95 °C	10 sec	
T_m1 + 6-8°C	30 sec	22-24 cycles
72°C	20 sec/Kb	
72°C	10 min	
4°C	∞	

7.1.2   Site directed mutagenesis

Introduction of point mutations, exchange or deletion of amino acids was done according to the Quick change Site-Directed Mutagenesis Kit (Stratagene). The method in principle utilizes a double-stranded DNA circular plasmid vector containing the insert of interest and two complementary synthetic oligonucleotide primers designed to contain the desired mutation flanked between ~15 bases of complementary sequence. The oligonucleotide primers were extended during temperature cycling by Turbo or alternatively Phusion DNA polymerase. The final PCR product contained the mutated insert within the vector plasmid and also contained staggered nicks within the DNA backbone. Following temperature cycling, the product was treated with DpnI. The DpnI endonuclease recognizes methylated and hemimethylated DNA and is used to digest the parental DNA template and to select for mutation-containing amplified DNA. The DNA isolated from bacteria is dam-methylated and therefore susceptible to DpnI digestion. After DpnI digestion, the nicked vector DNA containing the desired mutations was transformed into XL1-Blue competent cells which contain DNA repair mechanisms and will ligate the nicks in the backbone. DNA isolated from clones grown on selection media were sequenced.

The standard site directed mutagenesis PCR was as follows:

1 µl	Template DNA (30-50 ng/µl)
1.1 µl	Oligonucleotide 1 (10 pmol/ µl)
1.1 µl	Oligonucleotide 2 (10 pmol/ µl)
10 µl	5× High Fidelity Buffer
1µl	dNTPs (10mM of dATP, dCTP, dGTP, dTTP)
0.5µl	Phusion DNA polymerase
35.3 µl	H_2O

The general site directed mutagenesis cycle parameters were:

95°C	30 sec	1 cycle
95°C	10 sec	
55°C	30 sec	×12-18 cycles
68°C	20 sec /Kb	
4°C	∞	

7.1.3 Colony PCR

To check that an insert of interest is ligated into a cut vector in the correct orientation, screening of a large number of colonies can be done in a time saving method namely the colony PCR. In colony PCR, a forward oligonucleotide primer recognizing 5′ insert sequence and a reverse oligonucleotide primer recognizing an antisense vector sequence 3′, or vice versa, are selected so that a PCR product can only be detected if the insert is correctly ligated. Using a yellow pipette tip, tiny swabs of prenumbered colonies growing on the selective plate were placed directly into numbered tubes containing the PCR reaction mixture. After the PCR reaction, the product was separated with agarose-gel-electrophoresis and, if DNA of the correct size was amplified, the remainder of this colony were grown in 5 ml LB medium overnight at 37°C.

The general colony PCR reaction was as follows:

1.5 µl	Oligonucleotide 1 (10 pmol/ µl)
1.5 µl	Oligonucleotide 2 (10 pmol/ µl)
3 µl	10× PCR buffer
0.6µl	dNTPs (10mM of dATP, dCTP, dGTP, dTTP)
0.6µl	Taq polymerase
22.8 µl	H$_2$O
	+ Half of a colony picked from the agarose plate

The general site directed mutagenesis cycle parameters were:

98°C	5 min	1 cycle
98°C	30 sec	
58°C	30 sec	×24-27 cycles
72°C	1 min/Kb	
72°C	10 min	1 cycle
4°C	∞	

7.1.4 Alcohol precipitation of DNA

DNA is precipitated out of aqueous solution either for concentrating or purifying it. This was done by addition of 0.2 volume of 5M NaCl, mixing and then addition of 2.5 volumes absolute ethanol, followed by a 30 min centrifugation at high speed (14000 rpm). The DNA pellet was washed with 70% ethanol to remove excess salt, centrifuged for 10 min, air dried. DNA and finally resuspended in water or suitable DNA elution buffer.

7.1.5   DNA cleavage by restriction endonucleases

Most type II restriction endonucleases are able to recognize a 4, 6 or 8 nucleotide palindromic sequences where they cut double stranded DNA to create either overhanging or blunt ends. Restriction endonucleases are found in bacteria and are believed to play defensive role against invading DNA. Restriction enzymes are used as a tool to insert desired fragments into particular vectors that are cut and prepared so that ends match for ligation. They are also utilized to monitor the cloning process.

In general, a solution containing 0.5-4 µg of DNA was prepared in a total volume of 30 µl with 1 µl of the enzyme in an appropriate buffer (according to the recommendations of the manufacturer). Time and temperature of incubation also depend on the enzyme used.

7.1.6   Alkaline phosphatase dephosphorylation:

To reduce the possibility that a blunt-end cut vector religates into circular DNA resulting in colonies lacking the desired insert, the vector ends should be dephosphorylated to prevent religation. This was done by the enzyme alkaline dephosphatase directly after cutting the vector fragment.

The dephosphorylation reaction mixture contained:

30 µl	Vector cut fragment
4 µl	10×Antarctic phosphatase buffer
2 µl	Antarctic phosphatase
4 µl	H_2O

Reaction mixture was incubated at 37°C for 1 h then the enzyme was inactivated at 65°C for 5 min followed by vector fragment purification either by GTG-gel electrophoresis or by alcohol precipitation.

7.1.7   DNA phosphorylation (Kinase reaction)

The presence of a phosphate at the 5`-end of a DNA fragment is a prerequisite for a ligase reaction. PCR products that are used for ligation directly without being cleaved at their end with a restriction endonuclease, should therefore either be amplified with a phosphorylated pair of primers or phosphorylated after amplification. To phosphorylate DNA at its 5`-ends, DNA was incubated with T_4 Polynucleotide kinase in presence of a buffer containing ATP.

The kinase reaction mixture contained:

26 µl	PCR product precipitated then resuspended in bidistilled H_2O
3 µl	10×Ligase buffer
1 µl	T_4 Polynucleotide kinase

Reaction mixture is incubated at 37°C for 1 hour then the enzyme is inactivated at 75°C for 10 min followed by DNA purification either by GTG-gel electrophoresis or by alcohol precipitation.

7.1.8   Fill-in Reaction

To ligate DNA fragments with incompatible ends, a mixture of DNA polymerase with 3′to 5′or 5′to 3′ proofreading ability and a kinase was used to create blunt ends and simultaneously phosphorylate the ends

The fill-in reaction mixture contained:

22.75 µl	DNA fragment precipitated then resuspended in bidistilled H_2O
3 µl	10×Ligase buffer
2 µl	T_4 Polynucleotide kinase
1 µl	T_4 DNA polymerase
1.25 µl	1.25mM dNTPs mix

Reaction mixture was incubated at 37°C for 1 h followed by enzyme inactivation at 65°C for 10 min and DNA purification either by GTG-gel electrophoresis or by alcohol precipitation.

7.1.9   DNA analysis and purification by gel electrophoresis.

Agarose or PAGE gels provide the matrix for identification, separation or purification of DNA fragments based on charge migration. DNA molecules, being negatively charged, move through an applied electric field from the negative to the positive pole with a speed inversely proportional to their size (non linear). Ethidium bromide (EtBr) was used to visualize the DNA fragments. EtBr intercalated into DNA molecules becomes fluorescent when excited with 254 nm UV light. Gels were prepared with TBE buffer. Before loading into the gel pockets, DNA probes were mixed with loading buffer containing glycerol to make DNA sink into gel pockets and a dye to visualize the front. A standard DNA ladder was loaded for identification of fragment size.

The 10×TBE-buffer pH 8.0 is prepared as follows:

0.89 M	Tris-HCl
0.89 M	Boric acid
0.02 M	EDTA

The 10× Loading-buffer is prepared as follows:

40% (w/v)	Urea

40% (w/v)	Absolute glycerol
50 mM	EDTA, pH 8.0
10 mM	Tris-HCl pH 7.0
0.25%(w/v)	Bromophenolblue
0.25%(w/v)	Xylencyanol FF

7.1.10 Agarose gels:

The strength of agarose gel used depends on the size range of the fragments to be isolated. Regularly, 0.5 to 2% gels were used to resolve DNA fragments ranging in size from 0.05 to 10 Kb. Multipurpose agarose (Roth) was used for analytical gel electrophoresis while the low melting seakem GTG-agarose (Cambrex) was used for preparative purposes. To prepare the gel a slurry of the appropriate amount of agarose was mixed with 1× TBE, heated up in a microwave to dissolve the agarose and then stirred to cool down to a temperature of 55-60°C. Ethidium bromide solution was added to a final concentration of 0.001 mg/ml. The gel was poured into a chamber of a proper size with suitable combs and solidified at room temperature. Upon use, the gel was placed in the gel electrophoresis chamber and submerged in running buffer (1× TBE).

7.1.11 PAGE gels

Fragments of DNA smaller than 0.05 Kb were optimally isolated using 5-7% polyacrylamide gels. To prepare this gel, a (1:29) mixture of acrylamide and bisacrylamide was diluted with water to 40% (w/v) then used to prepare the gel with the desired concentration using 1× TBE buffer and adding 0.08% APS (w/v) and 0.12% (v/v) TEMED to initiate polymerization of the acrylamide solution. The mixture was poured between two glass plates and a comb was inserted. After running the DNA probes through the gel with 1× TBE in a vertical chamber, the fragments were visualized by staining the gel with ethidium bromide solution (0.5 µg/ml) for 10 min

7% PAGE gel

5 ml	40% Acrylamide:bisacrylamide (1:29)
3 ml	10 x TBE
35 µl	TEMED
80 µl	APS (30%)
Ad 30 ml	H_2O

7.1.12 Isolation of DNA by electroelution:

Small DNA fragments that were isolated by PAGE gel were thereafter purified by electroelution. The gel fragment was placed in an autoclaved semipermeable flexible tube (Dialysis Tubing MWCO 12000, Sigma) together with 300µl 1× TBE buffer and ends were tightly closed with clamps. The flexible tube was placed in 1× TBE buffer in an electrophoresis chamber and a 135 mA current was

applied for about 45 min at 4°C until the DNA was eluted into the buffer enclosed in the flexible tube. DNA solution was then carefully collected, and remains of DNA washed out of the flexible tube with 100 µl 1× TBE. DNA was precipitated with alcohol and salt as above.

7.1.13 Ligating DNA fragments:

The ligation reaction aims at joining together the compatible ends of a DNA fragment and a linearized vector. In presence of ATP and Mg^{2+} T_4-DNA ligase catalyzes, the formation of a phosphodiester bond between juxtaposed 5′ phosphate and 3′ hydroxyl termini of both fragments.

A standard ligation reaction consists of the following:

x µl   Insert fragment
y µl   Vector fragment
1.5 µl   10 x T_4 DNA ligase buffer
1 µl T_4 DNA ligase
Ad. 15 µl H_2O

The reaction mixture was incubated at 16°C over night or alternatively at room temperature for 4 h. The total amount of DNA used (x + y) was about 200 ng and the ratio was set to be 1:1 in case of ligating DNA fragments with cohesive (sticky) ends and to 6:1 in case of blunt ends

7.1.14 Preparation of chemically competent *E. coli* cells

Bacteria can be made competent for uptake of foreign DNA when treated with calcium or magnesium chloride in the mid-log phase of growth. From a stock solution of XL-1 Blue subcloning grade competent bacterial cells (Stratagene), single colonies were obtained by fractionation on an antibiotic-free agar plate. A single colony was used to inoculate 5 ml LB media over night from which one ml was diluted into 100 ml LB medium the next day. This culture was grown at 37°C to an OD_{600} of ~0.5. Cell pellets were obtained by centrifugation at 4°C, 6000×g for 10 min. The pellet was resuspended in 5-10 ml cold TSS buffer (calcium-rich buffer that facilitates plasmid uptake by cells) and aliquots of 100, 200 or 300 µl were immediately shock-frozen in liquid nitrogen and stored at -80°C (Chung et al. 1989).

To estimate transformation efficiencies (competency), defined as the number of colonies per µg transformed DNA, a test transformation was done with a test plasmid of known concentration.

From three different dilutions (1:10, 1:100, 1:1000) of cells in LB-medium, 100 µl was plated on agar plate containing the selection antibiotic corresponding to the test plasmid. After 24 h incubation at 37°C the competency of the cells was calculated from the following formula:

$$Competency = Number\ of\ colonies \times Dilution\ factor \times \frac{Total\ volume}{Plated\ volume} \times \frac{1}{Plasmid\ in\ \mu g}$$

Cells were considered competent for cloning if their transformation efficiency was in the range $10^6:10^7$ cfu/µg of DNA.

The composition of TSS buffer was as follows:

10%	PEG 3350
50 mM	MgCl$_2$
5%	DMSO
Ad. 50 ml	LB-medium

7.1.15 Transformation of plasmids into bacterial cells

An aliquot of competent cells was slowly thawed on ice. The DNA (ligation mixture) was gently mixed with the cells incubated on ice for 20-30 min. To induce DNA uptake by the cells, cells were heat shocked at 42°C for 90 seconds then placed on ice for 2 min. To recover, 1 ml of LB medium was added and cells were incubated at 37°C with 200 rpm shaking for 1 h. On an agar plate containing the corresponding selection antibiotic, 100 µl of the recovered bacterial suspension was plated with a Drigalsky spatula while the rest was concentrated by centrifugation at 5000 rpm for 5 min. The pellet was resuspended in about 100 µl LB medium and plated on the selective agar plate. Plates were incubated at 37°C overnight.

7.1.16 Small scale plasmid preparation (Miniprep)

For preparation of recombinant DNA plasmid DNA was amplified in bacteria. DNA was prepared on a small scale using the commercial kit (Qiaprep Spin Mini Kit, Qiagen). According to the provided "alkaline lysis" protocol, the desired number of colonies were picked with a sterile toothpick and grown overnight in 5 ml LB medium containing the corresponding selective antibiotic. A cell pellet was obtained by centrifuging a 1.5 ml of the preculture at 5000 rpm for 5 min. This step was repeated for low copy plasmids. Cells were resuspended in 250 µl resuspension buffer containing RNAse and mixed with 250 µl detergent-rich lysis buffer. To precipitate RNA, proteins and low-molecular weight impurities 350 µl neutralizing buffer was added. Contents were mixed immediately by inverting the tube. The mixture was spun at full speed for 10 min. The resulting clear lysate was added to an anion-exchange resin packed in a spin column, spun for 1 min at 13000 rpm to bind DNA under low salt conditions. The bound DNA was washed with 750 µl buffer with medium salt content, dried by further spinning after removal of the flow-through and finally eluted with 50 µl elution buffer. Using a spectrophotometer absorbance of UV light at 260 nm and the ratio of absorbance at 260/280 nm were measured to check the quantity and purity of DNA, respectively. The prepared DNA was used for further restriction mapping or sequence analyses.

7.1.17 Large scale plasmid preparation (Maxiprep)

When a recombinant DNA was proven to be of the correct sequence, DNA plasmid was amplified to a larger scale to yield enough DNA for further applications. Overnight cultures (200-400 µl) were diluted into 400 ml LB medium and grown at 37°C for 12-15 hours with the corresponding selective antibiotic. Plasmid purification follows the modified alkaline lysis protocol as above using buffer

volumes and column sizes suitable for the larger scale preparation and according to instructions of the manufacturer. DNA was eluted with high-salt containing buffer. Salts were removed by isopropanol-precipitation followed by a 70% ethanol washing step.

7.1.18 Sequencing DNA

Sequence of prepared recombinant DNA was analyzed using the "Cycle Sequencing Method" (Sanger et al., 1977). In this method, a polymerase synthesizes a complementary DNA strand, using a mixture of dNTPs and dideoxyribonucleotides tagged with fluorophors (ddNTPs). The latter nucleotides are reaction terminators because they lack the terminal hydroxyl group essential for extension. This way a number of DNA strands of different lengths are synthesized which contain one terminator ddNTP that can be recognized by detectors as they emit light of definite wave length when excited by a laser beam. Strands are sorted according to their size and aligned by the accompanying software "Sequence Analysis" that creates the full sequence of aligned bases. Sequencing was either done in Prof. Flockerzi's laboratory using the sequencer "Genetic Analyzer 310" (Applied Biosystems) controlled by "Data Collection" software and using "Big Dye TM FS Terminator Cycle Sequencing Ready Reaction Kit V 1.1" (Applied Biosystems) to prepare the DNA copies in a modified PCR reaction or sent for sequencing to the commercially available sequencing services of MWG/Operon or SeqLab.

The modified PCR reaction for sequencing:

1 µl	Primer
1.5 µl	BigDye® Terminator Ready Reaction Mix
x µl	Template DNA = 500 ng
Ad.12 µl	HPLC water to 12 µl

The cycle parameters were:

95°C	1 min	
95°C	30 sec	
58°C	2 min 30 sec	× 35 cycles
4°C	∞	

A 96-well plate was used for purification of the modified PCR products. In each well a filtration entity (Whatman Microplate Devices Unifilter) covered with sepharose (Sephadex^{TM} G-50, Amersham Pharmacia) was swelled with 300 µl HPLC-grade water for 3 h. The plate was centrifuged at $2930 \times g$ and sepharose was washed with 150 µ HPLC-grade water. Finally probes are loaded in individual wells and the plate was centrifuged so that the purified probe was collected into PCR tubes containing 8 µl HiDi-Formamide (Highly deionized Formamide). The probes were stored at 4°C until they were assembled into the sequencer.

7.2   Biochemical Technologies

7.2.1   Cell culture

Cells were cultivated in humified incubators kept at 37°C and supplied with 5% CO_2. Handling the cells for passage, transfection or splitting was done aseptically in a laminar flow hood (Biological safety cabinet, HERAsafe) using sterile equipment and containers sprayed with 70% ethanol before placing into the cabinet. Cell passage was done with trypsin (0.5 mg/ml trypsin + 0.2 mg/ml EDTA). Harvested cells were collected by centrifugation at room temperature, 1000 rpm for 5 min.

7.2.1.1 HEK293 cells

HEK293-cells (CRL-1573, ATCC, Manassas, VA USA) were cultured in Minimal Essential Medium (MEM, Invitrogen), supplemented with 200 unit/ml penicillin-G-sodium, 100 µg/ml streptomycin, 4 mM L-glutamine and 10 % fetal calf serum (FCS, Invitrogen).

7.2.1.2 Stable transfected cell lines

Stable cell lines were created (Dr. Ulrich Wissenbach) from TRPV6a or b expressing vector (hTRPV6a/b_pcDNA5-Plasmid) transfected into Flp-In™-293 cells (In-vitrogen) using Superfect Transfection-Reagent (Qiagen). Cells were cultivated in HEK293 medium with 500µg/ml Geneticin (G-418, Invitrogen) for selection. For I_{CRAC} measurements, a cell line stably expressing STIM1 was kindly provided by Dr. Soboloff. This cell line was cultured in the same medium as HEK293 cells.

7.2.2   Transient transfection

For transiently expressed TRPV6 wild-type or mutants, constructs were cloned into the bicistronic pCAGGS_IRES_EGFP vector. Two µg of the DNA to be transfected was mixed with 100 µl of Optimem-I Medium/Glutamax-I (Glibco) and 5 µl of the transfection reagent Fugene 6 (Roche). After 15-45 min incubation at room temperature, the transfection mixture was directly added to 60-70% confluent HEK293 cells in penicillin/streptomycin-free medium. After 24h cells were trypsinated and seeded at low density for electrophysiological recordings or at higher density for Ca^{2+} imaging. Experiments were performed 48h after transfection.

For ORAI expression, constructs were cloned into pCAGGS_IRES_EGFP (unless otherwise indicated) and 1 µg of the DNA was transfected into HEK-STIM1 cells using Nucleofector™II electroporator (Amaxa Biosystems) and Cell Line V Nucleofector kit (Lonza). Cells were transfected according to instructions of the manufacturer and seeded at suitable density in 50µM ß-mercaptoethanol-containing medium. Experiments were done 24h after transfection

7.2.3   Co-Immunoprecipitation (Co-IP)

Co-immunoprecipitation is a widely applied method for investigating protein-protein interaction. In this method, an antibody is used to precipitate a target protein out of solution (mostly cell lysate) in which it is believed to exist in complex with other interacting partners that will be precipitated along. Therefore, it is a prerequisite that the epitope of the target protein remains accessible to the antibody.

The protein complexes are analyzed by SDS-PAGE and presence of a candidate interaction partner is tested for by probing with a specific antibody against the potential interacting protein.

Cells were grown in 75 cm^2 cell culture flasks to 70% confluence and transfected with the plasmid encoding the target protein cDNA. Forty eight hours later cells were checked for transfection efficiency (GFP fluorescence) and harvested with trypsin with intermittent shaking for 1 min. Reaction was stopped by adding 7 ml of culture medium. Cells were resuspended and transferred to 15 ml falcon tube, centrifuged at 1000 rpm for 5 min at 4°C. Steps following cell harvest were done at 4°C (on ice). Cell pellets were washed with 10 ml PBS and resuspended in RIPA buffer containing a mixture of proteinase inhibitors and shaken vigorously, 700 rpm, at 4°C for 15 min. To solubilise cellular proteins, cell lysates were sheared through 0.7, 0.55 and 0.4 mm cannulae, shaken again vigorously at 4°C for 15 min. Clear lysate was obtained by centrifugation at 13000 rpm for 15 min at 4°C.

To complex the protein of interest together with its potential interacting partners, if associated, 2-6 µg of the polyclonal antibody was added to the cell lysate. Interaction was allowed overnight at 4°C with overhead rotation. To purify the protein complex, 90 µl of RIPA buffer-prewashed protein A beads were added to the Co-IP mixture then rotated again for 3 hours at 4°C.

To exclude non-specific binding to the beads, an equal fraction of the cell lysate is incubated with the same amount of beads for 3 hours without the antibody. To purify the protein complexes the beads were centrifuged at 500×g for 2 min, a control probe was taken from the supernatant and mixed with equal volume of 2× Laemmli, beads were washed with 4×1 ml RIPA buffer and finally resuspended in 45 µl of 2× Laemmli. All controls, prebeads and test probes were denatured (5 min at 95°C or 30 min at 37°C). Proteins were separated by SDS-PAGE analysis followed by blotting to nitrocellulose membranes that is subsequently probed with an antibody against the investigated interacting partner.

RIPA buffer

150 mM	NaCl
5 mM	Tris.HCL, pH 8
0.5 %	Sodium deoxycholate
1 %	Nonident P40
0.1 %	SDS
5 mM	EDTA, pH 8

2 × Laemmli (Protein loading buffer, pH 6.8)

8 %	SDS
120 mMM	Tris-HCl
20 % (v/v)	Glycerol
10 % (v/v)	ß-Mercaptoethanol
0.01 % (w/v)	Bromophenol blue

Proteinase inhibitors mix

1 µg/ml	Leupeptin
0.1 mM	PMSF
1 mM	Pepstatin A
0.3 µM	Aprotinin
1 mM	Benzamidin

7.2.4   SDS-PAGE

When a mixture of proteins was analyzed by SDS-PAGE, proteins were separated according to their size prior to visualization and analysis. Secondary structures of proteins were denatured and molecules became negatively charged by hydrophobic interactions with the anionic detergent SDS. A polyacrylamide matrix loaded with proteins to be separated was immersed in $1\times$ SDS running buffer in a vertical chamber within an electrical field. Proteins migrated to the positive pole with a speed relative to their charge-to-mass ratio. The loaded protein samples were first run through a stacking gel, a large-pore polyacrylamide gel of about 2 pH units lower than the buffer of the separating gel. At the border between the gels, proteins were condensed. Protein molecules were resolved in the separating gel according to their molecular mass. The percentage of polyacrylamide can be modified to the size range of proteins to be separated. Lower percentage gels were used for large proteins and higher percentage gels were used to separate small proteins. The stacking gel should be at least 3% less than the separating gel.

Stacking gel buffer, pH 6.8

0.5 M	Tris-HCl
0.4 %	SDS

Separating gel buffer, pH 8.8

1.5 M	Tris-HCl
0.4 %	SDS

$10\times$ SDS-electrophoresis buffer, pH 8.8

1 % (w/v)	SDS
250 mM	Tris-HCl
1,92 % M	Glycin

7.2.5   Coomassie staining of protein gels

As little as 200 ng protein can be visualized with the Coomassie protein-stain. To stain the gels they were placed in the Coomassie solution for 30-60 min. Excess staining solution was removed and destaining solution was added to remove unbound stain. Protein bands as well as marker bands were visualized in a clear back ground of the gel.

Coomassie stain solution

0.125 % (w/v)	Coomassie Brilliant Blue R-250
45 %	Ethanol
10%	Acetic acid

Destain solution

6 % (w/v)	Ethanol
9 %	Acetic acid

7.2.6   Western blot analysis

This method aims at transferring the SDS-PAGE separated proteins onto a membrane where they can be detected using the proper mono- or polyclonal antibody. In electroblotting, a PAGE gel was brought in contact with the nitrocellulose membrane (8 Hybond-C extra, Amersham Pharmacia) or PVDF membrane (for smaller proteins) and together they were placed between 2 pairs of filter paper and a pair of pads to assemble the so called "blotting sandwich". In the blotting apparatus (Mini Trans-Blot, Bio-Rad), the blotting sandwich was immersed in a blotting chamber filled with blotting buffer. A 350 mA current was applied and the negatively charged proteins migrated out of the gel onto the positively charged membrane. Blotting time depends on protein size and type of membrane. Transfer efficiency can be checked either by staining the remaining gel with Coomassie or by transiently staining the nitrocellulose/PVDF membrane with Ponaceau-S stain. Nitrocellulose membranes have high affinity to proteins and bind them by hydrophobic as well as charge interaction. PVDF membranes offer better protein retention, physical strength and broad chemical compatibility (Lauritzen and Pluskal, 1988). Areas on the membrane unoccupied by target protein were blocked by a 5% solution of non-fat dry milk in TBST for one hour to prevent unspecific antibody effects. The membrane was usually incubated over night with the primary antibody at 4°C with gentle rocking.

Blotting buffer, pH 8.3

1 %	SDS
250 mM	Tris-HCl
1.92 M	Glycin
20 %	Methanol

7.2.6   Enhanced chemiluminescence development (ECL-Reaction):

Commonly, a horseradish peroxidase-linked secondary antibody is used to bind the immune complex "protein-primary antibody". Adding the substrate of the antibody-bound enzyme results in a chemiluminescent product that can be visualized and the signal can be quantified. The nitrocellulose membrane containing the immune complex was washed 3×10 min with TBST (TBS buffer + 0.1 % Tween 20), incubated for 1h at room temperature with secondary antibody in 5% solution of non-fat dry milk in TBST buffer. Excess antibody was washed 2×10 min with TBST and finally 1×10 min with TBS. The ECL reagents were mixed in 1:1 ratio and added to the blot for 1 min. Luminescence was captured by a charge-coupled device (CCD) camera. The intensity of the digitized luminescence signal was analyzed in relation to an input control signal from known amounts of loaded protein.

10 × TBS-Buffer pH 7.5

5 mM	Tris-HCl
9 %1.5 mM	NaCl

7.2.7   Redetection (Stripping)

Using ß-mercaptoethanol and a detergent, the primary antibody bound to target protein can be cleaved allowing the usage of a different antibody for redetection of the same protein or another protein on the same blot. This was usually done to confirm the identity of test protein with a different antibody or to control for the expression of a house keeping gene. To strip a blot it was washed 4× 5 min with TBST incubated at 55°C with the stripping buffer and washed 6 × 5 min with TBST before blocking and incubating with the new primary antibody.

Stripping Buffer

62.5 mM	Tris-HCl pH 6.8
2 %	SDS

7.2.8   Protein determination (Bicinchoninic acid reaction)

A common method for quantification of protein content is based on the Biuret reaction. In an alkaline medium containing sodium potassium tartrate, proteins reduce cupric (Cu^{2+}) to cuprous (Cu^{1+}) and the latter chelates bicinchoninic acid forming a light blue complex which can be detected with a spectrophotometer. From a test protein solution, 1:100, 1:200 and 1:300 dilutions were made and in parallel, a standard BSA stock solution was diluted to yield 0.01, 0.02, 0.04, 0.06, 0.08, 0.1 mg/ml probes to establish a standard calibration curve. In a 96-well plate, 200 µl of the reagent mix (Pierce ECL Western Blotting Substrate, Thermo Scientific) were mixed with 25 µl of either the test or standard protein probes to obtain triplicates for each concentration. The plate was incubated at 65°C for 30 min with shaking, absorbance was measured at λ=540 nm in a plate spectrophotometer. The concentration of test protein was calculated using the standard calibration curve.
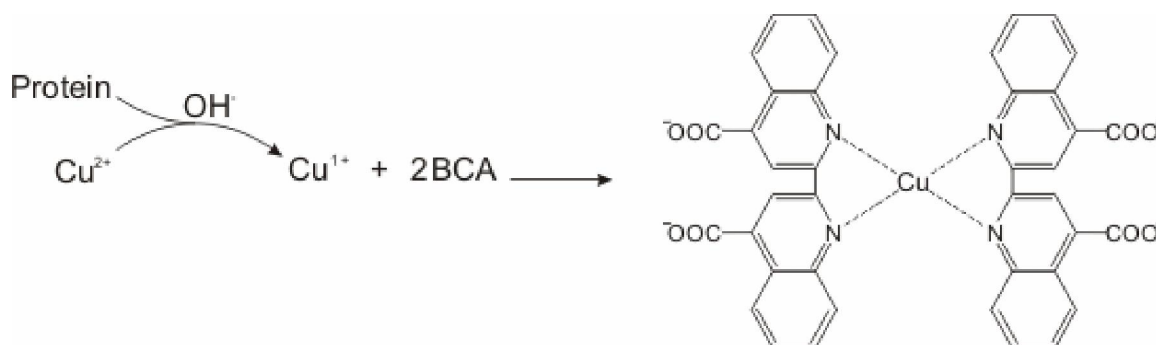
Figure 7: Bicinchoninic acid method for determination of protein concentration. In an alkaline medium proteins reduce cupric (Cu^{2+}) to cuprous (Cu^{1+}) which chelates bicinchoninic acid forming a light blue complex detected with a spectrophotometer.

7.2.9   Detection of surface proteins by biotinylation

Biotin (Vitamin H) is a small molecule with a versatile valeric acid side chain that can bind proteins. Polar derivatives of biotin made with sulfonated linkers e.g N-Hydroxysulfosuccinimide (Sulfo-NHS) esters are charged and readily water soluble and thus are cell membrane impermeable. As long as the cell remains intact, only primary amines exposed on the surface can be biotinylated. Biotinylated proteins bind avidin (a glycoprotein of four subunits each binds one molecule of protein) with extraordinary affinity via noncovalent interaction with $K_a=10^{15}M^{-1}$. The protein-biotin complex can therefore be isolated using avidin cross-linked to agarose beads. This way Sulfo-NHS-Biotin/Avidin reagents facilitate differential detection of plasma membrane proteins and give an estimate of the fraction of protein inserted at the plasma membrane relative to the total protein synthesized.

Cells expressing the protein of interest were cultured in 75 cm^2 culture flasks (BD), culture medium was removed and cells were washed 2× 10 ml PBSB (PBS containing 1 mM $MgCl_2$ and 0.5 mM $CaCl_2$, pH 8). To label membrane proteins cells were incubated with 9 ml NHS-Biotin; (0.5 mg/ml) for 30 min at 4°C. Unbound biotin was removed and cells were washed 2× 10 ml PBSB pH 8 containing 0.1% BSA. 10 ml of 2 mM EDTA in PBS pH 7.4 were added to cells for ~1 min with intermittent shaking to detach the cells. Cells were harvested by resuspension and transferred to a 15 ml Falcon, centrifuged for 5 min at 1000 rpm at 4°C, washed with 10 ml PBS. Pellets were resuspended in lysis buffer (PBS containing 1% Triton and 1 mM EDTA, pH 7.4) containing freshly added protease inhibitors and shaken for 15 min at 4°C then sheared through cannulae of decreasing sizes (0.7, 0.55 and 0.4 mm). Finally, lysates were incubated for 15 min at 4°C with agitation. Cleared cell lysates were obtained by centrifugation at 13000 rpm for 15 min at 4°C. Protein content of cell lysate was determined by BCA method. An aliquot equivalent to 50 µg was kept as an input control. A volume of the cell lysate equivalent to 1 mg was incubated with 90 µl slurry of avidin beads (Pierce) on a rotating wheel at 4°C for 3 hours. Beads with bound complexes were collected by centrifugation at 5000g for 2 min, washed with lysis buffer containing 0.25M NaCl to remove any unbound protein, resuspended in 2× Laemmli, denatured at 95°C for 5 min and analyzed with SDS-PAGE.

7.2.10 Detection of reactive thiol groups

A chemically modified form of biotin (MTSEA biotin-XX, Biotrend) selectively labels thiol (-SH) groups under mild condition with XX-linker optimizing biotin-avidin interaction. MTSEA-biotin can, therefore, be used to detect reactive cysteine residues either at the cell surface when applied to intact cells or within the cytosol when applied to permeabilized cells. Cells were permeabilized by 5 min incubation in PBSB containing 0.001% digitonin. Cells were washed afterwards 2× 10 ml PBSB and incubated for 40 min at room temperature with 0.5 mg/ml MTSEA in PBSB (MTSEA-biotin was predissolved in the minimal possible volume of DMSO then diluted to the aforementioned final concentration). The protocol proceeds as mentioned above for regular biotinylation.

7.2.11 In vitro phosphorylation

To test whether TRPV6 channel protein is directly phosphorylated, microsomal fractions prepared from TRPV6-expressing cells were incubated for 30 min at 30°C with recombinant $PKC_{\beta II}$ and ^{32}P labelled ATP together with either a $PKC_{\beta II}$ activator or inhibitor mix. Alternatively, lysates of TRPV6-expressing cells that were transfected with GFP-$PKC_{\beta II}$ or untransfected control cells were used for the phosphorylation reaction. In a total volume of 25 µl kinase assay buffer cell lysates were mixed with 2.5 µl of either activator or inhibitor mix and 5 µl of $[^{32}P]$-ATP Assay cocktail

Kinase assay buffer

2.5 mM	MOPS pH 7.2
0.5 mM	EGTA
0.2 mM	EDTA
2.5 mM	$MgCl_2$
0.25 mM	DTT freshly added

$[^{32}P]$-ATP Assay cocktail

15 µl	cold ATP (10 mM stock)
10 µl	hot ATP (1 mCi/100 µl → total 100 µCi)
575 µl	Kinase assay buffer

Activator mix

1 µl	PS (10 mg/ml)
2 µl	100 µM PMA (1:10 predilution of 1mM stock in MOPS $CaCl_2$ buffer)
17 µl	Buffer containing 20 mM MOPS, 1 mM $CaCl_2$

Inhibitor mix

1 µl	PS (10 mg/ml)
2 µl	100 µM Ro (1:50 predilution of 5mM stock in MOPS $CaCl_2$ buffer)

| 17 µl | Buffer containing 20 mM MOPS, 1 mM $CaCl_2$ |

Proteins were analyzed by SDS-PAGE, blotted to nitrocellulose membrane and phosphorylated proteins were detected by exposure to phosphoimager plates or x-ray film, scanned later using Fuji scanner. Identity of phosphorylated bands was confirmed by incubating the membrane with specific anti-TRPV6 antibody and subsequent detection with ECL reagent as above.

7.2.12 Cloning and Expression of His-tagged proteins

The cDNA coding for different fragments of the human TRPV6 N- and C-termini were amplified with PCR from hTRPV6b cDNA and subcloned into the BamHI or XhoI sites, respectively, of the pET19b vector. This vector contains a N-terminal located 10×HIS tag in frame with the cloned fragments. The fusion protein covering aa 1-117 was made from mouse TRPV6 (Marcel Meissner). Plasmids were expressed in *Escherichia coli* BL21 strains. Overnight cultures were diluted 1:20, grown to an OD_{600} of 0.5 and protein production was induced with 100 µM IPTG for 4 hours at 30°C. Cells were collected by centrifugation at 6000×g, 4°C for 15 min. Pellets are initially resuspended in 5 mM imidazole, 500 mM NaCl, 20 mM Tris pH 7.9 (BB). Lysates were sonicated 3×30 sec, centrifuged at 13.000 rpm for 20 min. Pellets were resuspended in BB with a repeat of sonication and centrifugation. The final resuspension buffer also contains 6M urea (BBU). Lysates were then shaken for an hour at 4°C for 1h and pottered with a Dounce homogenizer. Finally, lysates were ultracentrifuged at 24000×g for 25 min at 4°C and supernatants were incubated overnight with Ni-NTA beads (Qiagen). Columns were washed once with BBU then with BBU containing 15 mM imidazole. Proteins were eluted with BBU containing 1M imidazole. The integrity and size of the purified proteins were checked by Coomassie stained PAGE gels and protein concentration was determined by BCA (Pierce).

Alternatively, fusion proteins were purified under non-denaturing conditions. Fragments encoding for ARD (42-266) and CT (633-725) were cloned into a modified pET21b vector (Jin et al., 2006), bacteria were induced at an OD_{600} of 0.5 with 75µM IPTG for 16h at 25°C. Pellets were resuspended in 20 mM Tris-HCl (pH 8.0), 300 mM NaCl, 20 mM Imidazole, 1mM PMSF, 0.1% Triton-X-100, 0.2 mg/ml lysozyme, 50 µg/ml RNAse and 25 µg/ml DNAse and treated as above. The cleared lysates were incubated with Ni-NTA beads for 2h at 4°C, washed with 20 mM Tris-HCl (pH 8), 300 mM NaCl and 20 mM imidazole. For elution, imidazole was increased to 200 mM.

7.2.13 ATP-Agarose binding (Pulldown)

To test whether a His-tagged protein is retained by ATP-agarose, pull-down experiments were performed. The fusion protein (40 µg) is diluted in 900 µl binding buffer with or without 6 (15) mM ATP or adenosine and incubated at 4°C for 20 min. Seventy five µl prewashed ATP-agarose beads (bound by a C_6-spacer to C-8 of ATP, Sigma) were added for 2 hours with gentle rotation.

For native proteins, DTT was excluded from the binding buffer. After incubation, beads were centrifuged, washed 4× 1 ml binding buffer and resuspended in 2× Laemmli or Tricine loading buffer, depending on the type of gel used. Probes were denatured at 37°C for 30 min and separated by 15% SDS-PAGE or 10-20% TRIS/Tricine PAGE (Biorad). Probes can be split where 80% of bound fraction

is loaded on gels to be Coomassie-stained and 20% on gels to be blotted to nitrocellulose or PVDF membranes and probed with antibody against the His-tag. Binding experiments were repeated at least three times also with different batches of expressed protein.

ATP-agarose binding buffer contains:

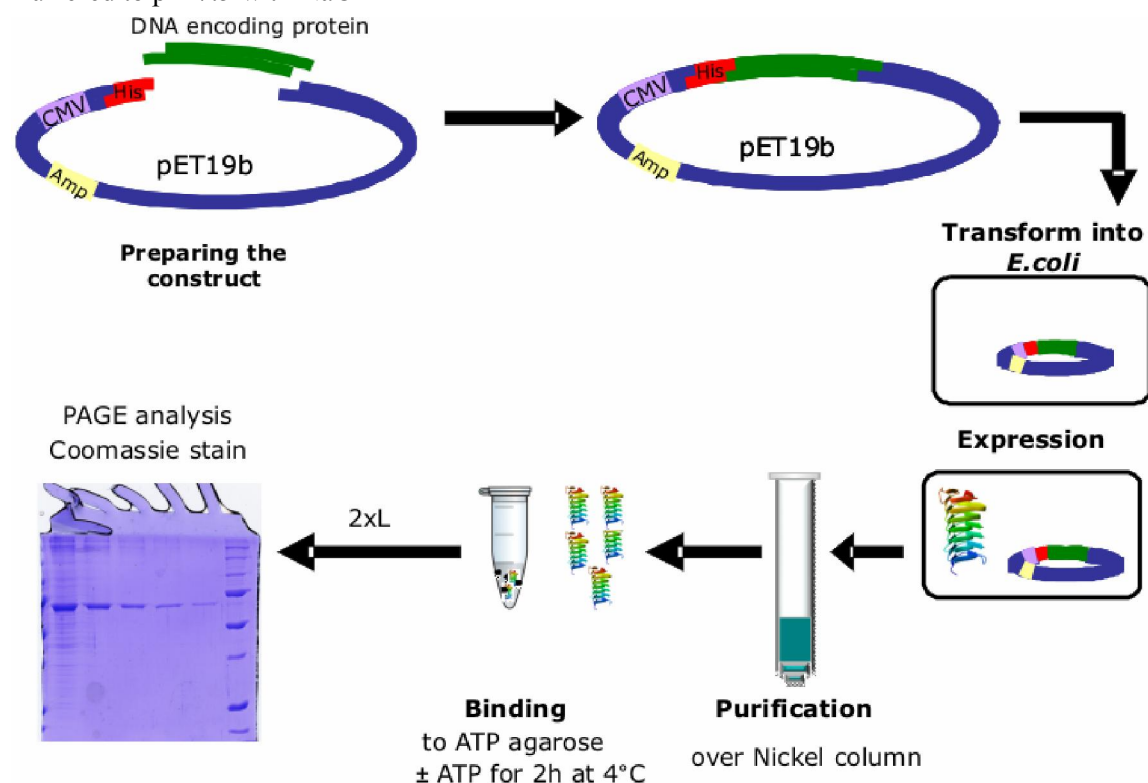|	
10 mM	Tris,
50 mM	NaCl
1 mM	DTT
0.15%	dodecyl-ß-D-maltopyranoside

Buffered to pH 7.5 with NaOH

Figure 8: Schematic representation of expression, purification and pull down of His-tagged fusion proteins. DNA encoding for desired fragment is cloned into pET vector expressed in *E.Coli* BL-21 and purified either under denaturing or native conditions. Fusion protein is bound to ATP-agarose and bound fraction is analyzed by SDS-PAGE

7.2.14 *In vitro* translation of TRPV6 and ATP-agarose pull down

The TNT-Quick Coupled Translation System (Promega) was used to translate full length TRPV6 protein *in vitro*. This system utilizes lysate of reticulocytes (rich in ER membranes) that are able to transcribe and then translate protein from circular plasmids, e.g. TRPV6 in pCDNA$_3$. The plasmid must contain a T7 RNA polymerase promoter, polymerase, nucleotides, salts and recombinant RNAsin

Ribonuclease Inhibitor were supplied as a reaction master mix. Radioactive methionine (^{35}S-Methionine) was added to be incorporated into the translated protein.

One *in vitro* translation reaction contains:

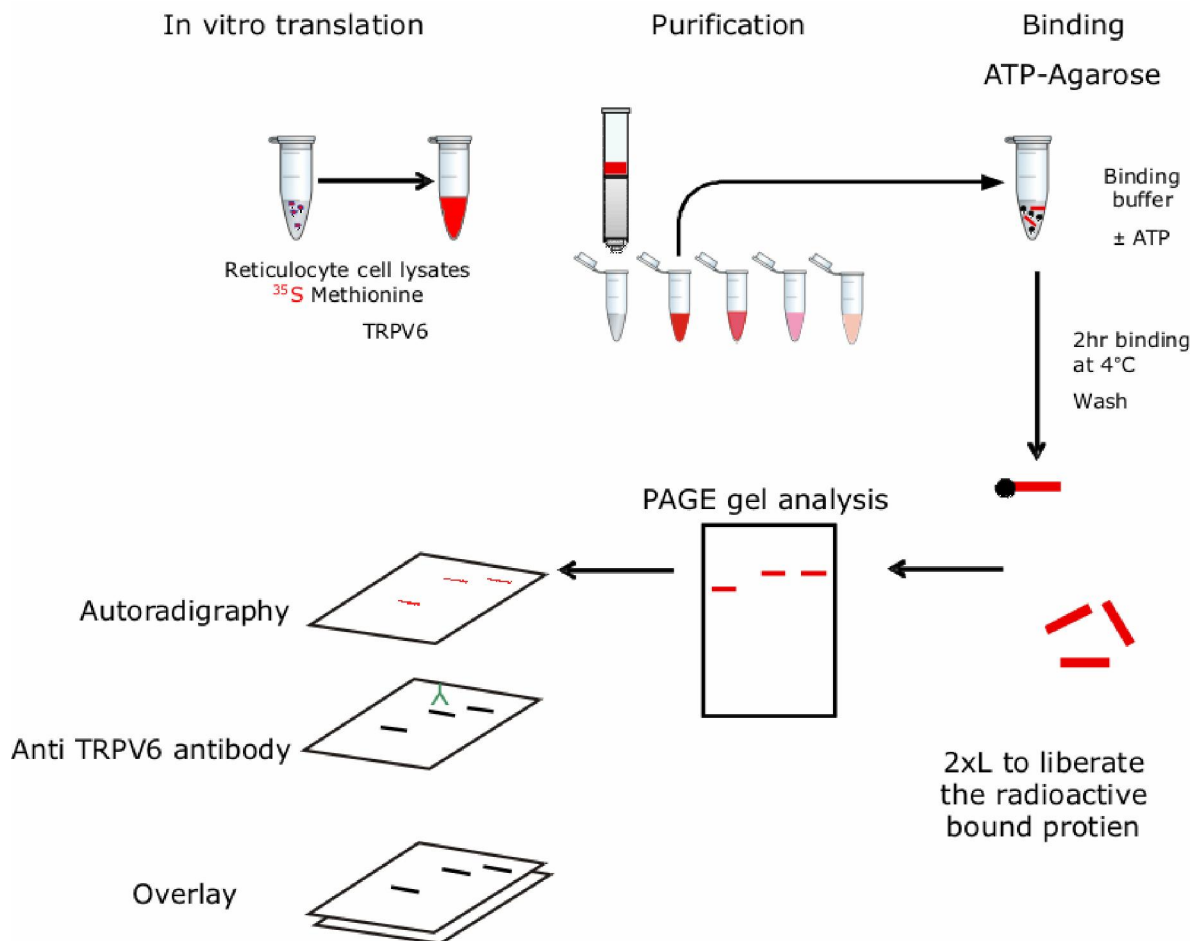| 25 µl	TNT-reaction master mix
1 µl	^{35}S-Methionine
2 µl	Plasmid (1 µg/µl)
2 µl	Nuclease free water

Figure 9: Schematic representation of invitro translation, purification and pull down of ^{35}S-Methionine-labelled TRPV6. Reticulocytes in vitro translate TRPV6-pCDNA3 in presence ^{35}S-Methionine. Labelled protein purified on G-50 columns and incubated with ATP-agarose for 2 hours at 4. Bound fractions analyzed by SDS-PAGE and detected with phosphoimager. Identity of detected bands was confirmed by incubating the membrane with anti-TRPV6 antibody.

The reaction components were mixed gently and incubated at 30°C for 90 min. The mixture was transferred to pre-equilibrated Probe Quant™ G-50 Micro Columns (GE-Healthcare) to purify labelled proteins, and fractions were eluted with 1 ml of the same buffer used afterwards for ATP-agarose binding (see below). The first fraction, containing the void volume was rejected, and the subsequent fractions containing the radioactive proteins were collected sequentially. Probes of the eluted fractions

54

(1 µl) were measured in a scintillation counter. A volume of the eluted protein corresponding to 710000 cpm was mixed with 30 µl pre-washed ATP-agarose beads and volume completed to 300 µl with binding buffer. Binding buffer contained (in mM): 140 caesium aspartate, 10 NaCl, 10 HEPES, 10 glucose, 10 EGTA and 0.016 $MgCl_2$ with or without 6 mM ATP containing 0.1% Triton. Binding was allowed for 2 hours then beads were washed 4×500 µl with the corresponding binding buffer, resuspended in 2 × Laemmli, probes denatured at 65°C for 15 min and bound fraction analyzed by SDS-PAGE blotted to nitrocellulose membrane. Phosphorylated proteins can be detected by exposure to phosphoimager plates or x-ray film. Identity of phosphorylated bands can be confirmed by incubation with anti-TRPV6 antibody and overlaying both images afterwards.

7.2.15 Fluorescence-based Ca^{2+} imaging (Ivan Bogeski)

Imaging of free intracellular Ca^{2+} concentration ($[Ca^{2+}]_i$) was performed using an Olympus IX 70 inverted microscope (Olympus Deutschland GmbH, Hamburg, Germany) equipped with a 20x (UApo/ 340, N.A. 0.75) objective, a Polychrome V Monochromator, and a CCD camera (T.I.L.L. Imago, T.I.L.L. Photonics GmbH, Germany). HEK cells were loaded with 1 µM Fura 2/AM in DMEM growth medium, at 37°C for 15 min in a dark chamber. Images were analyzed using TILL Vision software.

Bath solution contained the following (in mM):

150	NaCl
2.8	KCl
1	$MgCl_2$
1	$CaCl_2$
20	Glucose
10	HEPES

pH 7.4 with NaOH

Calcium signals were monitored over time with bath solution containing either 1mM or 10 mM $CaCl_2$ and 135 NaCl. The switch to the 10 mM $CaCl_2$ containing bath was repeated twice with an interval of ~ 50 min. For ATP-depletion, cells were incubated with deletion medium after the first switch.

ATP depletion medium contained the following (in mM):

140	NaCl
2.8	KCl
1	$MgCl_2$
1/10	$CaCl_2$
20	Deoxyglucose
10	HEPES
10	Na azide

pH 7.4 with NaOH

55

The absolute intracellular Ca^{2+}-concentration is calculated as previously described (Grynkiewicz et al., 1985).

7.2.16 DCF ROS measurements (Ivan Bogeski)

As an indicator of oxidative stress (redox status), H_2O_2 concentration was measured in stable as well as transiently TRPV6-expressing cells using the fluorescent dye CM-H_2DCFDA (5-(and-6)-chloromethyl-2',7'-dichloro-dihydrofluorescein diacetate, acetyl ester, DCF), (Invitrogen, Molecular Probes). A standard calibration curve was constructed that relates the fluorescence of the dye to different concentrations of H_2O_2. TRPV6 stable cells or HEK cells transiently transfected with TRPV6b are incubated for 30 min at room temperature with 1 µM CM-H_2DCFDA. Cells were washed twice with PBS and loaded into the wells (200 µl buffer A/well). The measurements were performed in 96-well plates (353948, black/transparent bottom, BD Biosciences) using a GeniosPro universal microplate reader (Tecan) at 485 nm excitation and 535 nm emission. Absorbance was measured from bottom with 30 s initial shaking, 30 s shake settle time, 10 flashes, 40 µs integration time and a gain of 60.

7.3   Electrophysiology

TRPV6a or TRPV6b stable HEK293 (D11, C3) cells or transiently transfected wildtype or mutant constructs in pCAGGS-IRES-GFP were used for patch-clamp recordings. Recordings were performed at room temperature in the tight-seal whole-cell configuration using electrodes of 2-4 MΩ resistance. Cell capacitance and access resistance were monitored before each voltage ramp and measurements were discarded when a change in access resistance exceeded 5 MΩ. Series resistance was compensated to 80 %. Membrane currents were filtered at 1.5 kHz and digitized at a sampling rate of 5-10 kHz. Currents were recorded with an EPC-9 patch clamp amplifier controlled by Pulse 8.3 software (HEKA Electronics). Immediately after establishing whole-cell configuration, linear voltage ramps from -100 to +100 mV within 100 ms were applied every 10 seconds from a holding potential of +70 mV for 10 or 20 min as indicated. For analysis, currents at -80 mV ramp potential were divided by cell capacitance, normalized (CD/CD$_{max}$) and plotted against time.

The EGTA-pipette solution contained the following (mM):

140	Cesium aspartate
10	EGTA
10	NaCl
10	HEPES
0.016	$MgCl_2$

pH 7.2 with CsOH

The BAPTA-pipette solution contained the following (mM):

140	Cesium aspartate

20	EGTA
22	NaCl
10	HEPES
0.020	$MgCl_2$

pH 7.2 with CsOH

Using CaBuf software (ftp://ftp.cc.kuleuven.ac.be/pub/droogmans/cabuf.zip), we calculated that 1 mM $MgCl_2$ had to be added to keep the free Mg^{2+} at 11 µM in presence of 6 mM ATP in both EGTA- and BAPTA- containing solutions. In BAPTA and ATP-containing solution, Cs aspartate was reduced to 135 mM.

<u>TRPV6 bath solution contained the following (in mM):</u>

115	Tetraethylammonium chloride
10	Cesium chloride
2.8	KCl
2	$MgCl_2$
30	$CaCl_2$
10	Glucose
10	HEPES

pH 7.4 with NaOH

Similarly for I_{CRAC} measurements, we made use of a STIM1-stable cell line that was transiently transfected with the wildtype or mutant Orai constructs. Human Orai1, 2 and 3 contructs were amplified from the HA-tagged constructs provided kindly by Annette Lis and Reinhold Penner then cloned into the bicistronic vector pCAGGS_IRES_GFP. Recordings of I_{CRAC} were performed under same conditions as above except for using EPC-10 as the patch clamp amplifier and Patch Master as the controlling software (HEKA Electronics). When whole-cell configuration was established, linear voltage ramps from -150 to +150 mV within 50 ms were applied every 2 seconds from a holding potential of 0 mV over a 5-minute recording period. Currents at -80 mV ramp potential were divided by cell capacitance, and plotted against time. Cells that showed an initial inward current of > 10 pA/pF were considered preactivated and were therefore excluded from the analysis also were the cells identified as outliers by the online available GrafPad software applying Grubb's test.

<u>I_{CRAC} pipette solution contained the following (mM):</u>

120	Cesium glutamate
20	Tetracesium BAPTA
10	HEPES
3	$MgCl_2$
0.05	IP_3

pH 7.2 with CsOH

The I_{CRAC} bath solution contained the following (mM):

120	NaCl
10	Tetraethylammonium chloride
10	$CaCl_2$
2	$MgCl_2$
30	Glucose
10	HEPES

pH 7.2 with NaOH

7.4   Statistical Analysis:

Data obtained are presented as mean ±S.E.M. Statistical significance was tested by performing unpaired, two-tailed Student t-test. Asterisks indicate significant differences. * $p<0.05$, ** $p<0.01$, *** $p< 0.001$.

8   Results

8.1   Regulation of TRPV6 activity

8.1.1 Regulation of TRPV6 activity by ATP

8.1.1.1   ATP prevents rundown of TRPV6 calcium currents

Heterologous expression of TRPV6 results in a constitutively active channel showing large inward rectifying currents that dramatically increase in value when cells are held at positive holding potential in whole-cell mode (Wissenbach et al., 2001). We recorded currents exhibiting typical TRPV6 characteristics from stable cell lines expressing either human TRPV6a or b alleles, thus profiting from the targeted insertion that minimizes transcriptional differences in locus. Currents were recorded in whole-cell mode placing the cells in high calcium containing bath solution. The internal solution was EGTA buffered and contained 11μM free Mg^{2+} keeping it at a concentration lower than the observed IC_{50} (Voets et al., 2003). We extended the recording time to 20 min to observe regulatory processes and thereby seeking a potential difference between the two alleles that might emerge under conditions of longer observation. In our protocol cells were kept at holding potential of +70 mV and a linear voltage ramp from -100 to +100 mV was applied. Analyzing the current at -80 mV we observed fast development of current (Fig. 10a). The maximum current density (in pA/pF ± SEM) recorded for TRPV6a was -105±15, n=17 which was not significantly different from that recorded for TRPV6b (155±27, n=11). Similar kinetics of current development were observed for both alleles which reached maximum value within the first 2 min of recording time (Fig. 10f). An interesting observation was the phenomenon of rundown where current values decreased over time to 31 and 35% of their corresponding maxima (Fig. 10a). For a quantitative description of this phenomenon, we termed the percent of maximum after 20 min "remaining current-densities (% REM)" (Fig. 10e). We also analyzed $t_{1/2}$ which is the time required for development of half maximal current density (Fig. 10f). Because our aim was to investigate regulatory mechanisms over longer recording time, we wanted to impede rundown. We included 6 mM Na_2ATP in our internal solution, keeping the free Mg^{2+} at 11 μM to bar its potential interference. A significant alteration of current development was observed. The initial currents after break-in were small and showed small increments with each ramp in a continuous run up mode throughout the recoding time that ended with minimal or no rundown (Fig. 10c). Maximum current densities after 20 min [-98±16 (V6a); -153±11 (V6b)] were not different from the corresponding values observed without ATP in the recording solution. To exclude the development of other conductances in our recording conditions, we plotted I-V relationship that actually retained the typical features of TRPV6 (Fig. 10b, d). Both alleles had comparable characteristics in both control and +ATP conditions with no significant differences detected in %REM or $t_{1/2}$.
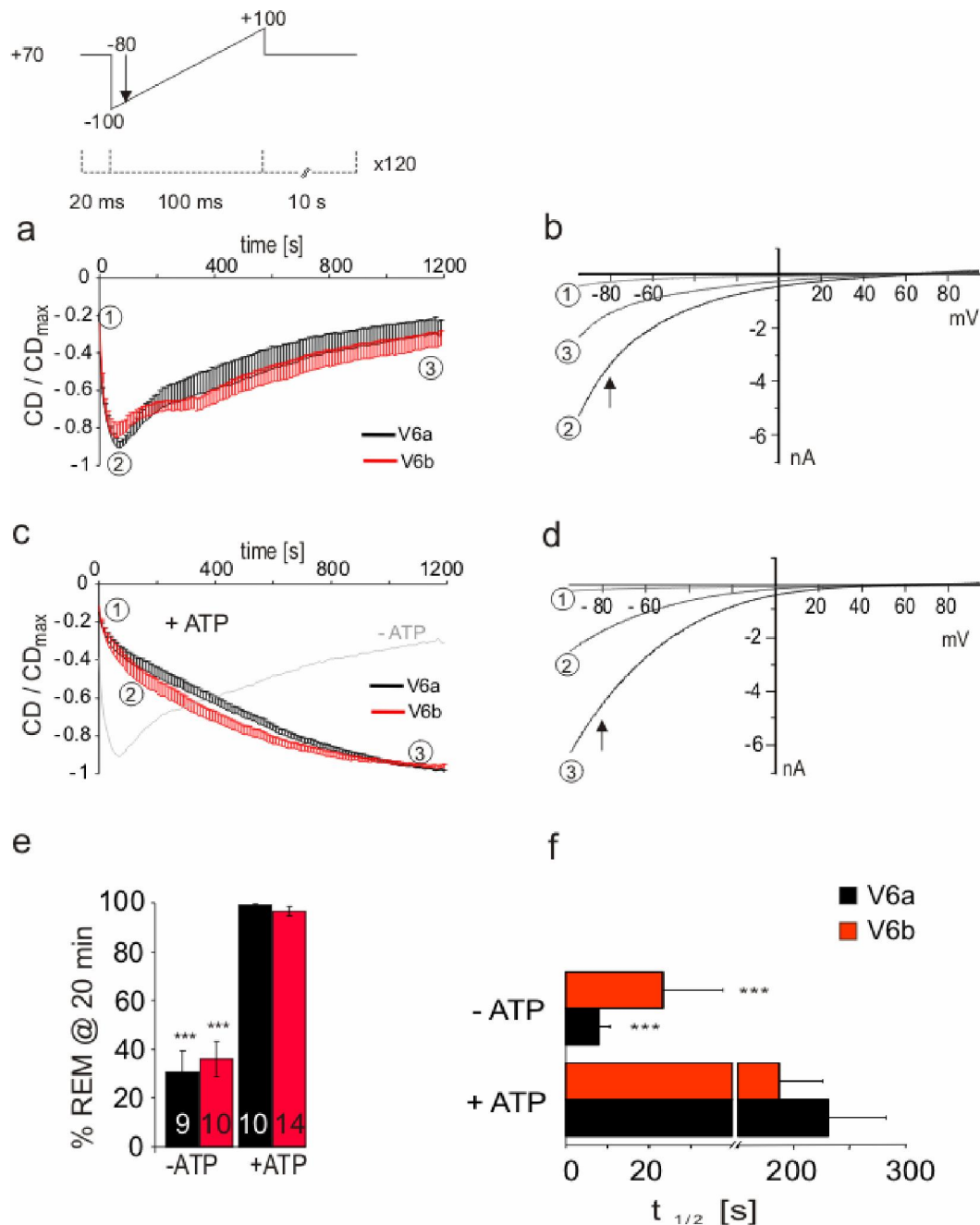
Figure 10: Whole-cell inward current densities (CD) measured at −80 mV ramp potential normalized to CD_{max} and plotted over 20 min recording time. On top of the figure is the performed ramp protocol: from holding potential of +70 a voltage ramp was performed from -100 to +100 mV over 100 ms and ramp repeated after 10 s pause for 120 times over total recording time of 20 min. Black trace is an average of TRPV6a expressing cells, red trace of TRPV6b expressing cells. Error bars represent mean + SEM. **a.** Pipette solution without ATP contains 11 μM free Mg^{2+}. **b.** Sample I/V relationships immediately after break-in (1), at 1 min (2) and after 20 min (3), showing the typical inwardly rectifying TRPV6 currents. **c.** Normalized current densities over time in the presence of 6 mM Na_2ATP for TRPV6a and TRPV6b expressing cells. **d.** Sample I/V relationships as described in (b) but in the presence of ATP. **e.** Bar graph showing the % remaining current (REM) after 20 min for TRPV6a and TRPV6b in the absence and presence of ATP. Numbers on bars represent number of cells. **f.** Quantification of the time to half-maximal activation for V6a and V6b in the absence and presence of ATP.

60

8.1.1.2   ATP effect on transiently expressed TRPV6

Because we wanted to further investigate the mechanism underlying the ATP effect by introducing point mutations and/or making deletions in TRPV6 subsequent recording from cells transiently expressing TRPV6 constructs was necessary. Therefore, we had to verify that the phenotype observed in the stable cell lines in presence or absence of ATP is similar for transiently expressed TRPV6. Recordings from HEK cells transiently expressing TRPV6a or b in pCAGGS expression vector showed comparable rundown in absence (Fig. 11a) and in presence (Fig.11b) of ATP to those of the stable cell lines. Since transient cells could often not be held for 20 min, currents were analyzed after 10 min recording time. After 10 min of recording, the rundown observed in absence of ATP in the transient cells was quite similar to that of the stable (45 ± 9; $59\pm9\%$, respectively). Though slow-down of current development was still evident for transiently expressed TRPV6 (Fig. 11d), stably expressed TRPV6 was significantly more slowed down ($t_{1/2}117\pm22$ vs. 57 ± 10). The difference in the kinetic component of the effect of ATP was complicated to interpret especially with the similar current densities (-160 pA/pF stable vs. -168 pA/pF transient). Therefore, we directed further analyses to effects on rundown. The difference in kinetics of current development in presence of ATP is addressed under regulation by ROS (chapter 7.1.4).
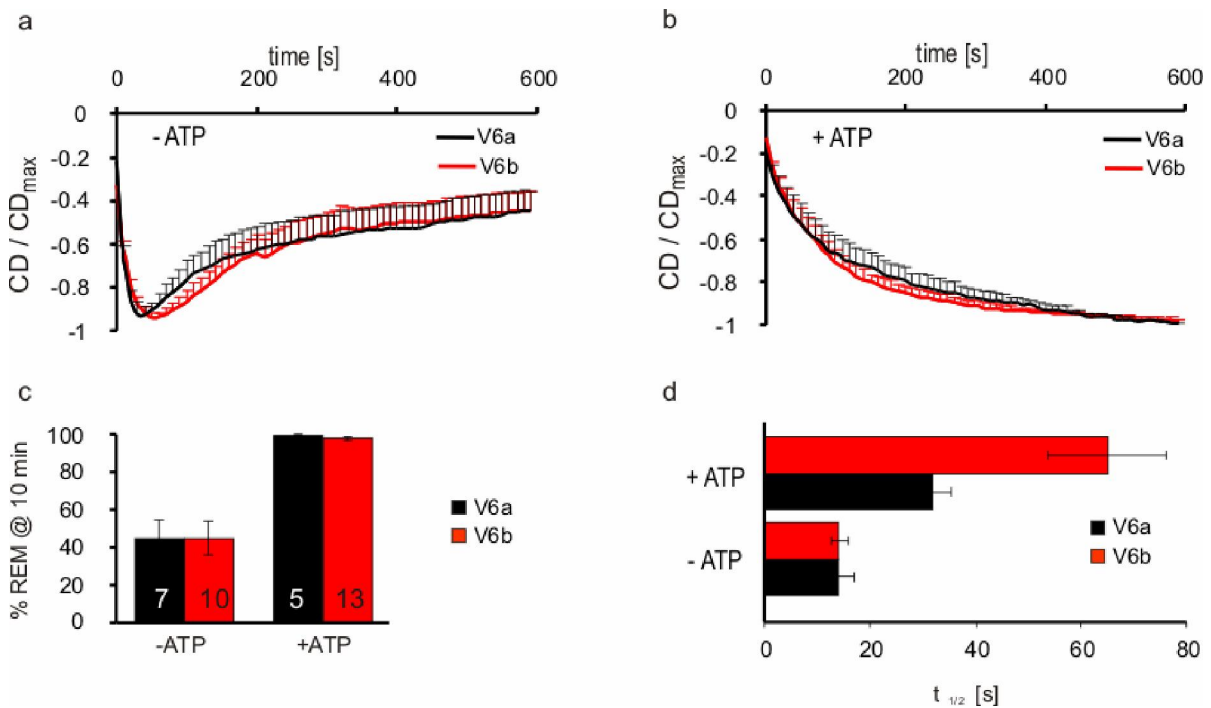

Figure 11: Whole-cell inward current densities (CD) measured at -80 mV ramp potential normalized to CD_{max} and plotted over 10 min recording time. Traces are averages of HEK cells transfected with TRPV6a (black) or TRPV6b (red) in pCAGGS-IRES-GFP. Error bars represent mean + SEM. Shown are the normalized current densities in absence **(a)** or presence of 6 mM ATP **(b)**. **c.** Bar graph showing the % remaining current (REM) after 10 min for TRPV6a and TRPV6b in the absence and presence of ATP. Numbers on bars represent number of cells. **d.** Quantification of the time to half-maximal activation for V6a and V6b in the absence and presence of ATP.

8.1.1.3   Influence of ATP on Ca^{2+}-dependent inactivation

A well-documented regulatory mechanism for TRPV6 is Ca^{2+}-dependent inactivation. When cells expressing TRPV6 are subjected to a hyperpolarizing voltage step they show strong time-dependent multiphasic inactivation in presence of Ca^{2+} but not Ba^{2+} as the charge carrier (Niemeyer et al., 2001). To investigate whether inclusion of ATP alters the pulse inactivation behaviour we applied a 1 s hyperpolarizing pulse following the voltage ramp protocol. To quantify pulse-induced inactivation we analyzed the residual current fraction at 930 ms (r930) relative to the peak current. Compared to the no ATP condition, the residual current fraction was significantly increased when 6 mM ATP was included in the pipette solution. However, this effect is not seen when 10 mM EGTA was substituted with 20 mM BAPTA (Fig. 12a, b), suggesting that the effect may be due to ATP's buffering capacity towards Ca^{2+}. The higher Ca^{2+}-buffering capacity of BAPTA and abrogation of ATP effect indicate that ATP can only interfere with Ca^{2+}-dependent inactivation mechanisms that are not buffered by 10 mM EGTA. Nevertheless, in the voltage ramp protocol ATP was still able to significantly suppress rundown as well as alter the current on-set kinetics even in the presence of the faster buffer (Fig.12d, e). This finding indicates that the effect of ATP is not entirely mediated by interference with Ca^{2+}-dependent mechanisms. This conclusion is in agreement with prevention of rundown in divalent free condition observed by Hoenderop and coworkers (Hoenderop et al., 2001). To test potential influence of ATP on Ca^{2+}-dependent mechanisms, we deleted a C-terminal domain calmodulin-binding domain (ΔCAM) (Niemeyer et al., 2001). The ΔCAM mutants were still influenced by ATP and showed slower current development and significantly less rundown than the wildtype (Fig.12c), indicating that ATP and calmodulin do not have overlapping interaction sites.
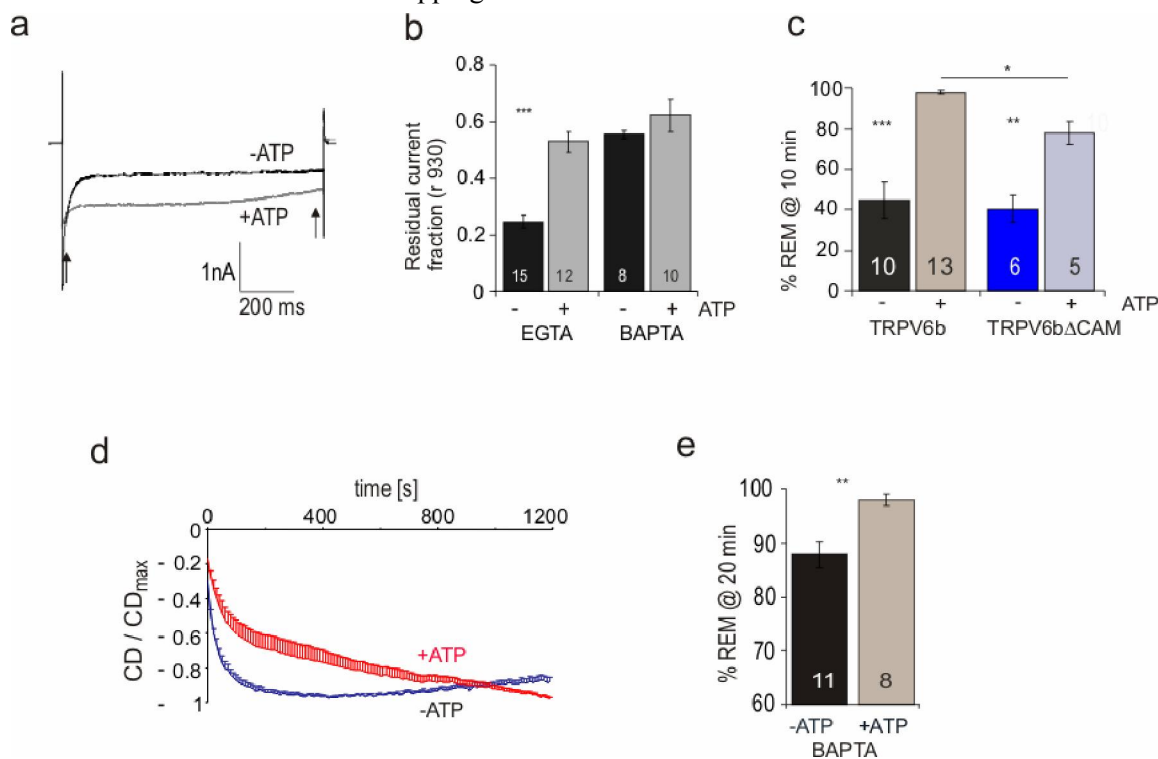
Figure 12: a. TRPV6b current traces in the presence (grey) and absence (black) of 6 mM ATP in response to a 1 s voltage step to -100 mV. **b.** Quantification of residual current fractions at 930 ms (r930) relative to the peak current with either 10 mM EGTA or 20 mM BAPTA. **c.** Quantification of rundown for transiently expressed wildtype TRPV6b and TRPV6ΔCAM mutants in the presence and absence of ATP. **d.** TRPV6b whole-cell current densities (CD) measured at -80 mV ramp potential normalized to CD_{max} with 20 mM BAPTA in presence (red) or absence (blue) of 6 mM ATP. **e.** Quantification of rundown with 20 mM BAPTA with and without ATP.

8.1.1.4 ATP depletion inhibits TRPV6-mediated Ca^{2+} influx

To investigate the ATP effects in a more physiological milieu we measured the Ca^{2+} influx in intact control TRPV6 cells and in cells kept in ATP-depleting buffer containing a metabolically non utilizable form of glucose and sodium azide (Schwoebel et al., 2002). Fura2 loaded control TRPV6 cells showed a transient increase in intracellular calcium concentration ($[Ca^{2+}]_i$) upon shifting the external calcium concentration ($[Ca^{2+}]_e$) from 1 to 10 mM. This transient could again be evoked after ~ 50 min when cells were kept at physiological conditions (Fig. 13 upper panel). Depriving the cells of ATP hampered the subsequent Ca^{2+} influx (Fig. 13 lower panel) indicating that an adequate concentration of ATP or of a metabolite is a prerequisite for a TRPV6 response to an increased $[Ca^{2+}]_e$. In our protocol, $[Ca^{2+}]_e$ was brought back to a lower level (1 mM) during incubation time. Interestingly, the ATPases were still functional as indicated by retrieval of the resting $[Ca^{2+}]_i$. A set of control experiments using HEK cells kept at the same conditions was done in parallel. HEK cells showed a lower resting calcium $[Ca^{2+}]_i$ and were lacking the rapid transient increase in $[Ca^{2+}]_i$ upon exposure to 10 mM $[Ca^{2+}]_e$
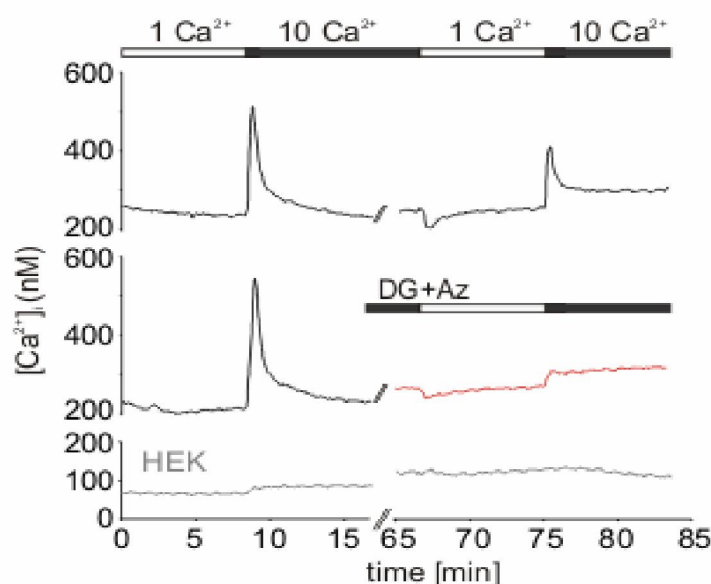

Figure 13: Upper panel: Fura-2/AM loaded HEK-TRPV6b cells showing a transient increase in $[Ca^{2+}]$ when extracellular $[Ca^{2+}]$ is increased to 10 mM. Influx can again be evoked after 50 min. **Middle panel:** Same protocol as above but bath solution after the first transient includes 20 mM deoxyglucose instead of glucose and

10 mM sodium azide. **Lower panel:** HEK-wt cells before and after depletion. Traces are averages of > 100 cells for HEK-TRPV6 and 75 cells for HEK-wt.

8.1.1.5   ATP effect is PIP$_2$-independent and does not require hydrolysis

ATP is essential for maintenance of intracellular PIP$_2$ levels. End of 2008, Thyagarajan et al. showed that Ca^{2+} influx induces depletion of PIP$_2$ and thereby mediating Ca^{2+}-induced inactivation of TRPV6 channels (Thyagarajan et al., 2008). To examine the probable involvement of PIP$_2$ in the ATP effect, we replaced ATP with 50 µM diC$_8$PIP$_2$, maintaining high intracellular [PIP$_2$] in absence of ATP. This water soluble PIP$_2$ derivative was unable to prevent rundown when solely included (Fig 14a,b). Furthermore, we mutated a highly conserved arginine residue, R606, equivalent to R599 in rTRPV5. The latter residue was shown to be essential for PIP$_2$-mediated regulation of TRPV5 (Rohacs et al., 2005). Site directed mutagenesis was done in TRPV6/pCDNA3 and the mutation containing EcoRV/MfeI-digested fragment replaced that of the wildtype in pCAGGS-IRES-EGFP (Fig 24b). The PIP$_2$-binding defective mutants (R606Q) still showed significantly reduced rundown when ATP was included in the pipette solution (Fig. 14c, d). Many regulatory effects of ATP were shown to require hydrolysis of ATP therefore we tested whether a non-hydrolyzable ATP analogue, AMP-PCP (Ashcroft and Kakei, 1989), is still able to prevent rundown. This analogue retained the ability to prevent rundown and slowed current development (Fig. 14a, b). When put together, this evidence indicates that ATP regulates TRPV6 in a PIP$_2$-independent manner and that this regulation does not require ATP hydrolysis.
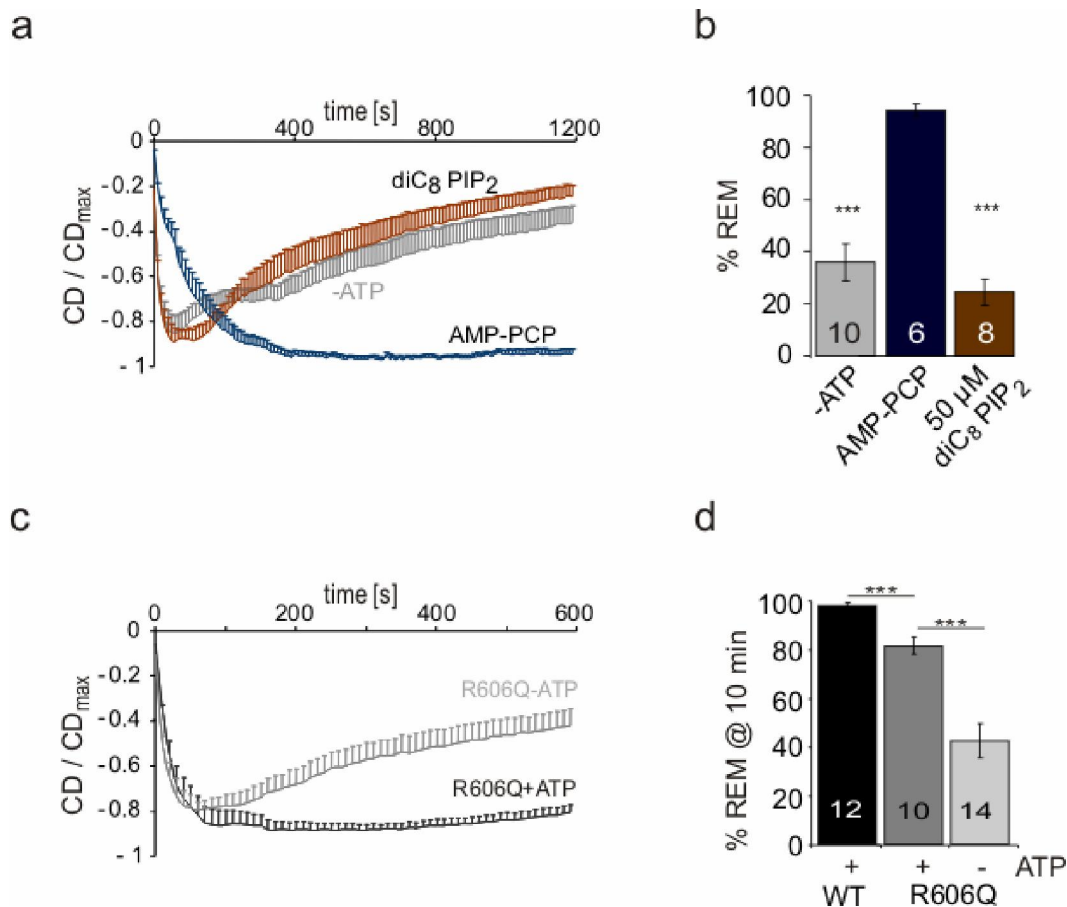
Figure 14: a. Normalized current densities over time in the absence of ATP (grey), in the presence of 50 μM diC$_8$PIP$_2$ (brown) or in the presence of 6 mM AMP-PCP (blue) in TRPV6 stable cell line, error bars represent mean + SEM. **b.** Bar graph of the % REM for traces seen in (a). **c.** Normalized current densities over time for transiently expressed TRPV6b-R606Q mutants with (black) and without (grey) ATP in the recording pipette showing that R606Q mutants retain the ATP effect. **d.** % REM after 10 min recording time, see also Fig.11b, c for transiently expressed wildtype.

8.1.1.6   The nucleotide specificity of the ATP effect

To test nucleotide specificity of the ATP effect we substituted ATP with an equal concentration of variable nucleotides having either fewer phosphate substitutions or a different nucleobase. For nucleotides known to chelate magnesium, the total added Mg^{2+} was adjusted to keep the free [Mg^{2+}] at 11 μM. Similar to recordings with ATP, we applied the voltage ramp protocol and analyzed the %REM. Figure 15 shows that having another nucleobase (UTP, IMP and GTP) reduces the nucleotide's ability to prevent rundown regardless of the number of phosphates. Similarly, adenine-based nucleotides with fewer phosphate substitutions were less effective than ATP in prevention of rundown with adenosine being ineffective. The second messenger cAMP was also unable to prevent rundown.
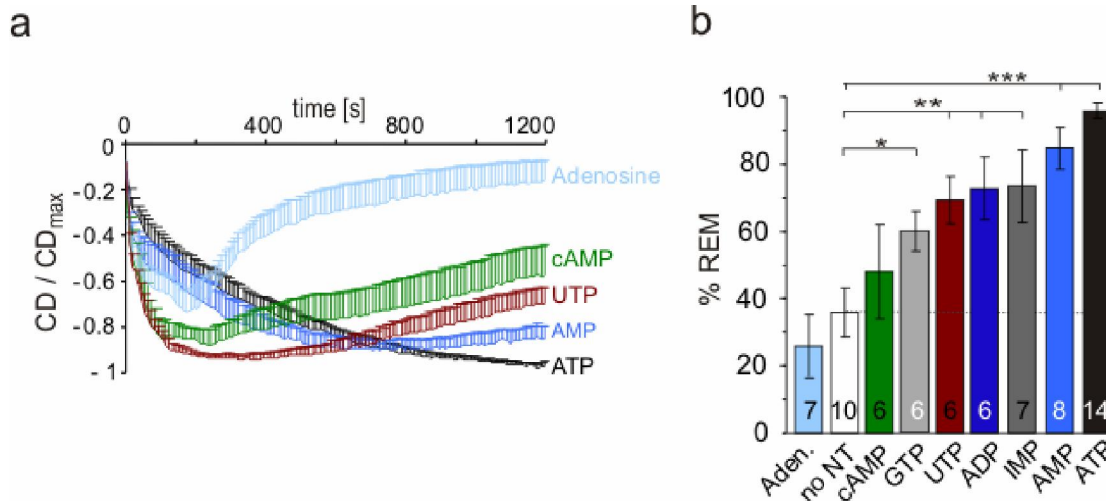
Figure 15: a. Sample traces of normalized current densities over time in the presence of different intracellular nucleotides at 6 mM concentration each, error bars represent mean + SEM. **b.** Quantification of the remaining current (%REM) for all nucleotides tested. Asterisks indicate significant differences of the %REM against the no added nucleotide (no NT) control. Numbers on bars represent number of cells. Recordings were obtained in stable TRPV6b cells.

These results indicate that: firstly, the effect of ATP is not due to an increased Ca^{2+}-buffer capacity because UTP and ATP have similar Ca^{2+}-buffering capacities but affect current kinetics quite differently. Secondly, the effect shows nucleobase specificity. Thirdly, at least one phosphate is necessary because AMP but not adenosine slows the current and prevents some of the rundown.

8.1.1.7   ATP effect is concentration-dependent

To find out whether and how concentration-dependent the ATP effect is, we analyzed the %REM for recordings from cells supplemented with different concentrations of ATP then plotted the dose response (Fig 16b). Our regular internal solution for the +ATP recordings contained 6 mM Na_2ATP, 1 mM $MgCl_2$ and 10 mM EGTA resulting in a free [ATP] of 3.7 mM which is higher than the estimated cellular free [ATP]. To obtain the dose response relationship we included free [ATP] of 609, 304, 124, 60 and 6µM always keeping free [Mg^{2+}] at similar levels and fitted the data points with a sigmoidal dose-response function of variable slope, where % REM_{MAX} is the maximal remaining current obtained after addition of 3.7 mM free ATP, EC_{50} is the half-maximal concentration of free ATP, and *n* is the Hill slope. The following equation was used to fit ATP concentration-response curve:

$$Y = base + \frac{(\max - base)}{(1 + \frac{X_{1/2}}{X})^{rate}}$$

As shown in Figure 16 the mean EC_{50} obtained from the graph was 378 µM free ATP and the Hill slope was 4.8. The EC_{50} value obtained is one order of magnitude greater than that normally required for a kinase-mediated phosphorylation reaction (Hilgemann, 1997) but conforms well with estimated free [ATP]$_i$ within cells (~ 0.5 mM) (Gajewski et al., 2003)
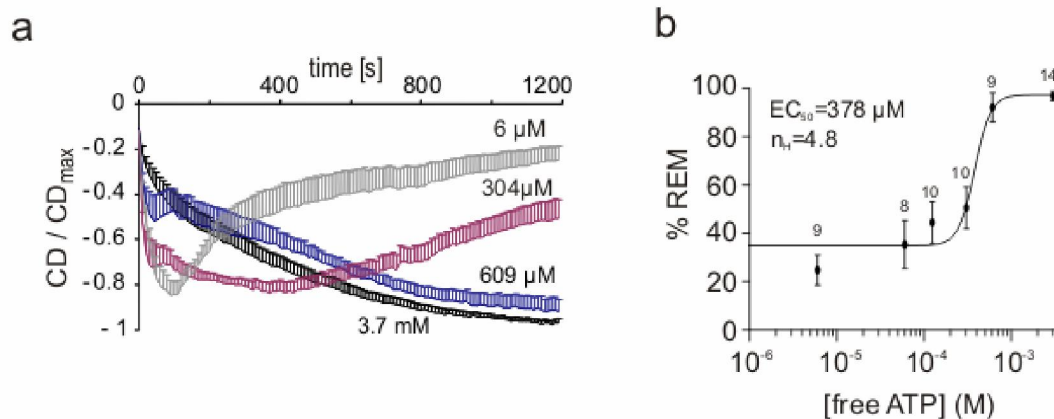
66

Figure 16: a. Normalized current densities over time for selected concentrations of intracellular free ATP, error bars represent + SEM. **b.** Mean relationship between free [ATP] and the degree of run-down after 20 min (%REM). Data points (number of cells above) were best fitted to equation (1), see text. EC_{50} = ATP concentration at which prevention of rundown is half-maximal. n_H = Hill slope.

8.1.1.8 ATP binds TRPV6 at atypical domains

ATP is shown to regulate the activity of several channels by means of direct binding. In an initial trial to test if this is also the case for TRPV6 we performed ATP pull down experiments using the *in vitro* translated full length TRPV6 protein and ATP-agarose. TRPV6 was retained by ATP-agarose and that retention was competed for by ATP in the binding buffer (Fig. 17). With this initial result at hand, we set out to further define ATP binding sites within TRPV6.
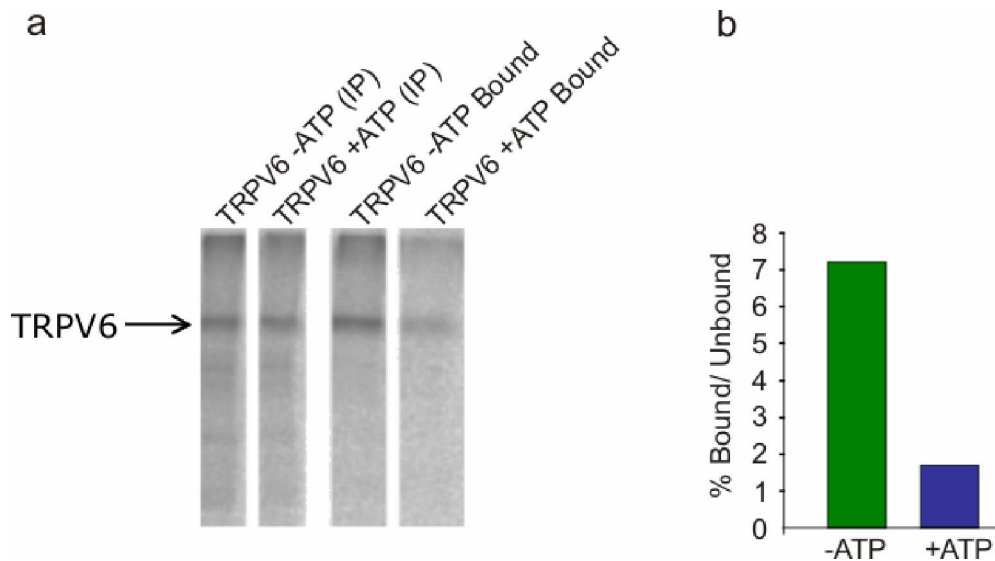

Figure 17 *In vitro* translated full length TRPV6 is retained on ATP-agarose. Using reticulocytes lysates, TRPV6 protein was *in vitro* translated, purified and bound to ATP-agarose in presence or absence of ATP in binding buffer. **a.** Autoradiographic image of SDS-PAGE analyzed in put (IP) and bound fractions. **b.** Quantification of signal of bound/unbound fractions in absence (green) and presence (blue) of ATP.

To map the potential ATP binding site(s), we made use of two mTRV6 histidine tagged fusion proteins, provided by Marcel Meissner (FP1 and CT1) and we cloned several additional N-terminally

67

10× histidine tagged proteins to cover the intracellular protein domains. At the N-terminus, the fusion protein FP1 started at the very beginning of TRPV6 and extended to the second ANK repeat (Fig. 18b), followed by a fusion protein covering the 6 ANK repeats (ARD) (Fig. 18c). The fusion protein (NP) covered the sequence downstream of the ANK repeats to the first transmembrane domain (NP) (Fig. 18d). Two fusion proteins covered the C-terminus with the first starting after the sixth transmembrane domain and including the TRP box (CT1) (Fig. 18e) while the second extended downstream to the very C-terminal end of TRPV6 protein (CT2) (Fig. 18f). We cloned the N- and C-termini fusion proteins into the BamHI and XhoI sites, respectively, of the pET19b vector. The fusion proteins were expressed in BL21 cells and purified from cell lysates by binding to Ni-beads. Retention of the eluted purified proteins by ATP-agarose was tested. Specificity of the binding was tested for by inclusion of free ATP or UTP.
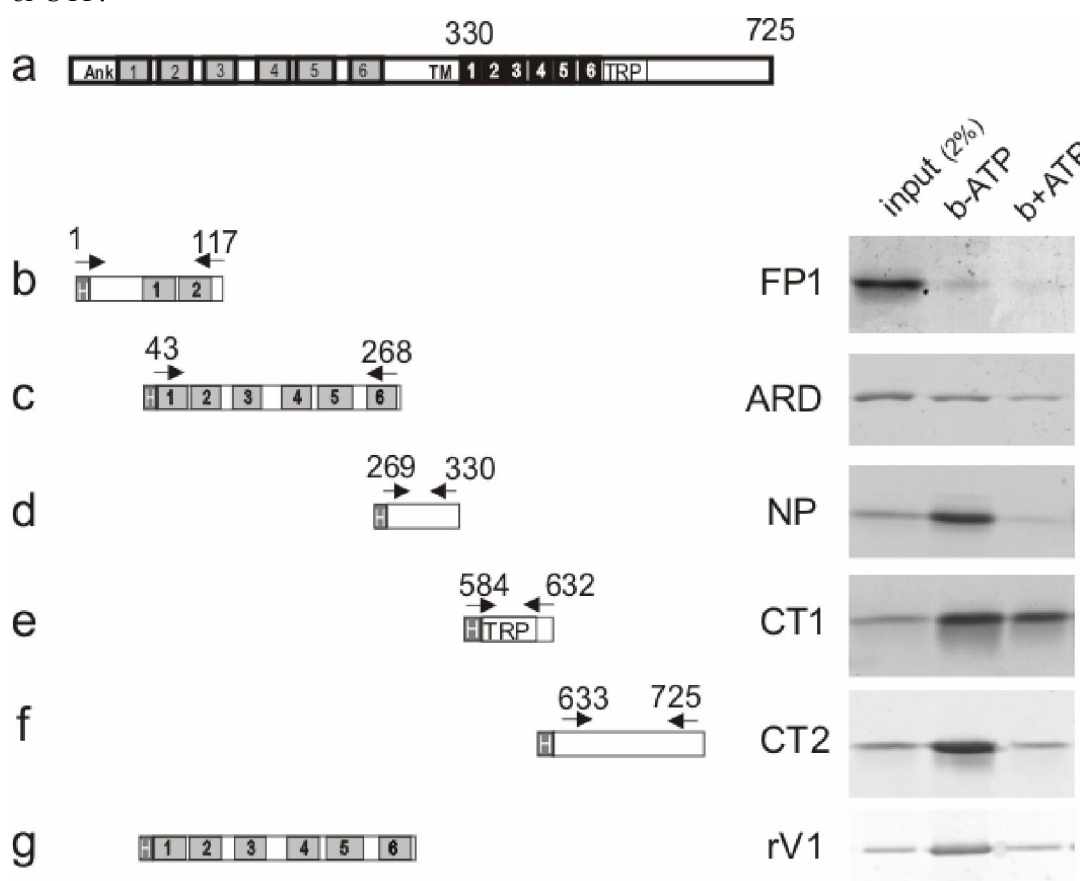

Figure 18: **a.** Schematic diagram of the TRPV6 protein domains. **b-f.** Schematic diagrams of the individual fusion proteins, numbers indicate amino acids next to Coomassie-stained PAGE gels of ATP-agarose pull down experiments. "input" 2% of total protein used for binding, "b-ATP" is the total fraction of protein retained by ATP-agarose in the absence of free ATP and "b+ATP" is the total fraction of protein retained in the presence of 6 mM free ATP in the binding buffer. **g.** Schematic diagram and ATP-agarose pull-down of rTRPV1 ARD fusion protein (aa 101-364).

Investigating binding at the N-terminus showed that P1 could not be retained on ATP-agarose (Fig. 18b) pointing to the fact that the His tag by itself does not confer unspecific binding to the agarose. On the other hand, ARD was weakly retained, an observation that remained consistent upon repetition of

the experiment also with different batches of purified protein. The NP was initially more strongly retained by ATP-agarose than ATP but this binding was variable when we repeated the experiment. (Fig. 18c,d). The proximal region of the C-terminal domain was efficiently but unspecifically retained on ATP-agarose as indicated by inability of free ATP to compete this binding (Fig. 18e). The distal part of the C-terminus was equally retained and the binding was, in contrast, specifically competed for by free ATP (Fig. 18f). Because the ARD region of rat TRPV1 had already been shown to bind ATP (Lishko et al., 2007), we also created a His tagged rTRPV1 ARD to serve as reference bound protein. This latter protein was retained by ATP-agarose in our experimental conditions (Fig. 18g). though with lower efficiency than the previously reported binding. Because no binding of TRPV6-ARD was detected in another independent study of the same group, (Phelps et al., 2008) which is in contrast to our results, we considered the differences in our experimental conditions. Among these differences is that we purified our proteins in presence of a denaturing agent (6M Urea). Based on results illustrated in the next chapter (regulation by protein kinase), that were obtained in parallel, we proposed that ARD and CT2 fusion proteins contain the functionally relevant ATP binding sites hence we wanted to confirm that both proteins still bind ATP when purified under native conditions.

Our trials to purify the N-terminal 10×His tagged proteins resulted in weakly soluble proteins that we could not keep in solution in absence of urea. Based on the cloning strategy described by Jin and coworkers (Jin et al., 2006), we constructed a new bacterial expression vector (Fig. 20) where we created a cloning site upstream of a 6× His tag to be C-terminally linked to the protein via a 3× alanine linker. Figure 19 shows that proteins purified under native conditions were still specifically retained by ATP-agarose to a comparable extent to that of the N-terminally tagged proteins
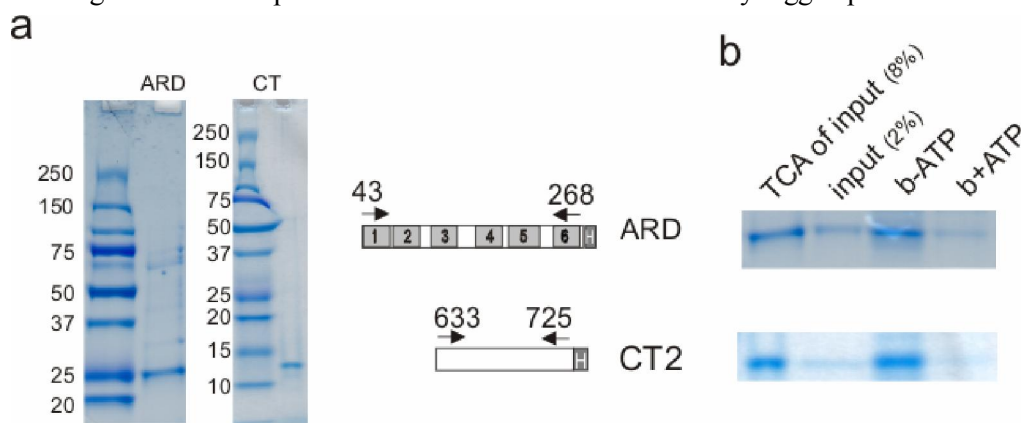

Figure 19: a. Coomassie stained PAGE gels showing expression of ARD and CT2 fusion proteins with C-terminal 6× His tag purified under native conditions. Middle panel is a schematic diagram of the two fusionproteins. **b.** Coomassie stained gels of ATP-agarose pull down experiments, TCA: 8% of trichloroacetic acid-precipitated total protein used for binding, "input": 2% of total protein used for binding, "b-ATP" is the total fraction of protein retained by ATP-agarose in the absence of free ATP and "b+ATP" is the total fraction of protein retained in the presence of 6 mM free ATP in the binding buffer.
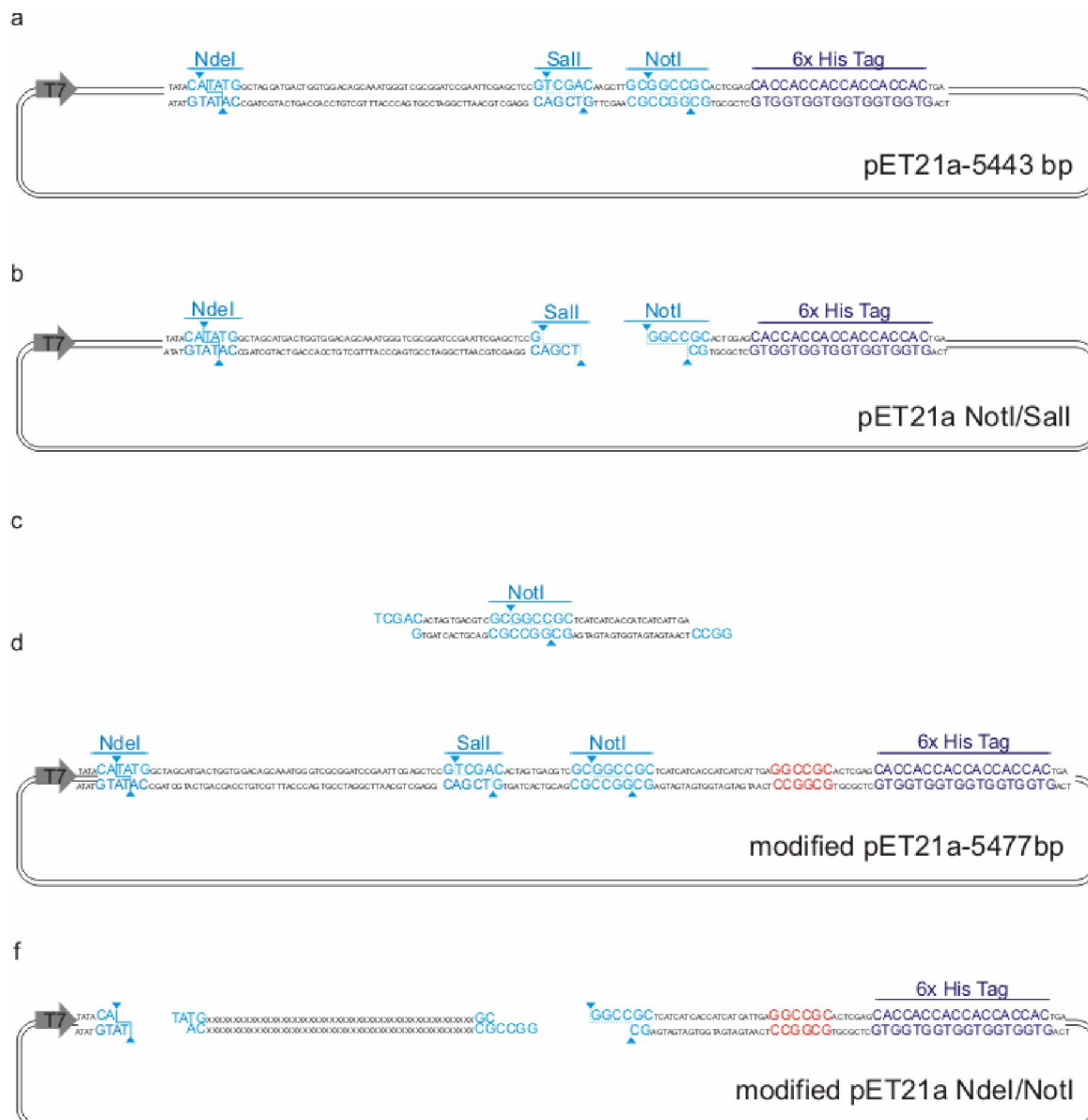
Figure 20: Modification of pET21a vector for cloning 6× His C-terminally tagged fusion proteins. Original pET21a **(a)** and a double stranded oligonucleotide containing a NotI recognition site **(c)** ligated into the NotI/SalI-digested fragment **(b)** reconstituting the SalI site and destroying the original NotI site **(d)**. cDNA of the desired fusion protein was PCR amplified and cloned into the NdeI/NotI of the modified vector **(f)**.

The results presented so far shed some light on how TRPV6 activity is linked to the metabolic status of the cell. Moreover, the results indicate that ATP modulates TRPV6 channel activity by direct binding at several binding sites. Because it is imaginable that not all the binding sites are functionally relevant, we performed further functional analyses presented in the following chapter to narrow down the relevant sites.

8.1.2   Regulation of TRPV6 activity by PKC modulation

8.1.2.1   Effect of stimulation of PKC

Because the human alleles TRPV6a/b differ in a potential phosphorylation site for PKC, we investigated whether we could uncover a functional difference under conditions of stimulated PKC. Accordingly, we incubated the stable cells with 500 nM of the phorbol ester PMA that, among other effects, is a potent activator of PKC. Surprisingly, preincubation with PMA resulted in reversion of the ATP effect where currents developed fast and attained the maximal values within the first 2 min despite the presence of ATP (Fig. 21a,c). Interestingly, the extents to which both alleles were affected by PMA stimulation were different. Whereas PMA annulled the effect of ATP on the ancestral allele (Fig. 21b) it could only partially revert it for the derived allele (Fig. 21d). With the polymorphic exchange (R158C) deleting a potential PKC consensus site (S/TxR) in the derived allele, this data reveals a unique though modest difference between the alleles that could have further functional relevance.
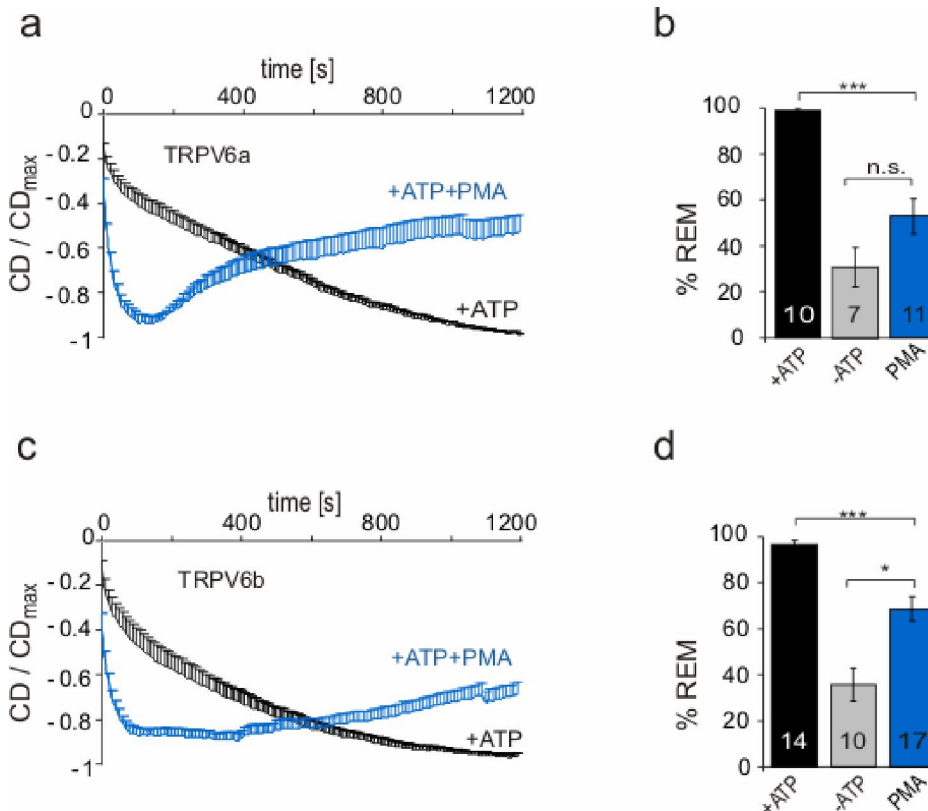

Figure 21: a. Normalized current densities over time for TRPV6a expressing control cells (black) and cells that were pretreated for 1hr with 500 nM PMA, also PMA present in bath solution (blue), for both 6 mM ATP included in patch pipette error bars represent +SEM. **b.** Quantification of run-down (%REM) after 20 min, in presence of ATP (black), absence of ATP (grey), and in presence of ATP with preincubation with PMA (blue). **c.** and **d.** Same as in (a) and (b) for TRPV6b stable cell line.

To test whether PMA has an effect in the absence of ATP, we recorded from cells preincubated with PMA without adding ATP to the internal solution. For both alleles currents developed fast. While the

ancestral allele showed similar rundown to that of the control recordings (25±8%), the derived allele showed more extensive rundown (17±3%) which could mean that at the ground state TRPV6a is more phosphorylated than TRPV6b.

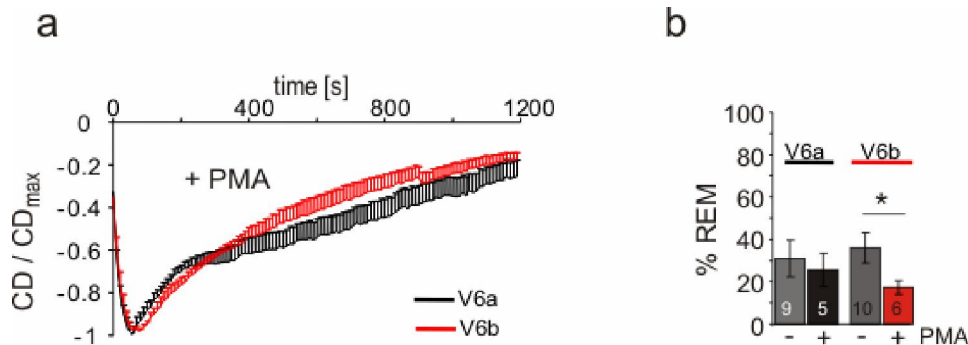**Figure 21: a**. Normalized current densities over time for TRPV6a (black) or TRPV6b (red) expressing cells pretreated for 1hr with 500 nM PMA, also included in bath solution pipette solution not containing ATP, error bars represent + SEM. **b.** Quantification of run-down (%REM) after 20 min from recording done in (a) compared to corresponding recording from cells not pretreated with PMA in grey (see Fig. 10).

8.1.2.2 PMA effect is isozyme specific

Considering the multiple effects of PMA, it was important to ascertain that the observed PMA effects were specific to PKC. Currents recorded from cells preincubated with 4αPDD (an inactive analogue that still binds C1 domains of proteins but is unable to stimulate PKC) were slow with no evident rundown indicating that PMA effect is PKC-mediated (Fig. 22a, b). In an attempt to block the effect of PMA, we pretreated TRPV6b cells for 1h with the inhibitor mix (Bisindolylmaleimide I and Gö 6983, Calbiochem), before stimulating with PMA. This pretreatment failed to prevent PMA-induced rundown (Fig. 22a, b). Screening the available literature about PKC inhibitors we noted that Bis/Gö have well characterized IC_{50} [6 – 60 nM, (Gschwendt et al., 1996; Toullec et al., 1991)] for most classical PKCs but not for the isozyme $PKC_{\beta II}$. Ro-31-8220 (Calbiochem), however, has a defined IC_{50} of 14 nM for $PKC_{\beta II}$ (Wilkinson et al., 1993). Pretreatment with 500 nM Ro-31-8220 abolished the PMA effect suggesting that the effect is mediated by $PKC_{\beta II}$ stimulation.

In line with the specificity of PMA effect to the isoform $PKC_{\beta II}$ are the findings obtained from the next set of experiments. Investigating the time required for the PMA effect we recorded from cells after descending incubation time periods: 30, 10 and 0 min, in the latter PMA was only acutely added to the bath solution and cells were recorded within 10 min. The PMA effect was either partial or gone with reduced incubation. To investigate why it takes an entire hour to see the PMA effect while, PKC activation and translocation to the plasma membrane occurs within min. A possible explanation is that HEK cells express very low levels of $PKC_{\beta II}$ (Feng et al., 1998) and the fraction of enzyme translocating to the plasma membrane might need longer to accumulate to a sufficient amount to exert a measurable effect. If this is the case, $PKC_{\beta II}$ overexpression should speed up the effect of PMA. We therefore overexpressed $PKC_{\beta II}$ as well as PKC_{α} in TRPV6 stable cells and as shown in Figure 22c,d, only overexpressing of $PKC_{\beta II}$ but not PKC_{α} obliterated the need to PMA preincubation though both of them translocated to the plasma membrane when PMA stimulated (Fig. 22e and data not shown). To

test whether PKC $_{\beta II}$ and TRPV6 share expression pattern, we examined its expression in the human placental DNA, from which TRPV6 was originally cloned (Wissenbach et al., 2001). We were able to amplify PKC $_{\beta II}$ using isoform-specific PCR primers (Fig. 22f). PCR products were of the expected size and the intensity correlated with the amount of template used. Taken together, this indicates that PMA specifically regulates TRPV6 activity via a PKC$_{\beta II}$ -specific pathway.
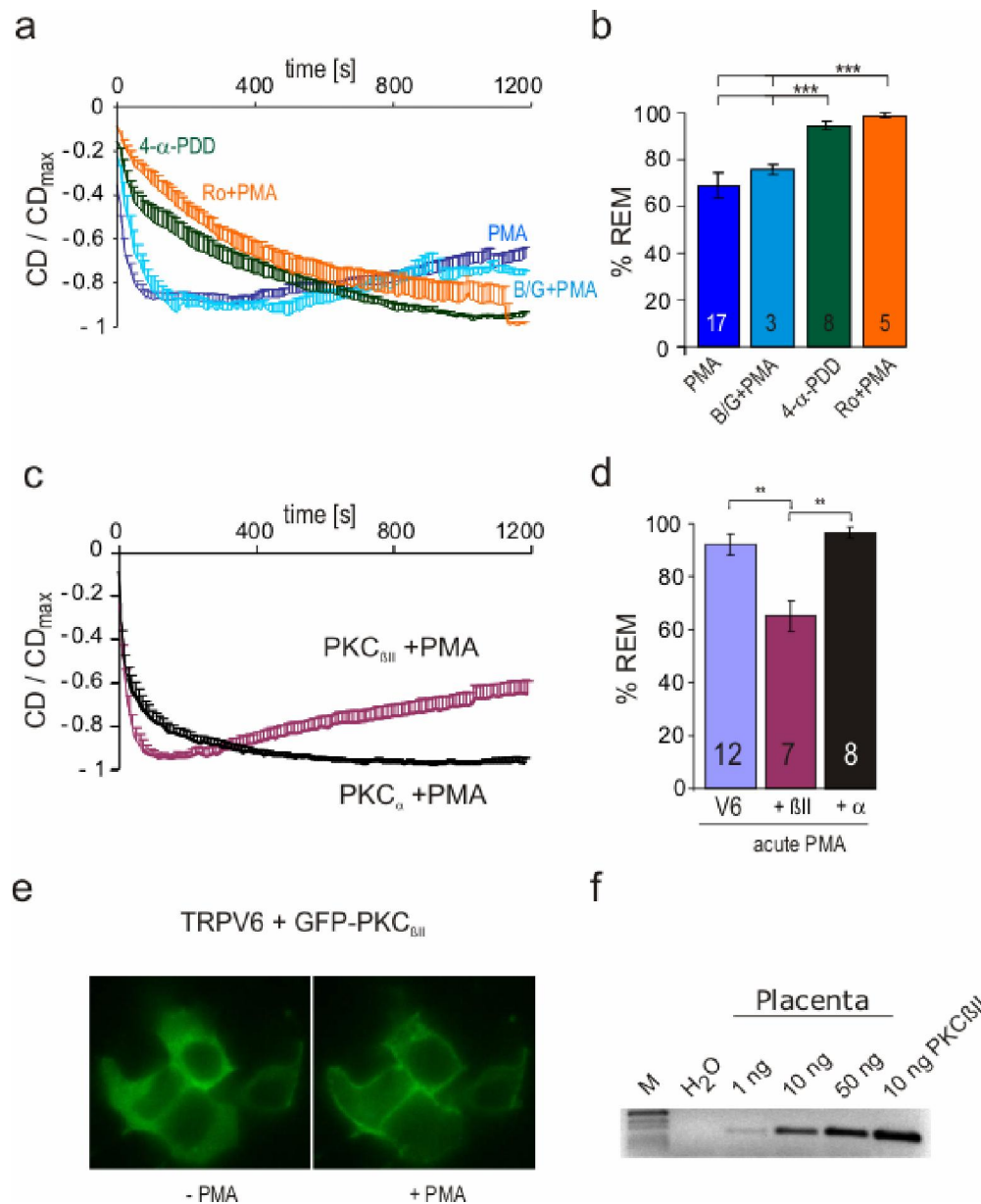

Figure 22: a. Normalized current densities over time for TRPV6b expressing cells that were pretreated either for 1 hr with PMA or 4-α-PDD or for 30 min with 500 nM each of inhibitors Gö6983/BIS or Ro-31-8220 then 500 nM PMA for 1 hr, recordings with ATP included in pipette solution and PKC modulators included in bath solution, error bars represent +SEM **b.** Percent REM for recordings with PKC modulators obtained in (a). **c**. Normalized current densities recorded from TRPV6b stable cells with transient expression of GFP-PKC$_{\beta II}$ or GFP-PKC$_\alpha$ with acute PMA treatment ($\leq$10 min in bath, no pretreatment), 6 mM ATP included in pipette solution. **d.** Bar graph of percent REM with acute PMA treatment for TRPV6b cells alone or TRPV6b cells transfected either with GFP-PKC$_{\beta II}$ or GFP-PKC$_\alpha$, as in (c). **e.** Fluorescent images from TRPV6b cells expressing GFP-PKC$_{\beta II}$ before and after induction of translocation with 500 nM PMA perfusion. **f.** Amplification products of

73

the 162 C terminal nucleotides distinctive of PKC$_{\text{ßII}}$ from PKC$_{\text{ßI}}$ out of human placental cDNA or from recombinant PKCßII vector, using the shown amount of templates in ng.

We next investigated whether PKC$_{\text{ßII}}$ directly phosphorylates the channel by incubating microsomal membrane fractions of TRPV6b expressing cells with recombinant PKC$_{\text{ßII}}$ or, alternatively, lysates of cells transfected with GFP-PKC$_{\text{ßII}}$, and [γ-^{32}P] labelled ATP. Proteins were blotted onto nitrocellulose membrane then phosphorylated proteins were detected by exposure to phosphoimager plates or x-ray film. Figure 23 shows that a band of a similar molecular mass as complex glycosylated TRPV6 is phosphorylated which could mean that PKC$_{\text{ßII}}$ specifically phosphorylates complex glycosylated TRPV6. The identity of the phosphorylated band was confirmed by incubating the same blot with antibodies against TRPV6.
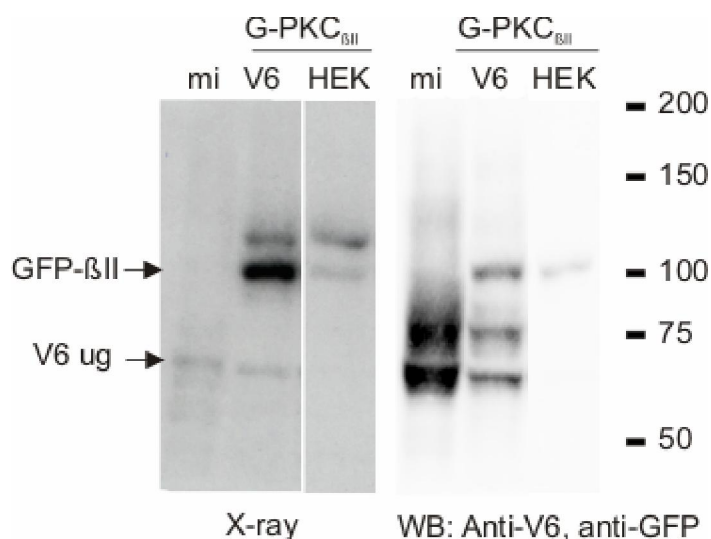

Figure 23: In vitro phosphorylation experiment. Proteins were labelled with [γ-^{32}P]-ATP by incubation of TRPV6 containing microsomes (mi) with lysates of HEK293 cells expressing GFP-PKC$_{\text{ßII}}$ Protein extracts were separated by SDS-PAGE and blotted to nitrocellulose film that was first incubated with an X-ray film (left panel) then the identity of phosphorylated bands was confirmed by incubation withTRPV6-antibody (right panel).

8.1.2.3   Mutational analysis of the putative phosphorylation sites mutants.

In an endeavor to reveal the functional relevance of effects of PMA, we mutated the putative phosphorylation sites identified by either the Prosite [http://www.expasy.ch/prosite, (Hulo et al., 2008)] or NetPhosk algorithms [http://www.cbs.dtu.dk/services/NetPhosK/, (Blom et al., 2004)]. We recorded from cells with and without preincubation with PMA. Control recordings without ATP were also done in parallel. Site directed mutagenesis was used to mutate the identified potential phosphorylation sites. Those sites were mutated by replacing the serine or threonine codons with alanine codons. The mutated fragments were confirmed by double stranded sequencing. Unless otherwise noted, mutations were done in the hTRPV6b background. To clone mutations within the N-terminal end of the protein (S144A, T150A, T298A/T299A, S318A, R153Q/R154P), mutagenic PCRs were initially done in TRPV6/pCDNA3, the mutated DNA was digested with BamHI and EcoRV (at 37°C) then BsmBI (at

55°C) and the BsmBI /EcoRV fragment hosting the mutations was swapped with the wildtype BsmBI /EcoRV fragment of TRPV6/pCAGGS (Fig. 24a). Resulting constructs were then used for electrophysiological recordings. Similarly, the mutation in the C-terminus (T688A) was first done in pCDNA3 and exchanged with the wildtype fragment in pCAGGS by MfeI/EcoRV-double digestion (Fig. 24b).
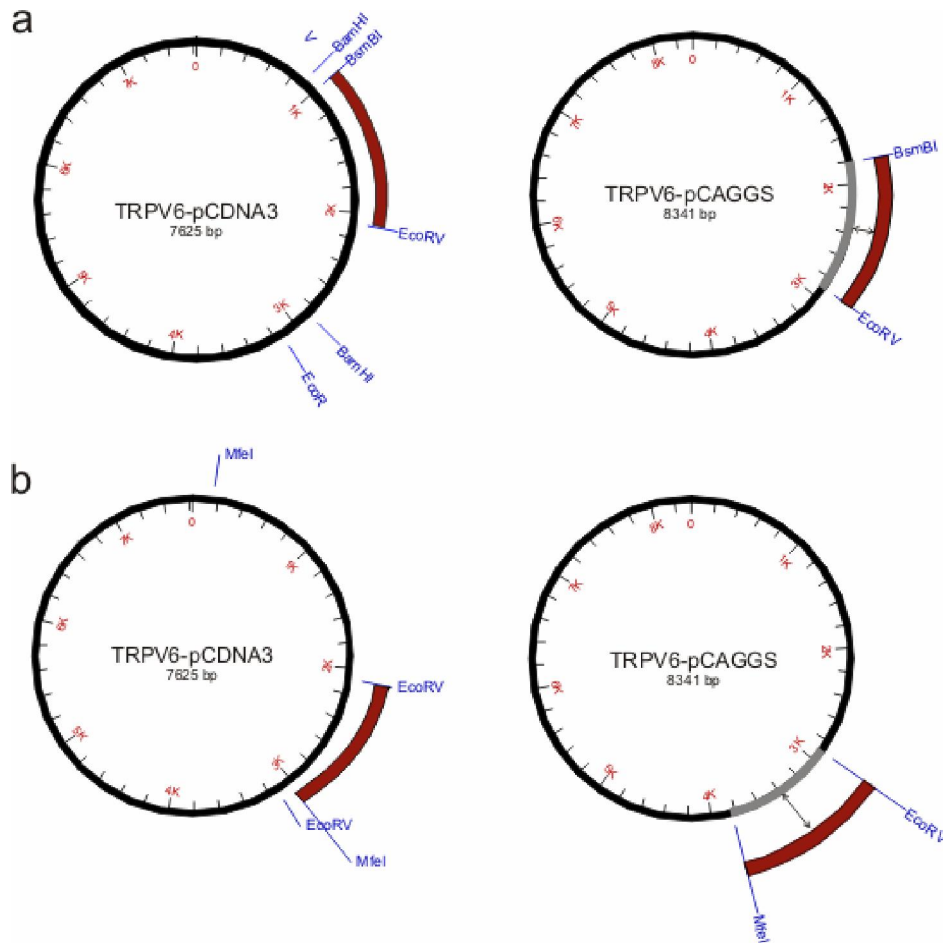

Figure24: Different TRPV6 mutageneses were done in TRPV6/pCDNA3 plasmid vector. **a.** For the N-term mutations, DNA confirmed to contain the desired base exchange was digested with BamHI/BsmB1/EcoRV then mutant BsmB1/EcoRV fragment (NT:66-1149) was exchanged with that of the wildtype in pCAGGS. **b.** Similarly, for C-term mutant, DNA was digested with EcoRV/MfeI and the mutant fragment (NT:1149-2079) replaced that of the wildtype in pCAGGS.

Recordings in absence of ATP from all mutants showed comparable rundown to the wildtype (Fig. 25b). In presence of ATP, for all mutants rundown is significantly prevented compared to the no ATP condition (Fig. 25 b-h). However, transient transfection of mutant constructs generally resulted in slightly altered kinetics of current development (see below: transient transfection and oxidative stress, subchapter 7.1.4). The first putative PKC site (S144) lies within the ARD in the solvent exposed finger loop between ANK3 and ANK4 and.is a potential functionally relevant site since mutants of this site did not show the effect of PMA (Fig. 25c) while in the same protein domain mutants of the threonine residue (T150A) still showed PMA-induced rundown (Fig. 25d). At the proximal end of the N-term,

the double mutant T298/299A showed a reduced PMA effect (Fig. 25e) while mutating the next putative serine residue (S318A) had no effect (Fig. 25f). Likewise, in the C-terminus mutating the first site T688 resulted in loss of PMA effect (Fig. 25g) while recordings from a stable cell line expressing the distal T702A mutants showed retention of the PMA effect (Fig. 25h). This data suggest that a PKC regulatory effect is mediated through phosphorylation at an N- as well as a C-terminal site.
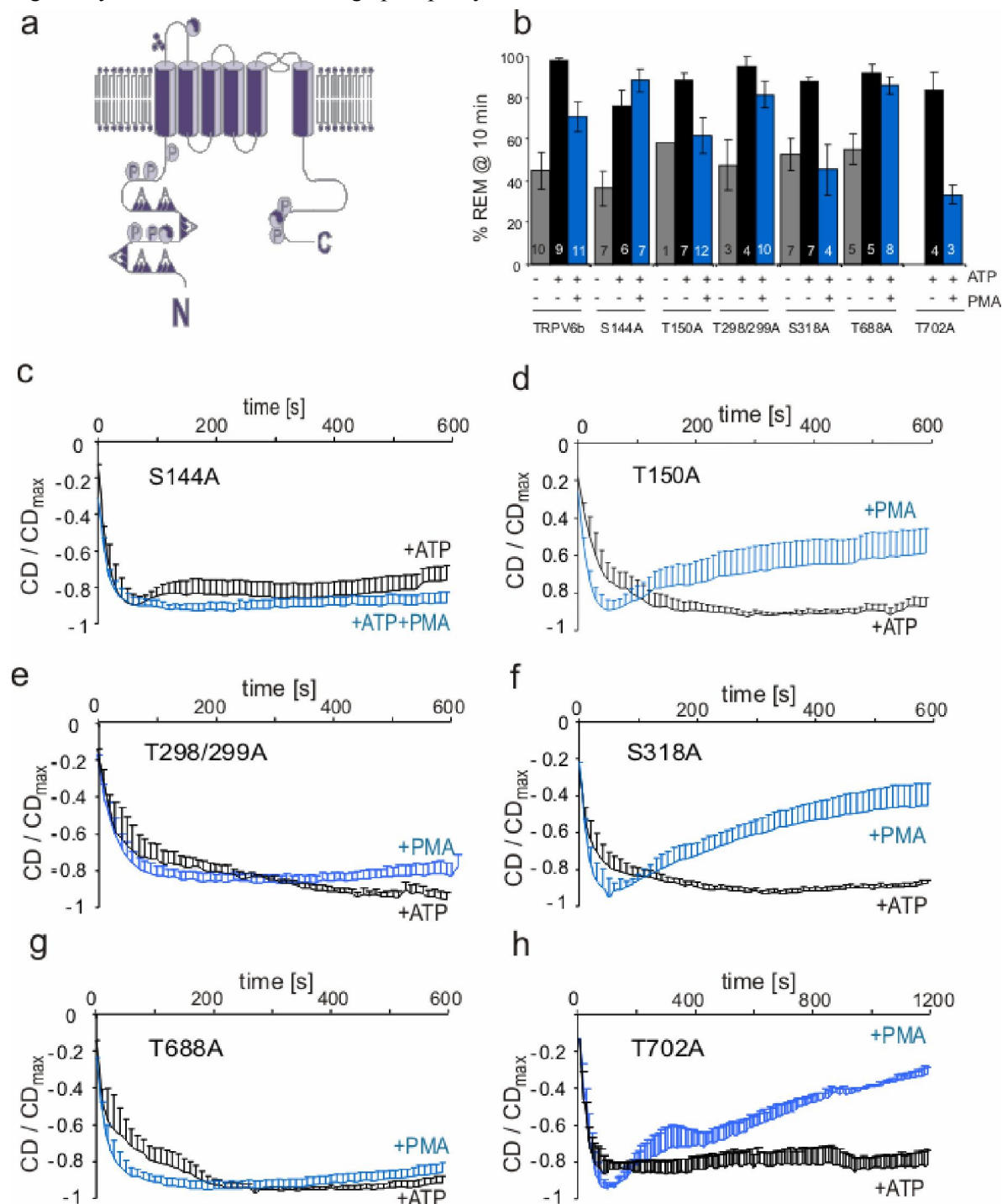
Figure 25: a. Schematic representation of putative PKC phosphorylation sites as found by the Prosite algorithm. **b.** Bar graph of percent REM from HEK cells transiently expressing mutants S144A, S150A, T298/299A, S318A and T688A or stably T702A. REM calculated after 10 min for transiently expressed mutants and 20 min for the stable T702A Pipette solution including no ATP (grey) or 6 mM ATP (black) in addition to pretreatment of cells with PMA for 1 hr and having PMA in bath solution during recording (blue), numbers on bars are numbers of cells. **c-h.** Normalized current densities over time from cells expressing the different mutants in (a) in presence of ATP (black) and with pretreatment with PMA (blue), error bars represent +SEM.

8.1.2.4   A double arginine mutation within the ARD region disrupts regulation by ATP

Our data show that the TRPV6 ARD region is able to bind ATP and that stimulation of PKC reverts the effects of ATP on current development and rundown. Because mutation of the S144 consensus site for PKC phosphorylation obliterated the effects of PMA on rundown, it is possible that the negatively charged phosphates added by PKC repel the binding of the phosphates of ATP and thereby shield an interactive site on the protein. If so, one would expect electrostatic attraction of ATP to positive residues within this domain to occur in the absence of channel phosphorylation. Two positively charged arginine residues (R153/R154) are present in the finger loop region between Ank3 and Ank4, close to the phosphorylation site S144 and also to the polymorphic phosphorylation site S155 (Fig. 26a). We mutated these residues to glutamine and proline (RR/QP, as present in hTRPV4) and recorded currents in the absence and presence of 3.7 mM free ATP. Indeed, this mutation rendered ATP incapable of slowing current development or preventing rundown. The %REM obtained (45±10%) is similar to that obtained in absence of ATP (51±11%) (Fig. 26b,d). To confirm the functional importance of this region we also included a peptide encompassing the sequence from aa 147-165 in patch pipette in presence of ATP assuming that this peptide being present in excess would bind ATP and make it unavailable for binding to the channel. Figure 26c,e shows that, in presence of the peptide, currents developed quickly and showed extensive rundown (48±12%). Because the peptide has limited solubility, we used a lower concentration of ATP that still showed the ATP effect as demonstrated in the dose response findings. Furthermore, we tested the binding of 10×His RR/QP-ARD fusion protein to ATP-agarose. To clone this construct, primers used for cloning the ARD into the BamHI site of the pET19b vector were used to amplify the same fragment using RR/QP mutant cDNA as template. This fusion protein showed reduced binding to ATP compared to the wildtype (Fig. 26f). Together, these results suggest that the ANK3-4 linker region encompassing residues R153 and R154 binds ATP's negatively charged phosphate moieties and is crucial for its physiological effects. Phosphorylation at S144 and possibly at S155 in the case of TRPV6a may prevent binding either by charge screening or by inducting conformational change.
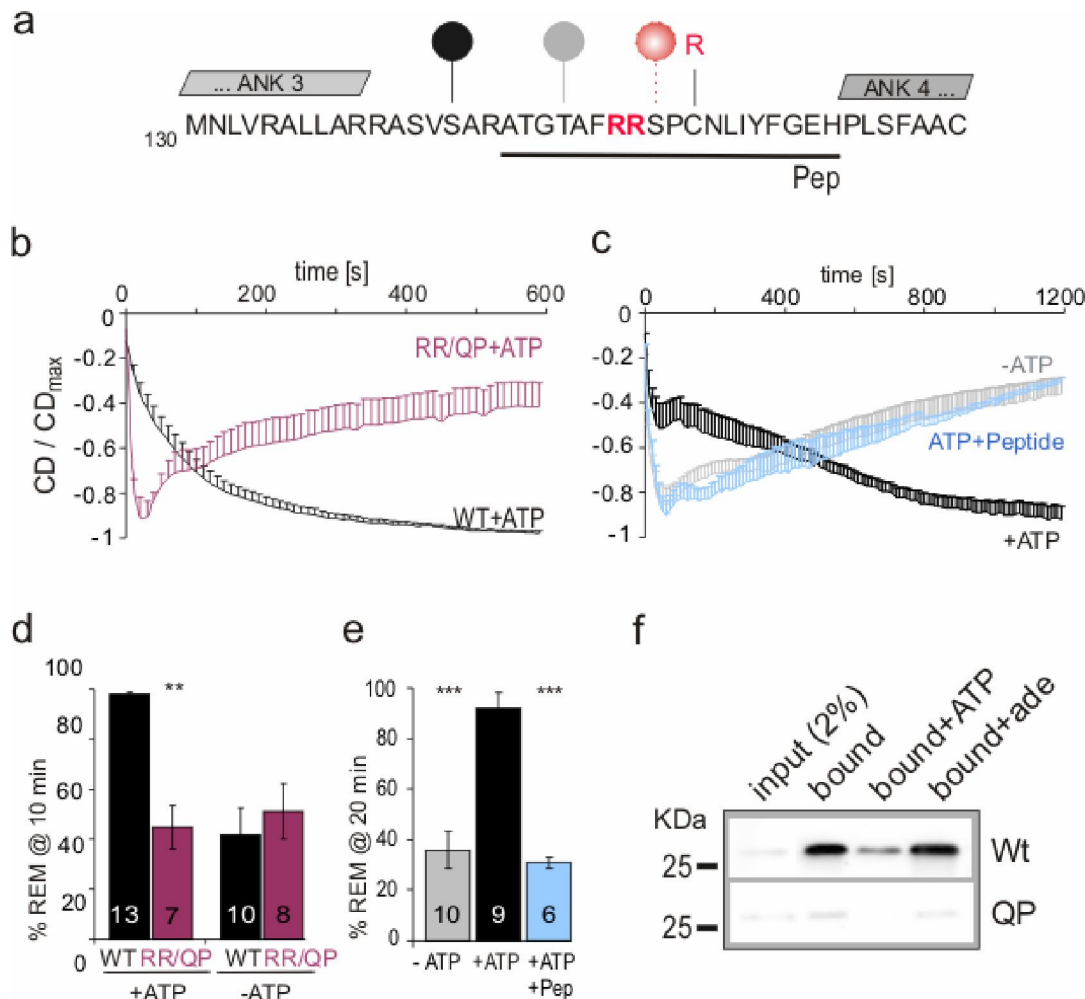
Figure 26: S144 is a critical PKC phosphorylation site**. a.** Linker region between ankyrin repeats 3 and 4 showing the first consensus site (S144, black circle) for PKC mediated phosphorylation according to the Prosite algorithm. Serine 155 (red circle) is a potential phosphorylation site only in TRPV6a. Threonine 150 (light grey) is the site most likely to be phosphorylated according to the NetPhosK algorithm. Underlined is the peptide sequence used for competition. **b.** Normalized current densities over time for transiently expressed TRPV6-wildtype (black) and R153Q/R154P mutants (purple) in the presence of 3.7 mM free ATP. **c.** Normalized current densities over time for transiently expressed TRPV6-wildtype recorded in the presence of 609 μM free ATP (black trace), 609 μM free ATP + 2 mM competing peptide (blue trace) or without added ATP (grey trace).**d-e.** Quantification of run-down of currents measured in (b) and (c), respectively. **f.** ATP-agarose pull-down experiment with wildtype and R153Q/R154P (QP) mutant fusion proteins of the ARD (aa 43-268). Input or bound His-tagged fusion proteins were detected by Western blot using an anti-HIS antibody. Binding was competed with 6 mM ATP but not with 6 mM adenosine (ade).

8.1.3 Regulation of mouse TRPV5 and mouse TRPV6 by PKC-mediated phosphorylation

Both mTRPV6 and mTRPV5 contain positive charges at position 153 and both show the ATP effect (Fig. 27b,c). Moreover, mTRPV5 shares the putative consensus sites of TRPV6 except the C-terminal T688. Therefore, we recorded from mTRPV5-expressing cells preincubated with PMA to test if mTRPV5 is similarly regulated by PMA despite the lack of the C-terminal site. PMA was not able to

revert the effects of ATP on mTRPV5 cells indicating the relevance of the C-terminal site for regulation by PMA (Fig. 27c). These results, in addition to the aforementioned ATP pull down and mutational analyses data, point towards a synergistic role of the C-terminal phosphorylation site together with the ARD region in mediating the effect of PMA.
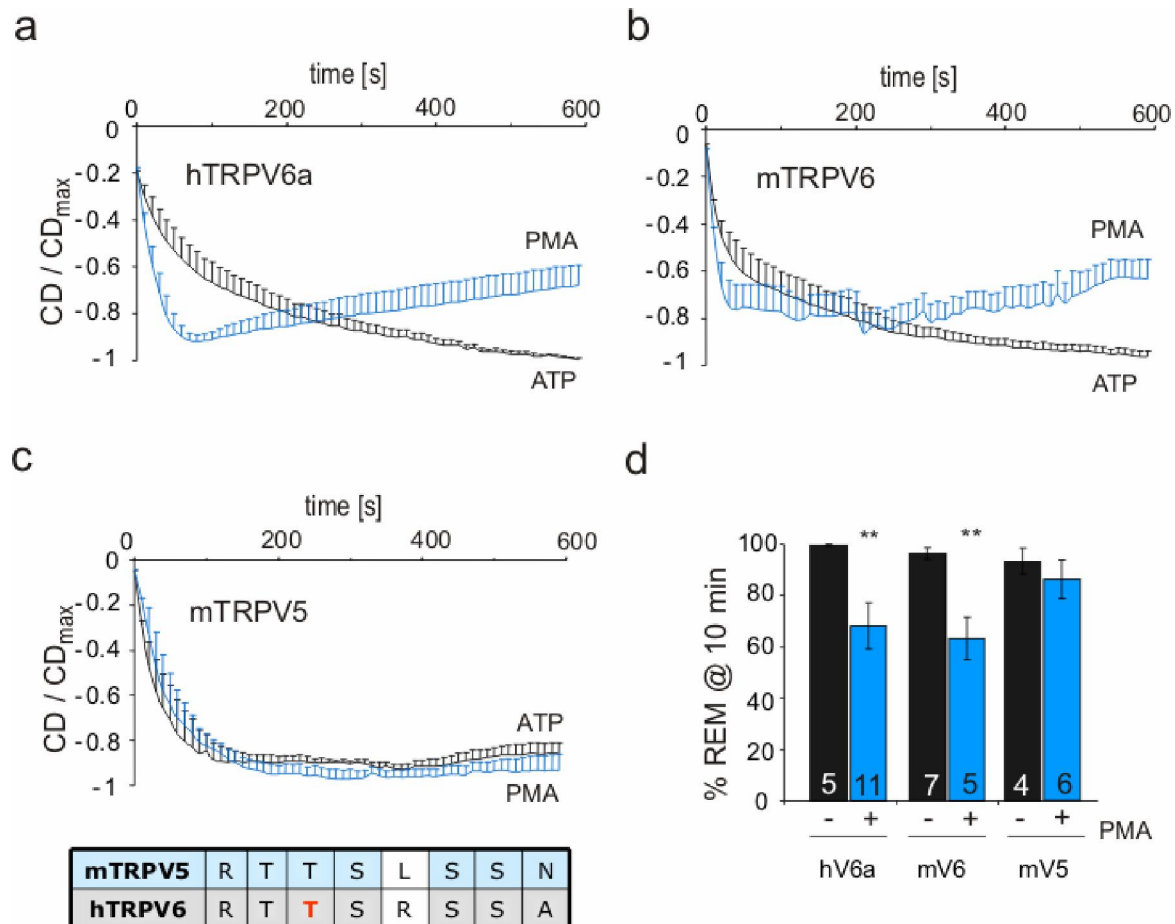

Figure 27: Regulation of other TRPV channels by PKC-mediated modulation: Normalized current densities over time for **(a)** transiently expressed TRPV6a, **(b)** mTRPV6, **(c)** mTRPV5-expressing control cells (black) and cells that were pretreated for 1hr with 500 nM PMA, also PMA present in bath solution (blue), for both 6 mM ATP included in patch pipette, error bars represent +SEM. **c.** lower panel is the alignment of mTRPV5 and hTRPV6 showing PKC consensus site T688 in hTRPV6 and lacking in mTRPV5. **d.** Quantification of run-down (%REM) after 10 min, in presence of ATP without (black), or with (blue) pretreatment with PMA.

8.1.4 Transient expression of TRPV6 is accompanied by increased oxidative stress

When we recorded from cells transiently expressing TRPV6 we noticed that current development was faster (Fig. 28b) despite the presence of ATP, but the extent of rundown was similar (Fig. 28a). It is well established that thiol oxidizing compounds, including hydrogen peroxide (H_2O_2), can influence ion transport mechanisms (Kourie, 1998) including calcium channels (Zima and Blatter, 2006). We therefore investigated if the altered kinetics of currents development could be due to oxidative stress accompanying transient transfection.
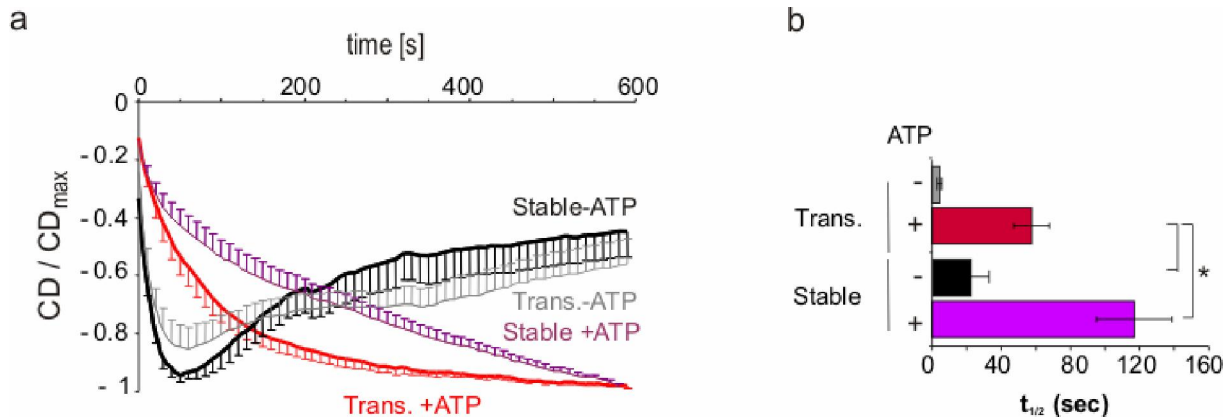
Figure 28: Whole-cell inward current densities (CD) measured at –80 mV ramp potential normalized to CDmax and plotted over 10 min recording time. **a.** Traces are averages of HEK cells stably expressing (black, violet) or transiently transfected with (grey, red) TRPV6b. Error bars represent mean ± SEM. currents recorded in absence or presence of 6 mM ATP as indicted on traces. **b.** Bar graph showing quantification of the time to half-maximal activation for stably and transiently expressing cells in absence and presence of ATP.

To check if transient transfection causes oxidative stress, we employed the oxidative stress indicator 2,7-dichlorofluorescin (DCF). The rate of DCF oxidation depends on the concentration of glutathione, another alternative target of reactive oxygen species (ROS). Therefore, intracellular oxidation of DCF can be used to measure the production of ROS and to monitor the oxidative status of a cell (Jakubowski and Bartosz, 2000). The fluorescent signal of DCF in transiently transfected cells was almost five times stronger than that of the stable cells (253±44 RU vs. 57±3 RU) (Fig. 29c-f) indicating that transient transfection was accompanied by increased oxidative stress which might interfere with the interaction between ATP and the channel alter kinetics of current development.
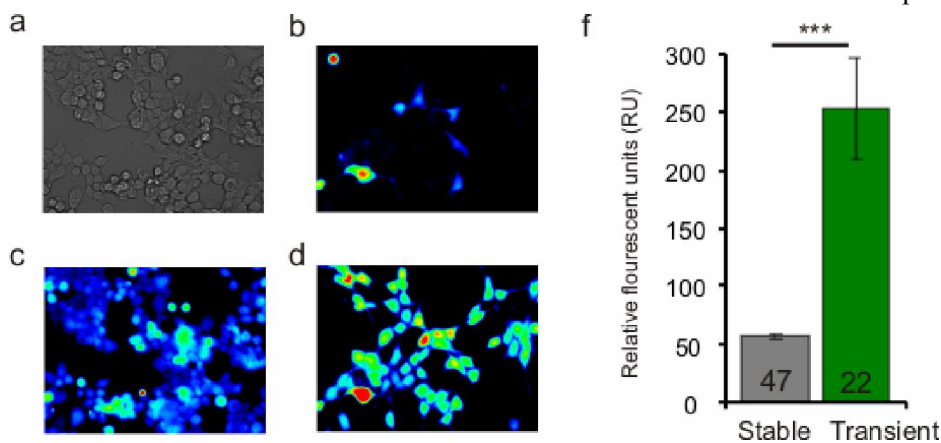
Figure 29: Measurement of H_2O_2 levels in stably and transiently-expressing TRPV6 cells preincubated with 1 μM CM-H_2DCFDA (DCF). The measurements were performed in 96-well plates at 485 nm excitation and 535 nm emission. **a.** Transillumination image of TRPV6b stable cell line **b.** Fluorescent image of HEK cells transfected with TRPV6b using GFP filter. **c-d.** DCF image of TRPV6 stable and transient cells, respectively. **f.** Quantification of DCF signal, numbers represent count of cells measured.

To confirm that increased oxidative stress is the reason for the faster kinetics of current development observed we recorded TRPV6 currents in stable cell lines in presence of H_2O_2. While in absence of

ATP we could not detect major oxidation-induced differences in current development or rundown (Fig. 30a, d), the slow-down of current development in the presence of ATP, but not the effect of ATP on rundown was much reduced (Fig. 30b-d). These results show that the faster kinetics accompanying transient expression in the presence of ATP are to a large extent due to increased oxidative stress, and also explain the variability of this parameter.
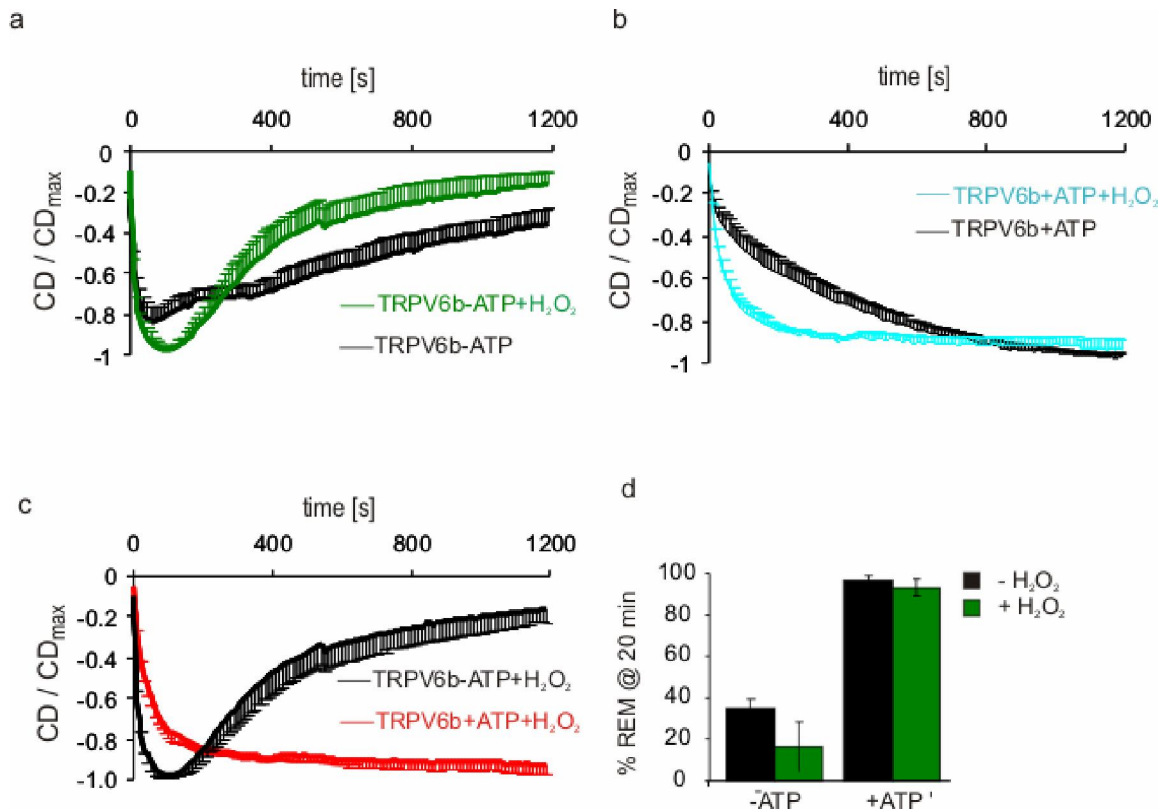
Figure 30: H_2O_2 speeds up current development in presence of ATP: Normalized current densities over time for TRPV6b stably expressing cells **a.** Pipette solution contains no ATP, recordings from control cells (black) or cells in bath solution containing 1mM H_2O_2 **b.** Cells treated as in (a) with 6 mM ATP included in pipette solution. **c.** Recordings from cells in bath solution containing 1mM H_2O_2 with (red) or without (black) ATP in the pipette solution. **d.** Quantification of run-down (%REM) after 20 min, in absence or presence of ATP in pipette solution and without (black), or with (green) inclusion of 1mM H_2O_2 in the bath solution.

8.2   Regulation of ORAI1 channel activity by ROS

8.2.1   ROS blocks ORAI1 mediated currents

Ivan Bogeski, Carsten Kummerow and Markus Hoth in our laboratory generated a set of data in which they investigated differential redox regulation of ORAI channels as a mechanism to tune T-cell responses (submitted manuscript). They show that H_2O_2 extensively reduced the viability of naïve T-helper (T_h) cells with an IC_{50} of ~40 µM while effector T_h cells were more tolerant with IC_{50} of ~200 µM. For the importance of Ca^{2+} influx in T cell proliferation, they investigated the Ca^{2+} signal in both naïve and effector cells. H_2O_2 induced a stronger Ca^{2+} influx in naïve cells with EC_{50} ~130 µM vs. 739 µM for the effector cells. Emptying the stores with thapsigargin (Tg) resulted in a store-activated Ca^{2+} influx that was dose-dependently inhibited by H_2O_2. Again the naïve cells were more sensitive to the effect of H_2O_2 with IC_{50} of ~ 10 µM (naïve) vs. 47 µM (effector). Because H_2O_2 could activate TRPM thereby hyperpolarizing the cell membrane and reducing the deriving force for Ca^{2+} entry, effects of H_2O_2 were also analyzed by comparing cells with similar intracellular Ca^{2+} concentration before Tg induced influx, the so called "iso-cells". The iso-cell analyses confirmed that naïve cells are more sensitive than effector cells to H_2O_2-evoked reduction of store activated Ca^{2+} influx. These results suggest that H_2O_2 inhibits CRAC channel activity. To investigate this, directly, they obtained whole-cell patch clamp recordings. Inclusion of 10 mM EGTA in the patch pipette led to passive depletion of stores and development of typically inwardly rectifying I_{CRAC} in Jurkat T or human effector T cells. The average current density was 2.2 pA/pF within 5 min recoding time. In presence of H_2O_2, current density was reduced to 16% in Jurkat T cells vs 40% for effector T cells, in agreement with the imaging data.

Because T-cell CRAC channel function is mainly encoded for by the Orai1 gene, the next aim was to identify the molecular target of oxidation in ORAI1. Here, our collaboration started. We made use of a HEK293 cell line stably expressing STIM1 (HEKS1) and co-expressed different Orai1 constructs that were necessary to investigate how ROS regulate I_{CRAC}.

To test how the heterologous expression system correlates with the native one, we transfected the HEKS1 stable cell line with Orai1-pCAGGS-IRES-GFP vector (HEKS1O1 cells) and repeated both Ca^{2+} imaging and whole cell recordings. Fura2-preloaded HEKS1O1 cells showed large sustained Tg-induced increases in $[Ca^{2+}]_i$ in absence of H_2O_2 (Fig. 31a black trace) which is ~ 5 fold larger than in HEKS1 cells (Fig. 31b, grey bar). Different concentrations of H_2O_2 inhibited up to 90% (Fig. 31b) of the increase in $[Ca^{2+}]_i$ subsequent to Tg addition with an IC_{50} of 40 µM (Fig. 31c).
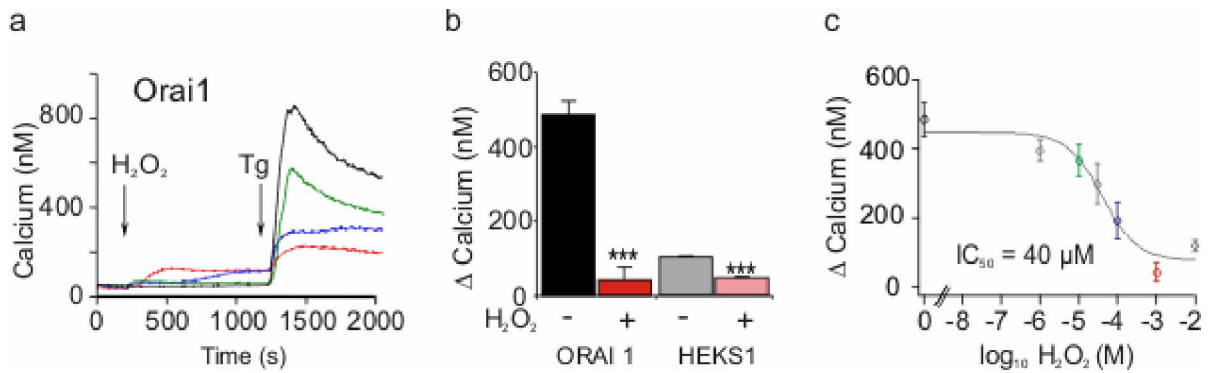
Figure 31: a. Calcium concentration in Fura 2/AM-loaded HEK-Stim1 (HEKS1) cells transiently transfected with Orai1 (HEKS1) before and after addition of different concentrations of H_2O_2, black trace: 0 µM (n=81), green: 10 µM (n=94), blue: 100 µM (n=71), red: 1 mM H2O2, (n=61). **b.** Quantification of the average change in $[Ca^{2+}]_i$ between 1200 s and 2000 s with 0 or 1 mM H_2O_2 in HEKS1O1 (black, red) and HEKS1 cells (grey, pink). (grey: n=244, pink, n=220). **c.** Dose dependence of Tg-induced rise in $[Ca^{2+}]_i$ on $[H_2O_2]$.

Similarly, patch-clamp analyses of HEKS1O1 cells revealed large IP_3-induced currents with an average current density of ~-30 pA/pF after 300 s (Fig. 32a black trace). Preincubation for ≥ 10 min with 1 mM H_2O_2 reduced current density to ~10 pA/pF (Fig.32a red trace). When tested against a range of different H_2O_2 concentrations and fitted to a sigmoidal dose-response function, the IC_{50} for H_2O_2 induced block of I_{CRAC} was 34 µM. In addition, H_2O_2 slowed current development.
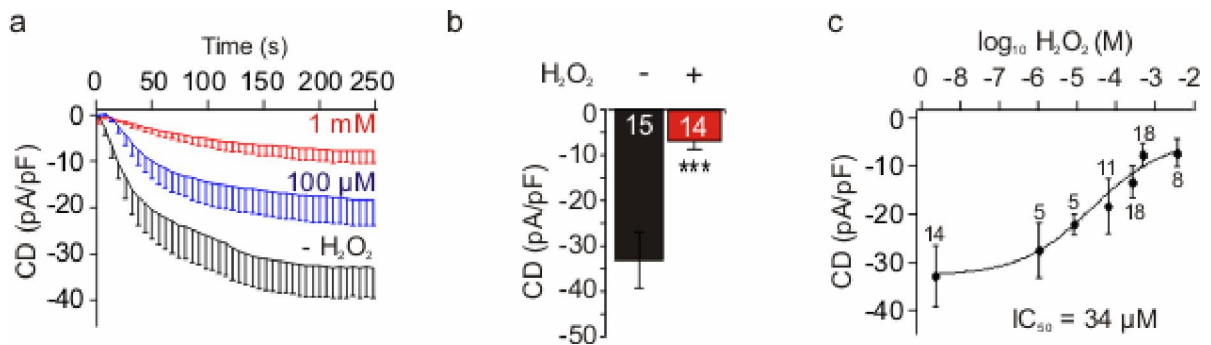
Figure 32: a. Whole cell currents were extracted at -80 mV ramp potential, normalized to cell capacitance and plotted versus time, from HEK-Stim1 (HEKS1) cells transiently transfected with Orai1 in absence (black, n=15) or presence of 100 µM (blue, n=14), or 1 mM H_2O_2, (red, n=14). For clarity, error bars represent SEM at every third data point. **b.** Average current densities analyzed 300 s after break-in in the absence or presence of 1 mM H_2O_2. **c.** Dose dependency of H_2O_2-induced current inhibition.

Interestingly, H_2O_2 only causes inhibition of calcium influx when cells are preincubated. Addition of H_2O_2 after CRAC channels activation blocks neither the Tg evoked increase in $[Ca^{2+}]_i$ (Fig. 33a), nor I_{CRAC} (Fig. 33b). This suggests that oxidation may either reduce activation or clustering of channels directly or of proteins involved in activation (e.g. STIM1).

Figure 33: a. Fluorescence (Fura 2/AM) based measurements of $[Ca^{2+}]_i$ in Orai1 expressing HEKS1 cells, n=72 500 µM H_2O_2 added after development of full Ca^{2+} influx induced by 1 µM Tg. **b.** I_{CRAC} in Jurkat T-cells was induced by passive store depletion and analyzed at -80 mV. 500 µM H_2O_2 added after 3 min recording were current was at stable value (representative experiment by Ivan Bogeski).

8.2.2 ORAI3 channels are insensitive towards oxidation

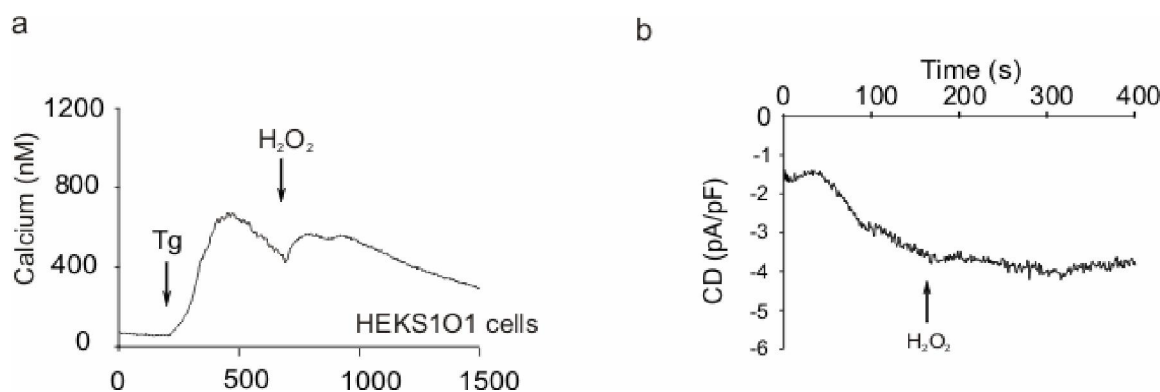As an approach to test whether H_2O_2 influences channel proteins mediating I_{CRAC} directly or affects other proteins involved in activation (e.g STIM) we investigated if and how H_2O_2 affects other homologues of ORAI1. HEKS1 cells transfected with Orai2 (HEKS1O2) showed similar Ca^{2+} signals and inhibition by H_2O_2 (data not shown). Conversely, the Ca^{2+} signal from Fura2 preloaded HEKS1cells expressing ORAI3 (HEKS1O3) showed a Tg-induced increase in $[Ca^{2+}]_i$ which is smaller than that of ORAI1. However, the increase in $[Ca^{2+}]_i$ persisted in the presence of 1 mM H_2O_2 (Fig. 33 a, b). While HEKS1 cells without overexpression of ORAI show a ~ 50% block of Tg induced increase in $[Ca^{2+}]_i$. (Fig. 31b), HEKS1O3 cells show no block, indicating that ORAI3 may have a dominant-negative effect on endogenous store-operated influx pathways. Whole-cell recordings from HEKS1O3 cells showed IP_3-induced currents with much smaller average current densities compared to ORAI1 (-4.9±0.4 vs -33±6 pA/pF), but significantly higher than in HEKS1 cells (-0.5 pA/pF). Similar to the results obtained with Ca^{2+}-imaging, currents were not blocked by preincubation with 1 mM H_2O_2 (Fig. 34 c, d).
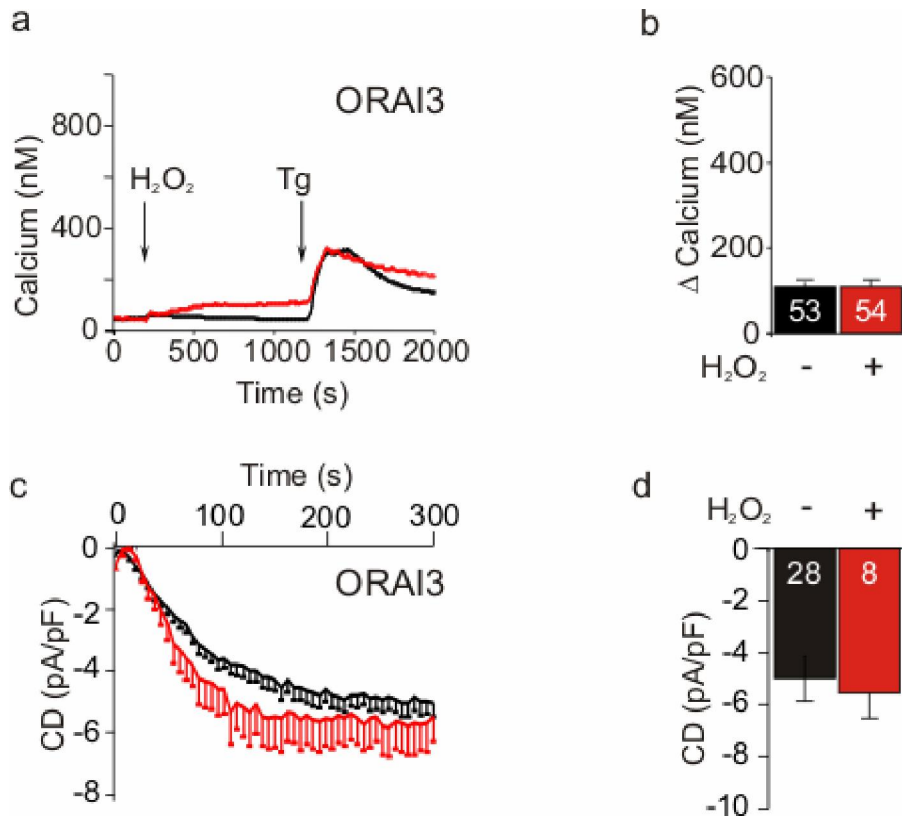
Figure 34: a. Ca^{2+} concentration before and after Tg-induced store depletion in Fura 2/AM-loaded HEK-Stim1 Orai3-transientlytransfected (HEKS1O3) control cells (black, n= 53) or cells treated with 1 mM H_2O_2 (red, n=54) at the shown arrow. **b.** Quantification of the average change in $[Ca^{2+}]_i$ between 1200 s and 2000 s for untreated (black) and cells treated with 1 mM H_2O_2 (red). **c.** Current densities of ORAI3 currents normalized to cell capacitance and plotted versus time of HEKS1O3 control (black) or 1 mM H_2O_2 pretreated cells (red). **d.** Quantification of current densities at 0 (black) and 1 mM (red) H_2O_2 from ORAI3-expressing cells.

8.2.3   Identification of ORAI1´s redox sensor

When a protein is subjected to a redox reaction, cysteines are usually the targets of the redox agent due to their nucleophilic oxidizable thiol group. Comparing the cysteine content of Orai1 and 3 we noticed that Orai1 contains 3 cysteines (C126, C143, C195) with C195 being the most extracellularly located site. On the other hand, Orai3 contains two additional closely spaced cysteines (likely to form disulfide bonds) within the extracellular loop between S3 and S4, but lacks the homolog of Orai1's C195.

Figure 35: Schematic diagram of ORAI1 and ORAI3 showing location of the cysteine residues (red circles). ORAI1 has an extracellular C195 residue lacking in ORAI3 that on the other hand contains two closely spaced cysteines likely to form disulfide bonds

To investigate whether this difference in cysteine content underlies the difference in redox sensitivities of the two proteins, we first performed site-directed mutagenesis on Orai1. We mutated the di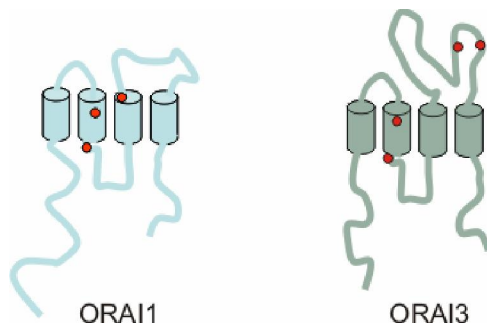vergent cysteine to serine (C195S) and tested regulation by H_2O_2. Because the bicistronic expression vector pCAGGS and Orai1 in pMAX vector were not amenable to site-directed mutagenesis, we subcloned a SmaI digested fragment of Orai1 (NT: 119-692) into pBlue. Site-directed mutagenesis was performed and mutated fragments were cloned into a SmaI digested EGFP-tagged Orai1 in pMAX vector. An additional pMAX vector SmaI site had been previously deleted. Finally, full length Orai1 sequence was amplified and cloned back into pCAGGS (Fig. 36).
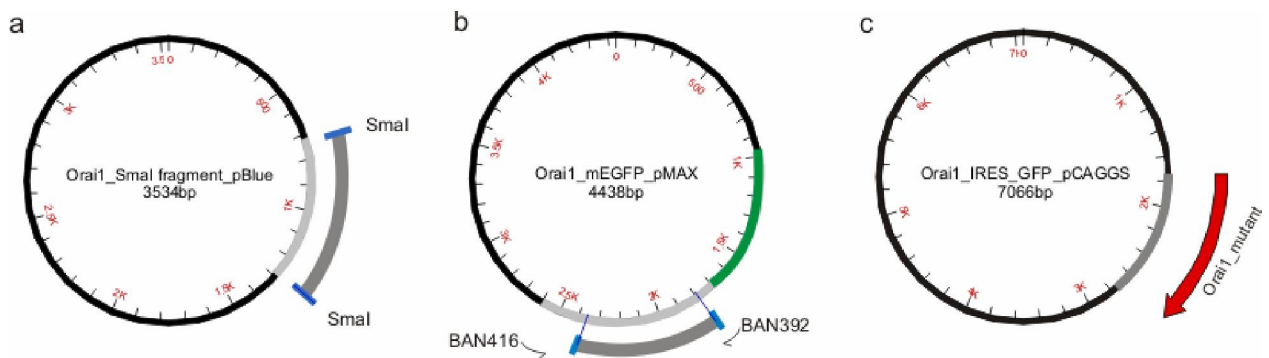
Figure 36: Strategy for cloning different Orai1-mutants. Site directed mutagenesis was done in the Orai1-SmaI digested fragment cloned in pBlue script. Fragments containing mutation exchanged with WT fragment of Orai1 in mEGFP-pMax from which multiple cloning site the SmaI site was previously removed. To obtain the untagged ORAI1, full length sequence was amplified out of mEGFP-pMax and cloned into ERV site of pCAGGS

Measurements of Ca^{2+} signals from C195S mutants showed that block of Tg-evoked increase in $[Ca^{2+}]_i$ by 1 mM H_2O_2 was much reduced compared to wildtype (Fig. 37b, h). Likewise, whole-cell patch clamp recordings from the C195S in presence of H_2O_2 showed an impaired blockade compared to wildtype (67 vs 37%) (Fig. 37c,i).

If C195 is the major reactive cysteine conferring redox sensitivity, then the introduction of cysteine residue at the equivalent locus in Orai3 may render Orai3 redox sensitive. We created a potential gain-of-function mutation by exchanging the glycine, at the cysteine 195 homologous position of Orai3, to cysteine (G170C). Both imaging data (Fig. 37e, h) and patch-clamp recordings (Fig. 37f, i) confirmed our hypothesis: ORAI3 turned sensitive to H_2O_2 blockade of both Tg-induced Ca^{2+} influx and IP_3-induced I_{CRAC} when a cysteine residue is introduced at the exterior side of the third transmembrane domain.
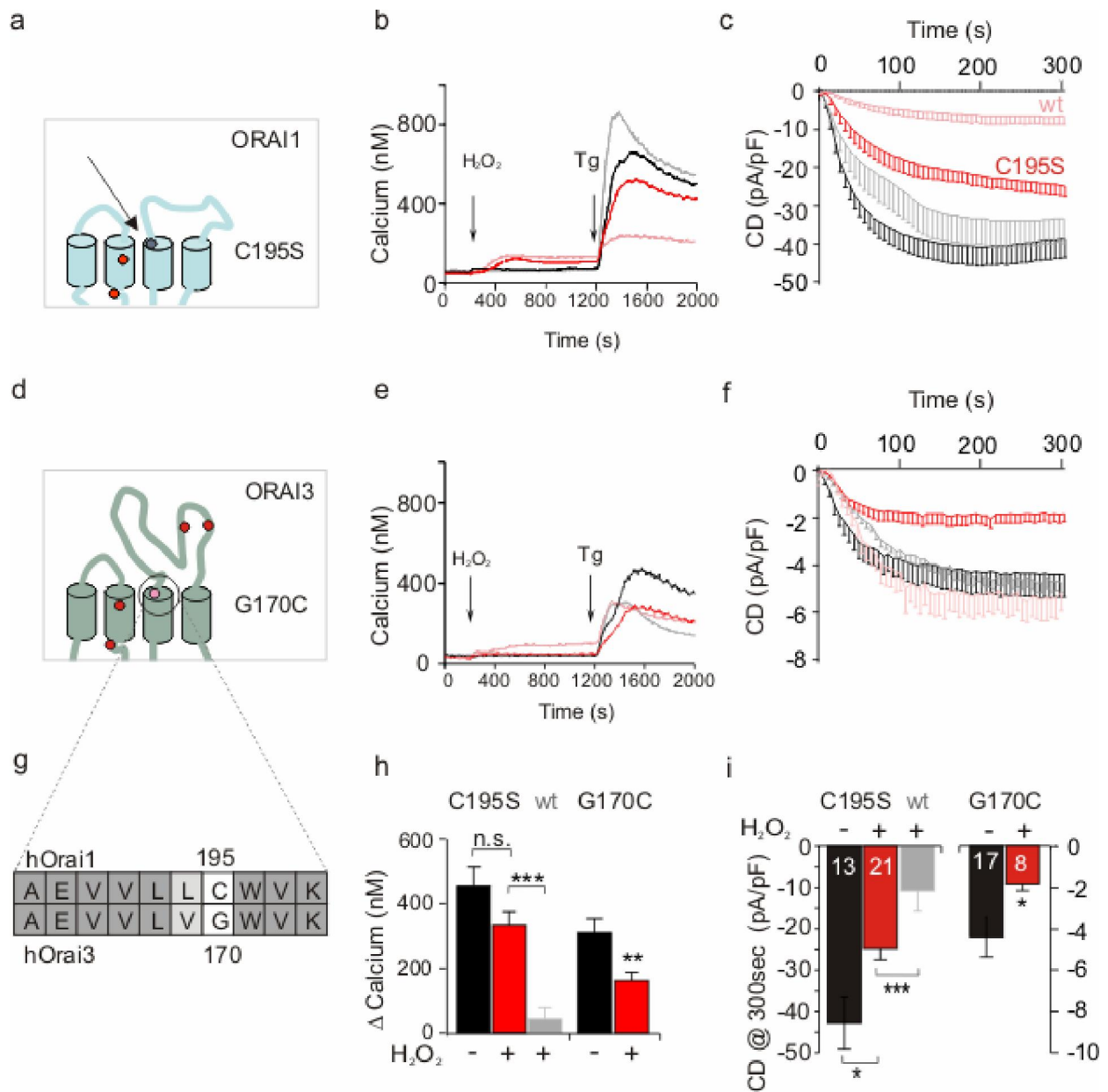
Figure 37: Identification of Cysteine 195 as the major redox sensor of ORAI1 **a.** Schematic topology of Orai1, its cysteines (red) and cysteine to serine mutations (blue). **b.** Calcium imaging experiments of HEKS1 cells expressing C195S mutant channels. The black trace (n=45) represents the average of calcium signal in the absence of H_2O_2, the red trace (n=58) the average after addition of 1 mM H_2O_2, grey and pink correspond to the signals without and with 1 mM H_2O_2 of ORAI1 wildtype. **c.** Current densities were plotted versus time, colour code like in (b). **d.** Same as in a-c for ORAI3_G170C mutant (n=48 for black and 53 for red), grey and pink are ORAI3 wild-type signals. **g.** Alignment of the C-terminal end of the third transmembrane helix of hORAI1 and hORAI3. **h.** Quantification of the change in $[Ca^{2+}]_i$ in HEKS1 cells transfected with ORAI1, ORAI1_C195S and ORAI3_G170C, treated or not treated with H_2O_2. **i.** Average current densities of ORAI1 (grey, untreated), ORAI1_C195S and ORAI3_G170C.

8.2.4 Cysteine195 is ORAI1's major reactive cysteine

To test whether C195 is the residue mainly involved in sensing redox status, we made use of a modified form of biotin (MTSEA-Biotin, Biotrend) that reacts specifically with reactive cysteine residues located at the extracellular sites of membrane proteins when applied to nonpermeabilized cells. Surface labeling of HEKS1O1 cells showed a weak signal corresponding to the presence of reactive sulfhydryl group at the plasma membrane. This signal was much reduced when cells were transfected with C195S or Orai3, respectively, indicating that C195 can serve as a sensor for changes in extracellular levels of oxidants.
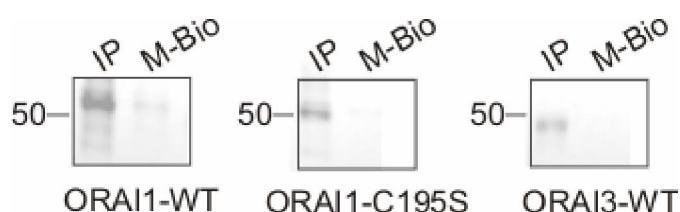
Figure 38: Biotinylation of reactive cysteine. HEKS1 cells transfected with C-terminally EGFP tagged ORAI1-WT, ORAI1_C195S or ORAI3-WT in pMAX were labelled with MTSEA-Biotin, lysed and incubated with avidin beads. Protein fraction were separated by SDS-PAGE and blotted to nitrocellulose membrane and detected by an anti-GFP antibody. IP is 5% of total input (50 μg), M-Bio is total fraction bound to avidin beads

8.2.5 Characterization of other cysteine mutants in ORAI1

We also mutated the other two cysteine residues in Orai1 to test if C195 is the sole sensor or other residues also contribute to redox sensitivity. The C143S mutants showed much smaller currents (-8.0±1.4 pA/pF) that were significantly reduced by pretreatment with 1 mM H_2O_2 to -2.7±0.7 pA/pF (Fig. 39c). Similarly, Ca^{2+} imaging showed reduced signal in HEKS1 transfected with C143S mutants (Fig. 39d). Mutating C126 resulted in currents smaller than wildtype (-18.6±3.4 pA/pF) that were, in contrast to wildtype, enhanced by treatment with 1 mM H_2O_2 likely due to alteration of ion selectivity. From whole cell recordings C126 does not contribute to H_2O_2 induced block of current development, although Ca^{2+} imaging still revealed inhibition (Fig. 39e,d). The triple mutant (TM: C195S, C143S, C126S) completely lost inhibition by H_2O_2 on both Tg-induced Ca^{2+} influx and IP3-induced I_{CRAC} with average current density (20.4±3.9 pA/pF) in between the larger wildtype value and the smaller value of the C143S mutants (Fig. 39a,b).
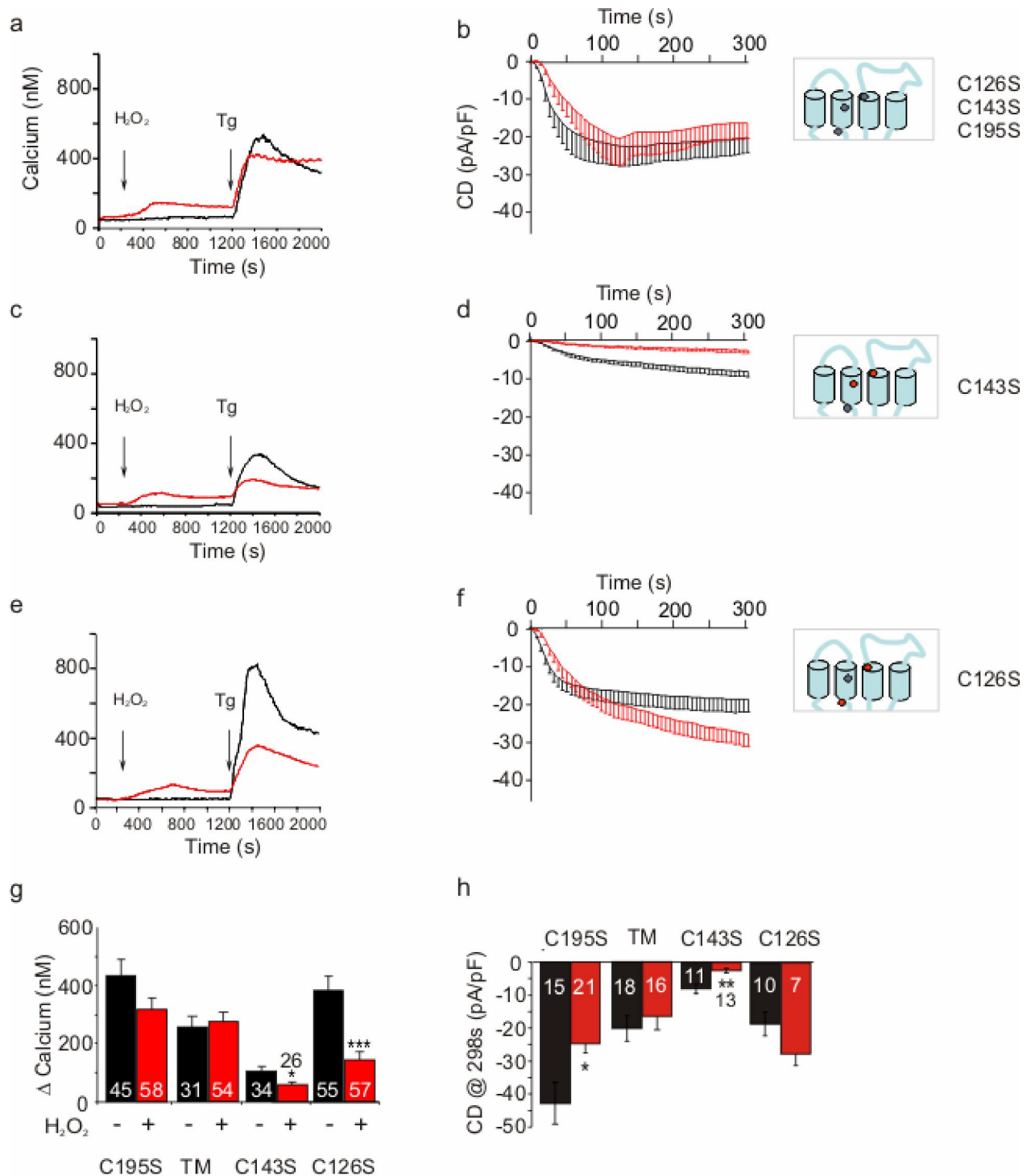
Figure 39: Effect of H_2O_2 on other cysteine residues in Orai1. **a., c., e.**. Ca^{2+} imaging experiments of HEKS1 cells expressing the triple mutant C126/143/195/S; C143S or C126S, respectively. The black traces represent the average of Ca^{2+} signal in the absence of H_2O_2, the red traces represent the average after addition of 1 mM H_2O_2 **b.,d.,f.** Current densities were plotted versus time of mutants as in (a, c, e) with same colour code for non- and pretreated cells. **g-h.** Quantification of the change in $[Ca^{2+}]_i$ or current densities of mutants as in (a-f). Black bars

89

are non treated cells and red bars represent average of 1mM-treated cells. The right panel shows the schematic diagram of the corresponding measured mutant with WT cysteine residue(s) in red and mutated residue(s) in blue.

8.2.6 Expression of Orai1 and Orai3 in naïve and effector Th-cells.

As mentioned above, differentiation of naïve into effector T_h cells was accompanied by an increased tolerance towards H_2O_2. In addition, differentiation was accompanied by an increase in Orai3/Orai1 ratio, as found from the qRT-PCR analysis (Fig. 39a,b) performed in our group (Eva Schwarz) as well as by another independent group (Lioudyno et al., 2008).The following primer pairs were used for amplification of a 193 bp fragment of Orai1 and a 159 bp fragment of Orai3.

Orai1 for   5′-GTACCGGGAGTTCGTGCA-3′

Orai1 rev   5′-GGTACTCGTGGTCACTCT-3′

Orai3 for   5′-GTGGGTAGTCGTGGTCAG-3′

Orai3 rev   5′-GTGGGTAGTCGTGGTCAG-3′

To test whether the altered relative expression of the H_2O_2-sensitive ORAI1 to the H_2O_2-insensitive ORAI3 upon differentiation is the reason for increased T_h effector cells tolerance, we transfected HEKS1 cells with both Orai1 and Orai3 at a ratio of 5/1. HEKS1O1/O3 cells showed significantly less inhibition of I_{CRAC} by H_2O_2 indicating that even a single subunit of ORAI3 in a heterotetrameric complex might be sufficient to alter H_2O_2 sensitivity (Fig. 39c).
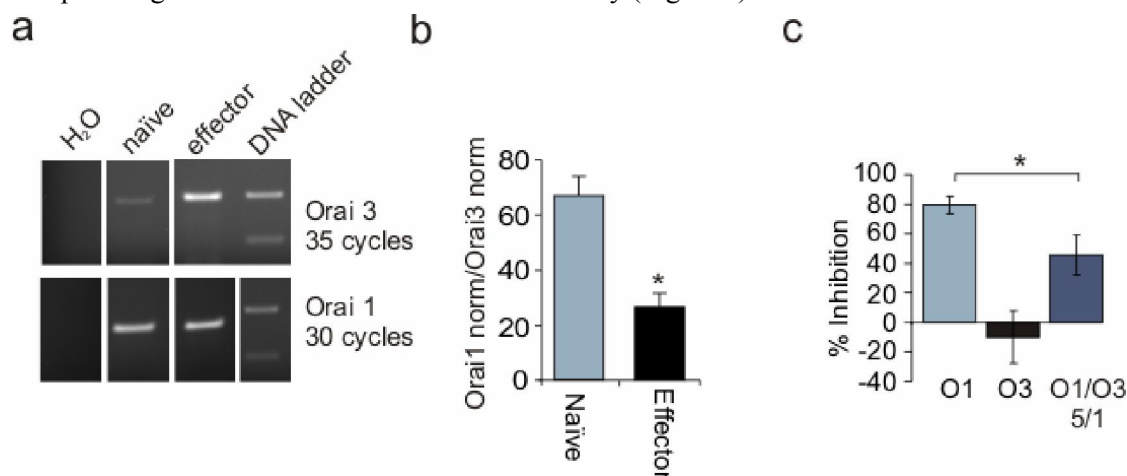
Figure 40: a-b.. Quantitative RT-PCR analyses of Orai1 and Orai3 expression in naïve and 72-96h effector Th-cells **b.** Averaged results from 5 independent blood donors with Orai expression normalized to RNA polymerase. **c.** Percent inhibition (CD $_{1\ mM\ H2O2}$ /average unblocked CD) for HEKS1 cells expressing Orai1 (light blue), Orai3 (black) or Orai1 together with Orai3 at a ratio of 5/1(dark blue). Total amount of DNA transfected was 1 μg for each condition

9 <u>Discussion</u>

Cell signalling involves communication between different intracellular components to mediate perception of stimuli from surrounding milieu while also securing cellular survival and efficiency. Fast cellular signalling works by means of second messengers: a complex system of diffusible components that convey the necessary molecular information within diverse signal transduction cascades. Calcium ions were recognized as second messengers more than 125 years ago (Ringer, 1883) and since then have been shown to be involved in synthesis and secretion of growth factors, hormones and neurotransmitters. Furthermore, Ca^{2+} is involved in direct and indirect modulation of processes such as proliferation, fertilization, muscle contraction, immune response and apoptosis. Not only is Ca^{2+} important for physiological processes but also an imbalanced $[Ca^{2+}]_i$ can lead to development of several diseases. Mutations in Ca^{2+} sensor or binding proteins or in Ca^{2+} channels lead to molecular dysfunction which ranges from altered gene expression to post-translational protein modification leading eventually to pathogenesis. For example, an EF-hand malfunction in the Ca^{2+} binding protein calpain-10 has been shown to mediate an increased susceptibility to diabetes (Baier et al., 2000). In addition, many neurological and retinal disorders involve neuronal sensor (NCS) proteins. One example is autosomal-dominant cone dystrophy which is caused by a mutation in the guanylate cyclase-activating protein-1 (Sokal et al., 1998). Moreover, several human diseases including autosomal-dominanat hypokalemic periodic paralysis, malignant hyperthermia, Huntignton's disease and several autoimmune diseases are linked to mutations in Ca^{2+} channels [reviewed in (Carafoli, 2004)]. A very tight control of Ca^{2+} homeostasis is therefore vital. Within the blood and the interstitial fluids, $[Ca^{2+}]$ is kept between 1-2 mM (Carafoli, 1987; Clapham, 2007) and is regulated via absorption from the intestine and mobilization from bones on one side and its excretion via the kidneys or deposition in bones on the other side. Intracellularly, $[Ca^{2+}]$ is kept at ~100 nM by the interplay of Ca^{2+} sources, namely Ca^{2+} channels at the plasma or endo- and sarcoplasmic reticula membranes, and a number of ubiquitous Ca^{2+} pumps and buffers, either soluble or intrinsic to membranes, that reversibly complex Ca^{2+} with variable affinities [Ca^{2+} signalling reviewed in (Bootman et al., 2001; Carafoli, 1988; Perez et al., 2008)].

The current work aimed at studying mechanisms regulating two Ca^{2+}-selective ion channels belonging to two different ion channel families. The results obtained present biochemical and electrophysiological evidence that the activity of the Ca^{2+} selective TRPV6 channel is linked to intracellular ATP levels where ATP directly binds to the channel protein and modulates its susceptibility to Ca^{2+}-dependent and independent regulatory mechanisms. In addition, the data shows that phosphorylation of TRPV6 at two distinct sites opposes the effects of ATP.

This work also shows that the concentration of extracellular oxidants is able to directly alter the activity of ORAI1, but not other closely related members of the same family of channels. The data also suggests that modulation by redox is the basis of how T cells become less sensitive when developing from the naïve to effector status. Importantly, the results identify a specific residue involved in interaction with oxidizing agents.

91

9.1   Sufficient intracellular ATP levels are able to sustain activity of TRPV6

While processes such as paracellular Ca^{2+} transfer in intestinal or renal epithelial cells, follow the concentration gradient and are energetically "favoured", cells have to invest a significant fraction of their energy to keep the free $[Ca^{2+}]_i$ in the nM range against a gradient that it ~10,000 fold higher. Therefore, one can anticipate that the activity of a Ca^{2+}-specific channel is regulated by ATP levels to allow for Ca^{2+}-influx only when sufficient energy equivalents are available for rapid extrusion. Among other channels shown to be regulated by ATP, regulation of K_{ATP} channels has been most thoroughly investigated. In our work we investigated if and how ATP regulates TRPV6 activity. Whole cell recordings show that inclusion of ATP slows down the "on" kinetics of TRPV6-mediated currents and protects channels against mechanisms causing inactivation or run-down. Though a related observation of the stabilizing effect of ATP on TRPV6 was previously reported, it was not further investigated (Hoenderop et al., 2001).

A well documented feature of TRPV6 currents is the two-component Ca^{2+}-dependent inactivation during application of hyperpolarizing pulses to negative potentials, an inactivation that is not observed when Ba^{2+} is the charge carrier (Hoenderop et al., 2001). Part of the ATP effect can be explained by interference with Ca^{2+}-dependent inactivation or possibly by a rapid, though low affinity, Ca^{2+} buffering effect of ATP since ATP prevents pulse inactivation with 10 mM internal EGTA but not with 20 mM BAPTA (Fig. 12). Nevertheless, the sole interference of ATP with Ca^{2+}-dependent mechanisms could be excluded by the ATP-induced prevention of rundown during repetitive voltage ramp stimulation of wildtype TRPV6 in presence of 20 mM BAPTA and of a mutant lacking the calmodulin binding site (ΔCAM). In addition, Hoenderop et al. demonstrated that ATP was able to prevent rundown in divalent free bath.

Thyagarajan and colleagues (Thyagarajan et al., 2008) have recently shown that PIP_2 (phosphatidylinositol-4,5-biphosphate) is, unlike other phospholipid metabolites tested, able to activate TRPV6 and prevent Ca^{2+}-induced inactivation. They also showed that Ca^{2+}- but not Ba^{2+}-influx via TRPV6 reduces intracellular level of PIP_2. In our hands, replenishment of PIP_2 via the patch pipette solution is not able to prevent rundown. Additionally, a mutant likely unable to bind PIP_2 (Rohacs et al., 2005) still shows ATP-induced prevention of rundown. Together this data shows that the ATP effect is not entirely dependent on PIP_2 production nor does it require hydrolysis. In line with a PIP_2-independent effect is the finding that the nonhydrolyzable analogue AMP-PCP is also able to slow current development and prevent rundown. Similarly, AMP which cannot be further hydrolyzed slows current development and prevents rundown though not as efficient as ATP. The fact that adenosine, mono- or diphospho-nucleotides and nucleotides having different nucleobase are either unable to or less efficient in preventing rundown than ATP indicates that the ATP effect requires at least one phosphate and is nucleotide-specific.

An additional argument for the link between functional TRPV6 and sufficient ATP is that ATP depletion was deleterious to the TRPV6-mediated Ca^{2+} influx triggered upon shifting to a higher $[Ca^{2+}]$-containing bath. We estimated the intracellular level of ATP that is needed to prevent TRPV6

rundown by measuring the % REM to different concentrations of free ATP. The obtained EC_{50} was ~378 µM. The cytosole contains 5-10 mM total ATP (Katz and Lorell, 2000), and 14-20 mM total Mg^{2+} (Grubbs and Maguire, 1987). However, Mg-ATP is the most abundant form in the cell leading to free $[Mg^{2+}]_i$ of 0.5-0.7 mM (Grubbs and Maguire, 1987; Romani and Scarpa, 1992) and free $[ATP]_i$ of less than 0.5 mM (Gajewski et al., 2003). Thus, the obtained EC_{50} is in agreement with the physiological levels of ATP.

9.2   Phosphorylation counteracts ATP regulatory effects on TRPV6

For many ion channels the crosstalk between ATP levels and protein kinases is shown to influence channel activities For example, in TRPV1-expressing cells ATP has been shown to increase currents evoked by capsaicin or protons through activation of P2Y metabotropic receptors in a PKC-dependent manner (Tominaga et al., 2001). Considering the fact that TRPV6 has several putative sites for PKC-mediated phosphorylation it was conceivable that a mutual influence between the two regulatory ligands exists for TRPV6 as well. If higher levels of intracellular ATP were to increase preactivated PKC activity and thereby prevent rundown, the prediction would be that inhibiting PKC would lead to rundown even when ATP is continuously supplied via the patch pipette. To our surprise, it was not inhibition (data not shown) but activation of PKC that led to significant rundown for both alleles (Fig. 21). Interestingly, TRPV6a showed more extensive rundown with a remaining current that completely reverted to the no ATP level. This means that stimulating PKC has distinct effects that are able to counteract the effects of ATP.

In order to analyze the effects of PMA on PKC-mediated phosphorylation we aimed to first prove those effects PKC-specific then link them to one or more of the putative phosphorylation sites. Specificity was demonstrated by the inability of the PMA analogue, 4-αPDD, which is able to bind to C1 domains but does not activate PKC, to simulate the effect of PMA. Site directed mutagenesis was used to disrupt PKC consensus sites. This enabled us to pinpoint two physiologically relevant PKC consensus sites, S144 and T688, which, when mutated to alanine, led to loss of the PMA effect. This finding indicates PMA effects involve PKC-mediated direct phosphorylation of the channel. Unexpectedly, we were not able to simulate the effects of PMA by mutating the serine or threonine to the phosphomimetic aspartic acid residues (data not shown). Though this finding questions whether the channel is directly phosphorylated, the *in vitro* phosphorylation experiment using recombinant $PKC_{\beta II}$ argues that it indeed is. The fact that mutation to aspartatic acid does not revert the ATP effect is maybe due to the smaller size of the substituting amino acid or smaller charge to mass ratio compared to that added by phosphorylation, hence being unable to sterically hinder the binding of ATP to an adjaced site, as discussed below.

A puzzling observation was that the classical PKC inhibitors (Bis and Gö6983) were not able to block the effects of PMA. A thorough screen of available literature revealed that this pair of inhibitors had well defined IC_{50} for PKC isoforms except $PKC_{\beta II}$. If phosphorylation were to be mediated by this particular isoform of PKC then a specific inhibitor would be needed to block the effect of PMA. This

was the case when Ro-31-8220 was applied and suggested that the PMA effect was mediated by PKC$_{\beta II.}$

Another puzzeling observation was that the effects of PMA could only be observed with a preincubation time that is much longer than needed for translocation of PKC to the membrane. We exploited this observation to further confirm that PMA is exquisitely mediated by PKC$_{\beta II}$. The expression level of this isoform is rather low in HEK293 cells (Feng et al., 1998) requiring prolonged preincubation for a sufficient number of enzyme molecules to find their targets at the plasma membrane. Overexpression of this isoform actually precluded the need for preincubation and the effects of PMA were immediate.

Besides direct phosphorylation of TRPV6 and steric hindrance of ATP interaction, it is possible that PMA has other indirect effects. PMA increases production of ROS within the cell (Chen, 2002) which can result in the observed faster current development (see below). In addition, it has been shown that stimulation of PKCδ is accompanied by membrane blebbing, as early as 20 min after stimulation with PMA (Goerke et al., 2002). Membrane blebbing is an early hallmark of apoptosis that we also observed when we investigated translocation of stimulated PKC$_{\beta II}$ (data not shown). Accordingly, it is possible that PMA-induced current rundown is part of the apoptotic process that the cell undergoes when stimulated with PMA.

9.3   Identification of ATP binding sites in TRPV6

The *in-vitro* translated full length TRPV6 protein is retained by ATP-agarose despite the fact that TRPV6 lacks typical ATP binding motifs such as Walker motifs A, B, C (Azzaria et al., 1989; Gottesman et al., 1996; Loo and Clarke, 1995). We used fusion proteins to "dissect" the protein and narrow down a potential ATP-binding site. Pull down experiments using the distal part of the N-terminus (NP) show variable and inconclusive binding. Whole cell recordings from mutants of the two phosphorylation sites within this domain (T298/299A) indicate that phosphorylation is still able to revert the effect of ATP although to a less extent than the wildtype. The proximal part of C terminus was consistently retained by ATP-agarose. Nevertheless, owing to the poor specificity we anticipate that this domain is not physiologically relevant. Conversely, the ARD and CT2 fusion proteins were consistently and specifically retained by ATP-agarose and the effect of phosphorylation was completely abolished in mutants of phosphorylation sites within both of these domains. These latter findings strongly indicate that a binding site at both domains is likely to regulate channel activity.

In a previous report investigating structural and ligand-binding properties of ARDs of TRPV5 and TRPV6, mTRPV6-ARD was not retained by ATP-agarose (Phelps et al., 2008). The discrepancy between previous and current findings could be explained by species difference (mouse vs. human), the use of different type of agarose which could alter accessibility of ATP to binding due to different linker lengths and differences in elution buffers. In contrast to Phelps et al, the elution buffer used in current work did not include 2 mM EDTA or 1 mM DTT. Inclusion of the latter components led to reduced binding (data not shown). However, taking into account that the binding we observed with rTRPV1 was weaker than that already demonstrated by the same group in an earlier study (Lishko et al., 2007),

we considered the differences in our experimental conditions. Proteins purified under native conditions showed similar binding and specificity to those purified in presence of urea.

Considering possible mechanisms explaining the effect of ATP on channel activity other than direct binding, an effect on single channel conductance is unlikely because both identified binding sites are distant from the selectivity filter identified in the pore region (Voets and Nilius, 2003). However, it is still interesting to perform single channel recordings and investigate whether ATP alters opening time duration or open channel probability that has been shown to be reduced by ATP for TRPC6 and TRPC7 (Shi et al., 2004) but increased for inositol (1,4,5)-triphosphate receptor (InsP3RI) (Betzenhauser et al., 2009). An effect on expression level or exocytosis of TRPV6-containing vesicles is argued against by the unchanged maximum current density without vs. with ATP.

9.4 The Ank3-Ank4 linker region contains essential amino acids for regulation by phosphorylation and ATP

The nature of interaction between ATP and channel protein is unclear. Yet, the opposition of two similarly charged moieties, ATP and phosphates added by phosphorylation, suggests an electrostatic nature of this interaction. With this assumption in mind we screened residues in the vicinity of physiologically relevant phosphorylation sites identified by our data that would mediate this interaction. Mutational analysis of the positively charged residues (R153, R154) within Ank3-Ank4 linker region argues for electrostatic interaction of ATP with TRPV6 at this region. In agreement is the competition for ATP by a peptide including sequence of this linker region.

Figure 41: Structure of TRPV6-ARD. The left panel is alignment of ARDs of mammalian TRPV channels separated into individual repeats (ANK1-6). Residues that conform to the ankyrin repeat consensus (indicated above each repeat) in all species are colored dark green, and ankyrin repeat residues conserved in just mammalian TRPVs are colored light green. Residues that are conserved in TRPV ARDs and either are not part of or deviate from the ankyrin repeat consensus are colored dark blue for residues conserved in all species and light blue for residues conserved in mammalian TRPV ARDs only. For ARDs where a structure is yet to be determined (TRPV3, TRPV4 and TRPV5) the human sequences are used. The sequence of crystallized species is used for ratTRPV1, ratTRPV2 and mouseTRPV6. The secondary structure of TRPV1-ARD (dark grey) is indicated above each repeat, and the secondary structure of TRPV6-ARD (light grey) is shown below. Insertions in TRPV1-4 commpared to TRPV5 and TRPV6 are shown in red. Left panel: Sequence similarities mapped onto the overall structure of TRPV6-ARD. The relative backbone is colored according to sequence similarity in the alighnment shown in the right panel (Phelps et al., 2008).

The crystal structure of TRPV6 ARD revealed six ankyrin repeats each having characteristic antiparallel inner and outer α-helices and finger loops connecting the helical layers (Fig. 41) (Phelps et al., 2008). Variable residues, most likely specify binding partners, are found on the exposed faces of the repeat helices and at the tip of the finger loops while the conserved ankyrin-repeat consensus residues consist the hydrophobic core. Hence, the location of the arginine residues at the solvent exposed tip of finger loop 3 makes it probable that ligands bind to this region. In addition to the arginine residues, the finger loop between ANK3 and ANK4 contains the phosphorylation site shown to be physiologically important for the PMA effect (S144) (Fig.25c). This region also contains the T150 phosphorylation site, mutants of which still showed the PMA effect, and the polymorphic phosphorylation site present only in the ancestral allele (Fig. 42). The variable relevance of different residues within this domain points to the importance of conformation of the channel that governs exposure of these residues and determines accessibility of the channel to different regulatory ligands.
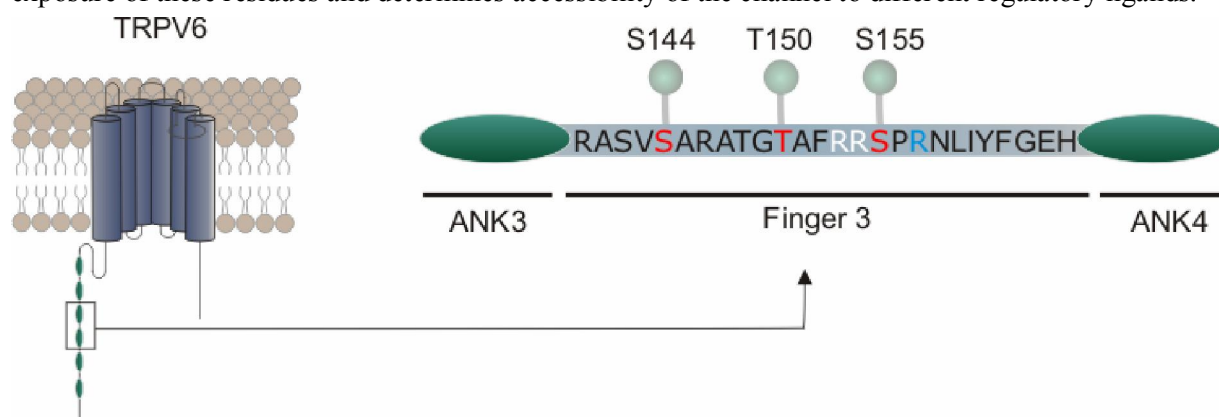

Figure 42: The ANK3-ANK4 linker region. Right panel is enlarged view of the ankyrin repeats 3 and 4 encircled in the schematic presentation of TRPV6 in the left panel. The finger loop3 between ANK3 and ANK4 contains three putative PKC phosphorylation sites (red: S144, T150 and S155) in TRPV6a, the S155 is lacking in TRPV6b. In addition, the finger 3 contains the arginine residues (white: R153, R154) shown to be essential for interaction with ATP.

9.5   TRPV6 acts as a signal integrator

Evidence gathered in this work indicates that TRPV6 is able to integrate signals reflecting cellular ATP levels on one side and activation of $PKC_{\beta II}$ on the other side. With sufficient intracellular ATP, influx of Ca^{2+} is permitted through TRPV6 raising $[Ca^{2+}]_i$ to a threshold initiating a chain of Ca^{2+} dependent and independent inactivation mechanisms. Ca^{2+}-ATPases sense the rise of $[Ca^{2+}]_i$ above the resting levels and start pumping Ca^{2+} in an ATP-consuming process. A drop in $[ATP]_i$ may then constitute a feedback signal that down regulates the activity of TRPV6 manifested experimentally as a rundown phenomenon. Conversely, at free $[ATP]_i > 400$ µM ATP binds at both C- and N-termini of the protein, maintaining the channel in an open conformation. The influx of Ca^{2+} can activate a plethora of regulatory mechanisms among which is phosphorylation. A fully functional PKC requires a rise in $[Ca^{2+}]$, binding of either diacylglycerol (DAG) or phorbol ester (Burns et al., 1990; Hannun et al., 1985; Kaibuchi et al., 1981) and anionic lipids, in particular L-phosphatidylserine (PS) (Burns et al., 1990; Lee and Bell, 1989). It is possible that a rise in $[Ca^{2+}]_i$ initiates an upstream signal via a G-

protein coupled receptor (GPCR) that in turn activates $PKC_{\beta II}$ (Shirai and Saito, 2002) leading to channel phosphorylation. If the channel is phosphorylated, the added negatively charged phosphate moieties shield the positive charges at the N-terminus and a yet not well defined putative binding site at the C-terminus preventing ATP binding and leaving both termini accessible to inactivation mechanisms. The C-terminal domain shown to bind ATP (CT2) contains 11 positively charged amino acids upstream to the calmodulin binding domain (Niemeyer et al., 2001) which we show not likely to overlap with ATP binding domain (Fig. 12e). Biochemical and mutational analyses can provide an insight to residues of most physiological relevance to ATP binding at the C-terminal end of the protein. The low binding affinity of ATP to TRPV6 as assessed by an EC_{50} of ~380 µM allows the channel to respond to small drops in $[ATP]_i$ due to ATP consumption or due to an increase in $[Mg^{2+}]_i$. (Romani and Scarpa, 2000). The consequent downregulation of TRPV6-mediated Ca^{2+} current is important to occur while $[ATP]_i$ is still sufficient for functional plasma membrane Ca^{2+}-pumps [EC_{50} for ATP 0.1-1 µM (Guerini, 1998)] to prevent Ca^{2+}overload.

The finding that phosphorylation of either the N- or the C-terminal site, while the other is mutated, is not sufficient to prevent the effect of ATP implies the need for concerted phosphorylation at both sites and provides additional evidence that ATP binds to multiple sites on the channel. Furthermore, PMA-induced reversion of ATP is observed for mTRPV6 but not mTRPV5, both containing positive charges at position 153 but only the latter lacks the C-terminal phosphorylation site, strongly indicating that regulation at C-terminal region is an ultimate requirement for tuning channel activity.

It is possible that ATP binds C- and N- termini on one subunit or on different subunits thus altering the channel's accessibility to inactivation mechanisms or favouring an open conformation. Antcliff and associates suggested a model of ATP binding to different subunits of the K_{ATP} channel $Kir_{6.2}$ In this model, ATP binds at the interface between two subunits where the phosphate tail of ATP interacts with R201 and K185 in the C-terminus of one subunit, and with R50 in the N-terminus of another; the N6 atom of the adenine ring interacts with E179 and R301 in the same subunit. In this model, contrary to our suggested model, ATP-dependent gating favours closure of the $Kir_{6.2}$ channel (Antcliff et al., 2005). Our data support a model in which TRPV6 has to decipher multiple signals regarding $[ATP]_i$ and phosphorylation status that determine the channel activity. A model of how TRPV6 might integrate these signals is depicted below (Fig. 43).
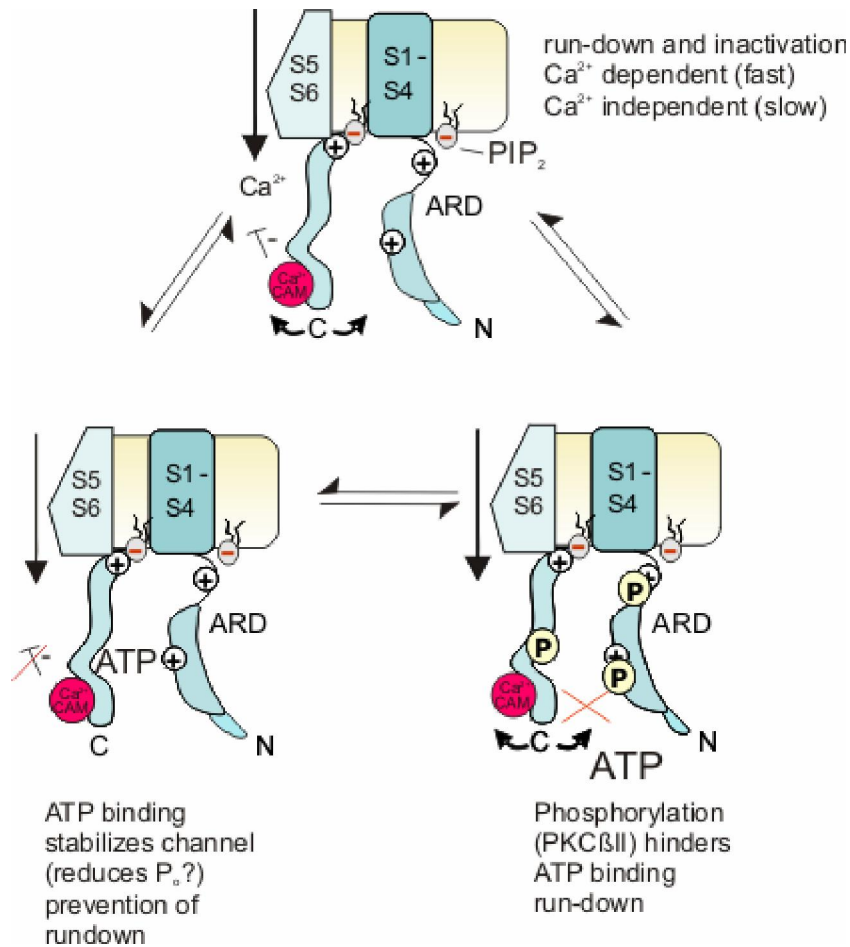
Figure 43: Model of regulatory mechanisms on TRPV6 by ATP and phosphorylation. To simplify graph, only one pore-forming subunit is represented. In the absence of ATP the channel is prone to both Ca^{2+}-dependent (calmodulin) and Ca^{2+}-independent regulation and run-down. Sufficient ATP stabilizes N-and C-termini and prevents channel run-down. Phosphorylation hinders ATP binding thus reduces its stabilizing effect.

9.6 Regulation by phosphorylation unravels a minor difference between the two human TRPV6 alleles

The disclosure of the unique geographical distribution of the two alleles of human TRPV6 prompted several groups to find functional differences that could have conferred a basis for selection. So far, the published studies could detect no difference in electrophysiological experiments (Hughes et al., 2008) or a minor clinical difference in occurrence rate of renal stones (Suzuki et al., 2008b) and, using $^{45}Ca^{2+}$ uptake assay, a higher Ca^{2+} transport activity of the ancestral allele (Suzuki et al., 2008b). In our hands no significant difference could be detected in whole cell recordings obtained from both alleles in absence or presence of ATP regarding current densities or kinetics of current development. The three non-synonymous substitutions in the derived compared to the ancestral alleles are C157R, M378T, M681V. The first substitution (C157R), deletes a putative PKC consencus site (R/SxT). Interestingly, minor but still significant differences were detected regarding regulation of both alleles by PKC phosphorylation. First: while the %REM of the ancestral allele (TRPV6a) was completely reverted by

98

PMA to the rundown seen in absence of ATP, the reversion was only partial for the new world allele (TRPV6b). Second: in absence of ATP, PMA induced no additional rundown for TRPV6a currents while TRPV6b %REM was smaller than without PMA preincubation. A possible interpretation of this difference is that TRPV6a is already phosphorylated at the ground state. That, in addition to the stronger susceptibility of TRPV6a to effects of phosphorylation might be due to the additional PKC phosphorylation site (S155) that the new world allele lost with the first polymorphic substitution.

9.7 Outlook: ROS regulation of TRPV6

The faster kinetics of current development despite the presence of ATP in HEK cells transiently expressing TRPV6 compared to the stably expressing cells support a hypothesis that increased oxidative stress alters kinetics of current development. Direct measurement of H_2O_2 levels and whole cell recordings in presence and absence of H_2O_2 verified the hypothesis (Fig. 29, 30).

Taking the difference in their cysteine content into consideration, it is interesting to find out whether the ancestral and derived alleles react differently to H_2O_2. Using MTSEA biotin-labeling of reactive cysteines can give an insight into susceptibility of the channel protein to regulation by H_2O_2. Therefore, further investigation of ROS regulation of TRPV6 and whether a difference between the alleles imposed a selective advantage will be an exciting field for future research.

9.8 Redox regulation of ORAI channels is a mechanism to tune T-cell responses.

An efficient but well tuned immune response requires exquisite balance between immune activator and suppressor mechanisms. Growing evidence indicates that ROS influence the outcome of an immune response. Both enhanced and deficient ROS production have equally been shown to be involved in initiation or progression of different diseases (Abramov and Duchen, 2005; Droge, 2005; Imai et al., 2008; Voss and Siems, 2006). ROS have also been shown to modulate multiple ion channels (Feissner et al., 2009). However, it was unknown whether ROS regulates ORAI channels. Our interest in regulation of ORAI stems from the fact that ORAI is the main component of CRAC currents in immune cells and thus contributes essentially to the Ca^{2+} signal mediating immune cells' propagation and differentiation in an immune response.

Current work shows that monocytes produce concentrations of H_2O_2 that are permissive for survival of effector but not of naïve T_h cells in their vicinity. Selecting for the effector T_h cells, production of ROS enhances the clonal proliferation of cells more useful in the immune response. In H_2O_2-tolerant T_h cells CRAC currents are likely mediated by heterotetrameric ORAI channels where the levels of ORAI3 are higher compared to their expression in naïve cells [Fig. 40 and (Lioudyno et al., 2008)]. ORAI3 upregulation attenuates the overall inhibitory effect of H_2O_2 on CRAC currents and permits persistence of Ca^{2+} influx necessary for the immune response. As identified by mutational analyses, C195 is the ORAI1's H_2O_2-sensitive residue. Introduction of cysteine residue at the homologous location rendered ORAI3 susceptible to H_2O_2.

Altogether, the data suggests that ROS production plays multiple roles during an immune response. At the periphery of the ROS gradients surrounding the producing APC, concentration of H_2O_2 is very low

(nM to low µM) and is able to actually enhance proliferation of nearby cells (Droge et al., 1987) likely due to an increase in Ca^{2+}-influx. In regions of slightly higher ROS concentrations, T_h -cells will already undergo partial CRAC channel inhibition that will not yet affect viability of effector –cells (Schwarz et al., 2007; Zitt et al., 2004). Within the center of inflammation, ROS concentrations within T-cells reach much higher levels through both increased macrophage activity and massive activation of the TCR mediated signaling (Reth, 2002) that may then activate TRPM channels (Hara et al., 2002), release Ca^{2+} from intracellular stores, affect phosphorylation, cause irreversible cysteine oxidation and ultimately apoptosis (Hildeman et al., 2003). Defects in the cellular H_2O_2 producing machinery (e.g. NADPH oxidases) can lead to autoimmune diseases in humans (Erickson et al., 1992) and mice (Hultqvist et al., 2004). This may be caused by inefficient migration of T_h-cells to sites of inflammation (Niethammer et al., 2009) or compromised T_h activation as well as the inability to derive activated T_h-cells into apoptosis. Our results suggest that redox regulation of Ca^{2+}-signaling can be a mechanism to control the T-cell mediated immune response.

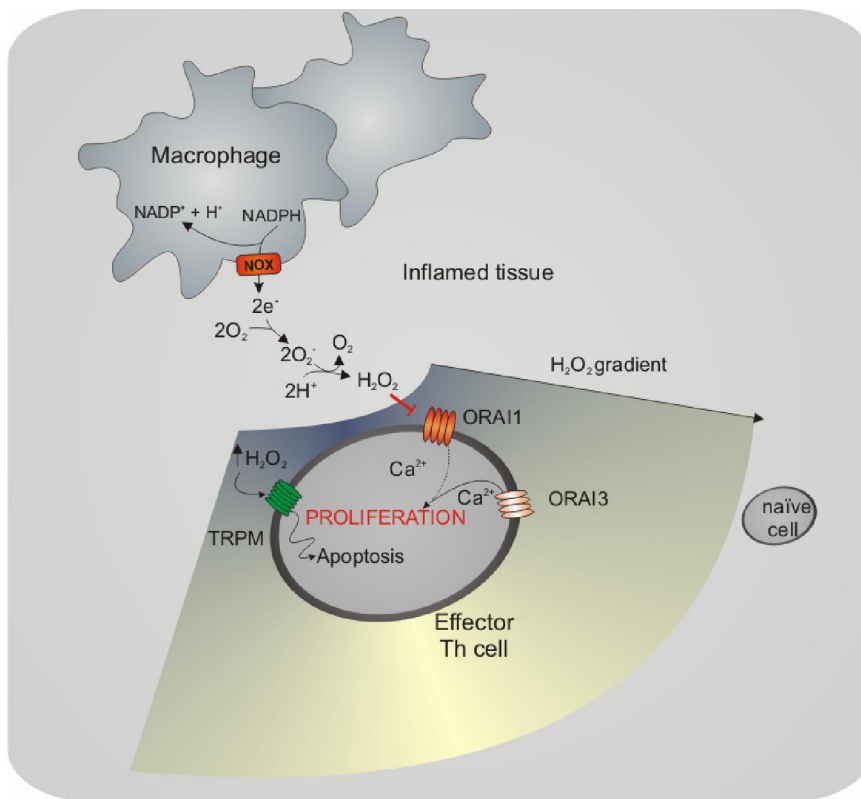**Figure 44:** Model of extracellular ROS production and its effects on Th-cell Ca^{2+} signaling in inflamed tissues.In inflamed tissues, activated macrophages generate H_2O_2 which affects several Ca^{2+} signaling pathways in neighboring effector Th-cells. H_2O_2-induced inhibition of ORAI1 but not ORAI3 tunes Th-cell function, while H_2O_2-induced activation of TRPM channels leads to apoptosis.

10 **Bibliography**

Aarts M., Iihara K., Wei W. L., Xiong Z. G., Arundine M., Cerwinski W., MacDonald J. F. and Tymianski M. (2003) A key role for TRPM7 channels in anoxic neuronal death. *Cell* **115**, 863-77.

Abdalla I., Ray P., Ray V., Vaida F. and Vijayakumar S. (1998) Comparison of serum prostate-specific antigen levels and PSA density in African-American, white, and Hispanic men without prostate cancer. *Urology* **51**, 300-5.

Abramov A. Y. and Duchen M. R. (2005) The role of an astrocytic NADPH oxidase in the neurotoxicity of amyloid beta peptides. *Philos Trans R Soc Lond B Biol Sci* **360**, 2309-14.

Akey J. M., Swanson W. J., Madeoy J., Eberle M. and Shriver M. D. (2006) TRPV6 exhibits unusual patterns of polymorphism and divergence in worldwide populations. *Hum Mol Genet* **15**, 2106-13.

Alvarez J., Coulombe A., Cazorla O., Ugur M., Rauzier J. M., Magyar J., Mathieu E. L., Boulay G., Souto R., Bideaux P., Salazar G., Rassendren F., Lacampagne A., Fauconnier J. and Vassort G. (2008) ATP/UTP activate cation-permeable channels with TRPC3/7 properties in rat cardiomyocytes. *Am J Physiol Heart Circ Physiol* **295**, H21-8.

Annunziato L., Pignataro G. and Di Renzo G. F. (2004) Pharmacology of brain Na+/Ca2+ exchanger: from molecular biology to therapeutic perspectives. *Pharmacol Rev* **56**, 633-54.

Antcliff J. F., Haider S., Proks P., Sansom M. S. and Ashcroft F. M. (2005) Functional analysis of a structural model of the ATP-binding site of the KATP channel Kir6.2 subunit. *Embo J* **24**, 229-39.

Arniges M., Fernandez-Fernandez J. M., Albrecht N., Schaefer M. and Valverde M. A. (2006) Human TRPV4 channel splice variants revealed a key role of ankyrin domains in multimerization and trafficking. *J Biol Chem* **281**, 1580-6.

Ashcroft F. M. and Kakei M. (1989) ATP-sensitive K+ channels in rat pancreatic beta-cells: modulation by ATP and Mg2+ ions. *J Physiol* **416**, 349-67.

Azzaria M., Schurr E. and Gros P. (1989) Discrete mutations introduced in the predicted nucleotide-binding sites of the mdr1 gene abolish its ability to confer multidrug resistance. *Mol Cell Biol* **9**, 5289-97.

Babior B. M. (1984) The respiratory burst of phagocytes. *J Clin Invest* **73**, 599-601.

Baier L. J., Permana P. A., Yang X., Pratley R. E., Hanson R. L., Shen G. Q., Mott D., Knowler W. C., Cox N. J., Horikawa Y., Oda N., Bell G. I. and Bogardus C. (2000) A calpain-10 gene polymorphism is associated with reduced muscle mRNA levels and insulin resistance. *J Clin Invest* **106**, R69-73.

Barley N. F., Howard A., O'Callaghan D., Legon S. and Walters J. R. (2001) Epithelial calcium transporter expression in human duodenum. *Am J Physiol Gastrointest Liver Physiol* **280**, G285-90.

Betzenhauser M. J., Wagner L. E., 2nd, Park H. S. and Yule D. I. (2009) ATP Regulation of Type-1 Inositol 1,4,5-Trisphosphate Receptor Activity Does Not Require Walker A-type ATP-binding Motifs. *J Biol Chem* **284**, 16156-63.

Bhave G., Hu H. J., Glauner K. S., Zhu W., Wang H., Brasier D. J., Oxford G. S. and Gereau R. W. t. (2003) Protein kinase C phosphorylation sensitizes but does not activate the capsaicin receptor transient receptor potential vanilloid 1 (TRPV1). *Proc Natl Acad Sci U S A* **100**, 12480-5.

Bhave G., Zhu W., Wang H., Brasier D. J., Oxford G. S. and Gereau R. W. t. (2002) cAMP-dependent protein kinase regulates desensitization of the capsaicin receptor (VR1) by direct phosphorylation. *Neuron* **35**, 721-31.

Blom N., Sicheritz-Ponten T., Gupta R., Gammeltoft S. and Brunak S. (2004) Prediction of post-translational glycosylation and phosphorylation of proteins from the amino acid sequence. *Proteomics* **4**, 1633-49.

Bootman M. D., Collins T. J., Peppiatt C. M., Prothero L. S., MacKenzie L., De Smet P., Travers M., Tovey S. C., Seo J. T., Berridge M. J., Ciccolini F. and Lipp P. (2001) Calcium signalling--an overview. *Semin Cell Dev Biol* **12**, 3-10.

Bootman M. D., Taylor C. W. and Berridge M. J. (1992) The thiol reagent, thimerosal, evokes Ca2+ spikes in HeLa cells by sensitizing the inositol 1,4,5-trisphosphate receptor. *J Biol Chem* **267**, 25113-9.

Brini M., Pinton P., Pozzan T. and Rizzuto R. (1999) Targeted recombinant aequorins: tools for monitoring [Ca2+] in the various compartments of a living cell. *Microsc Res Tech* **46**, 380-9.

Burns D. J., Bloomenthal J., Lee M. H. and Bell R. M. (1990) Expression of the alpha, beta II, and gamma protein kinase C isozymes in the baculovirus-insect cell expression system. Purification and characterization of the individual isoforms. *J Biol Chem* **265**, 12044-51.

Cahalan M. D. (2009) STIMulating store-operated Ca(2+) entry. *Nat Cell Biol* **11**, 669-77.

Carafoli E. (1987) Intracellular calcium homeostasis. *Annu Rev Biochem* **56**, 395-433.

Carafoli E. (1988) The intracellular homeostasis of calcium: an overview. *Ann N Y Acad Sci* **551**, 147-57; discussion 157-8.

Carafoli E. (2004) Calcium-mediated cellular signals: a story of failures. *Trends Biochem Sci* **29**, 371-9.

Caroni P. and Carafoli E. (1983) The regulation of the Na+ -Ca2+ exchanger of heart sarcolemma. *Eur J Biochem* **132**, 451-60.

Caterina M. J., Rosen T. A., Tominaga M., Brake A. J. and Julius D. (1999) A capsaicin-receptor homologue with a high threshold for noxious heat. *Nature* **398**, 436-41.

Caterina M. J., Schumacher M. A., Tominaga M., Rosen T. A., Levine J. D. and Julius D. (1997) The capsaicin receptor: a heat-activated ion channel in the pain pathway. *Nature* **389**, 816-24.

Cha S. K., Ortega B., Kurosu H., Rosenblatt K. P., Kuro O. M. and Huang C. L. (2008) Removal of sialic acid involving Klotho causes cell-surface retention of TRPV5 channel via binding to galectin-1. *Proc Natl Acad Sci U S A* **105**, 9805-10.

Chang Q., Gyftogianni E., van de Graaf S. F., Hoefs S., Weidema F. A., Bindels R. J. and Hoenderop J. G. (2004) Molecular determinants in TRPV5 channel assembly. *J Biol Chem* **279**, 54304-11.

Chang Q., Hoefs S., van der Kemp A. W., Topala C. N., Bindels R. J. and Hoenderop J. G. (2005) The beta-glucuronidase klotho hydrolyzes and activates the TRPV5 channel. *Science* **310**, 490-3.

Chen C. S. (2002) Phorbol ester induces elevated oxidative activity and alkalization in a subset of lysosomes. *BMC Cell Biol* **3**, 21.

Aarts M., Iihara K., Wei W. L., Xiong Z. G., Arundine M., Cerwinski W., MacDonald J. F. and Tymianski M. (2003) A key role for TRPM7 channels in anoxic neuronal death. *Cell* **115**, 863-77.

Abdalla I., Ray P., Ray V., Vaida F. and Vijayakumar S. (1998) Comparison of serum prostate-specific antigen levels and PSA density in African-American, white, and Hispanic men without prostate cancer. *Urology* **51**, 300-5.

Abramov A. Y. and Duchen M. R. (2005) The role of an astrocytic NADPH oxidase in the neurotoxicity of amyloid beta peptides. *Philos Trans R Soc Lond B Biol Sci* **360**, 2309-14.

Akey J. M., Swanson W. J., Madeoy J., Eberle M. and Shriver M. D. (2006) TRPV6 exhibits unusual patterns of polymorphism and divergence in worldwide populations. *Hum Mol Genet* **15**, 2106-13.

Alvarez J., Coulombe A., Cazorla O., Ugur M., Rauzier J. M., Magyar J., Mathieu E. L., Boulay G., Souto R., Bideaux P., Salazar G., Rassendren F., Lacampagne A., Fauconnier J. and Vassort G. (2008) ATP/UTP activate cation-permeable channels with TRPC3/7 properties in rat cardiomyocytes. *Am J Physiol Heart Circ Physiol* **295**, H21-8.

Annunziato L., Pignataro G. and Di Renzo G. F. (2004) Pharmacology of brain Na+/Ca2+ exchanger: from molecular biology to therapeutic perspectives. *Pharmacol Rev* **56**, 633-54.

Antcliff J. F., Haider S., Proks P., Sansom M. S. and Ashcroft F. M. (2005) Functional analysis of a structural model of the ATP-binding site of the KATP channel Kir6.2 subunit. *Embo J* **24**, 229-39.

Arniges M., Fernandez-Fernandez J. M., Albrecht N., Schaefer M. and Valverde M. A. (2006) Human TRPV4 channel splice variants revealed a key role of ankyrin domains in multimerization and trafficking. *J Biol Chem* **281**, 1580-6.

Ashcroft F. M. and Kakei M. (1989) ATP-sensitive K+ channels in rat pancreatic beta-cells: modulation by ATP and Mg2+ ions. *J Physiol* **416**, 349-67.

Azzaria M., Schurr E. and Gros P. (1989) Discrete mutations introduced in the predicted nucleotide-binding sites of the mdr1 gene abolish its ability to confer multidrug resistance. *Mol Cell Biol* **9**, 5289-97.

Babior B. M. (1984) The respiratory burst of phagocytes. *J Clin Invest* **73**, 599-601.

Baier L. J., Permana P. A., Yang X., Pratley R. E., Hanson R. L., Shen G. Q., Mott D., Knowler W. C., Cox N. J., Horikawa Y., Oda N., Bell G. I. and Bogardus C. (2000) A calpain-10 gene polymorphism is associated with reduced muscle mRNA levels and insulin resistance. *J Clin Invest* **106**, R69-73.

Barley N. F., Howard A., O'Callaghan D., Legon S. and Walters J. R. (2001) Epithelial calcium transporter expression in human duodenum. *Am J Physiol Gastrointest Liver Physiol* **280**, G285-90.

Betzenhauser M. J., Wagner L. E., 2nd, Park H. S. and Yule D. I. (2009) ATP Regulation of Type-1 Inositol 1,4,5-Trisphosphate Receptor Activity Does Not Require Walker A-type ATP-binding Motifs. *J Biol Chem* **284**, 16156-63.

Bhave G., Hu H. J., Glauner K. S., Zhu W., Wang H., Brasier D. J., Oxford G. S. and Gereau R. W. t. (2003) Protein kinase C phosphorylation sensitizes but does not activate the capsaicin receptor transient receptor potential vanilloid 1 (TRPV1). *Proc Natl Acad Sci U S A* **100**, 12480-5.

Bhave G., Zhu W., Wang H., Brasier D. J., Oxford G. S. and Gereau R. W. t. (2002) cAMP-dependent protein kinase regulates desensitization of the capsaicin receptor (VR1) by direct phosphorylation. *Neuron* **35**, 721-31.

Blom N., Sicheritz-Ponten T., Gupta R., Gammeltoft S. and Brunak S. (2004) Prediction of post-translational glycosylation and phosphorylation of proteins from the amino acid sequence. *Proteomics* **4**, 1633-49.

Bootman M. D., Collins T. J., Peppiatt C. M., Prothero L. S., MacKenzie L., De Smet P., Travers M., Tovey S. C., Seo J. T., Berridge M. J., Ciccolini F. and Lipp P. (2001) Calcium signalling--an overview. *Semin Cell Dev Biol* **12**, 3-10.

Bootman M. D., Taylor C. W. and Berridge M. J. (1992) The thiol reagent, thimerosal, evokes Ca2+ spikes in HeLa cells by sensitizing the inositol 1,4,5-trisphosphate receptor. *J Biol Chem* **267**, 25113-9.

Brini M., Pinton P., Pozzan T. and Rizzuto R. (1999) Targeted recombinant aequorins: tools for monitoring [Ca2+] in the various compartments of a living cell. *Microsc Res Tech* **46**, 380-9.

Burns D. J., Bloomenthal J., Lee M. H. and Bell R. M. (1990) Expression of the alpha, beta II, and gamma protein kinase C isozymes in the baculovirus-insect cell expression system. Purification and characterization of the individual isoforms. *J Biol Chem* **265**, 12044-51.

Cahalan M. D. (2009) STIMulating store-operated Ca(2+) entry. *Nat Cell Biol* **11**, 669-77.

Carafoli E. (1987) Intracellular calcium homeostasis. *Annu Rev Biochem* **56**, 395-433.

Carafoli E. (1988) The intracellular homeostasis of calcium: an overview. *Ann N Y Acad Sci* **551**, 147-57; discussion 157-8.

Carafoli E. (2004) Calcium-mediated cellular signals: a story of failures. *Trends Biochem Sci* **29**, 371-9.

Caroni P. and Carafoli E. (1983) The regulation of the Na+ -Ca2+ exchanger of heart sarcolemma. *Eur J Biochem* **132**, 451-60.

Caterina M. J., Rosen T. A., Tominaga M., Brake A. J. and Julius D. (1999) A capsaicin-receptor homologue with a high threshold for noxious heat. *Nature* **398**, 436-41.

Caterina M. J., Schumacher M. A., Tominaga M., Rosen T. A., Levine J. D. and Julius D. (1997) The capsaicin receptor: a heat-activated ion channel in the pain pathway. *Nature* **389**, 816-24.

Cha S. K., Ortega B., Kurosu H., Rosenblatt K. P., Kuro O. M. and Huang C. L. (2008) Removal of sialic acid involving Klotho causes cell-surface retention of TRPV5 channel via binding to galectin-1. *Proc Natl Acad Sci U S A* **105**, 9805-10.

Chang Q., Gyftogianni E., van de Graaf S. F., Hoefs S., Weidema F. A., Bindels R. J. and Hoenderop J. G. (2004) Molecular determinants in TRPV5 channel assembly. *J Biol Chem* **279**, 54304-11.

Chang Q., Hoefs S., van der Kemp A. W., Topala C. N., Bindels R. J. and Hoenderop J. G. (2005) The beta-glucuronidase klotho hydrolyzes and activates the TRPV5 channel. *Science* **310**, 490-3.

Chen C. S. (2002) Phorbol ester induces elevated oxidative activity and alkalization in a subset of lysosomes. *BMC Cell Biol* **3**, 21.

Clapham D. E. (2007) Calcium signaling. *Cell* **131**, 1047-58.

Colbert H. A., Smith T. L. and Bargmann C. I. (1997) OSM-9, a novel protein with structural similarity to channels, is required for olfaction, mechanosensation, and olfactory adaptation in Caenorhabditis elegans. *J Neurosci* **17**, 8259-69.

Corey D. P., Garcia-Anoveros J., Holt J. R., Kwan K. Y., Lin S. Y., Vollrath M. A., Amalfitano A., Cheung E. L., Derfler B. H., Duggan A., Geleoc G. S., Gray P. A., Hoffman M. P., Rehm H. L., Tamasauskas D. and Zhang D. S. (2004) TRPA1 is a candidate for the mechanosensitive transduction channel of vertebrate hair cells. *Nature* **432**, 723-30.

Cosens D. J. and Manning A. (1969) Abnormal electroretinogram from a Drosophila mutant. *Nature* **224**, 285-7.

Craig T. J., Ashcroft F. M. and Proks P. (2008) How ATP inhibits the open K(ATP) channel. *J Gen Physiol* **132**, 131-44.

Dattilo M., Penington N. J. and Williams K. (2008) Inhibition of TRPC5 channels by intracellular ATP. *Mol Pharmacol* **73**, 42-9.

de Bono M. (2003) Molecular approaches to aggregation behavior and social attachment. *J Neurobiol* **54**, 78-92.

den Dekker E., Hoenderop J. G., Nilius B. and Bindels R. J. (2003) The epithelial calcium channels, TRPV5 & TRPV6: from identification towards regulation. *Cell Calcium* **33**, 497-507.

Derler I., Hofbauer M., Kahr H., Fritsch R., Muik M., Kepplinger K., Hack M. E., Moritz S., Schindl R., Groschner K. and Romanin C. (2006) Dynamic but not constitutive association of calmodulin with rat TRPV6 channels enables fine tuning of Ca2+-dependent inactivation. *J Physiol* **577**, 31-44.

DiPolo R. and Beauge L. (1998) Differential up-regulation of Na+-Ca2+ exchange by phosphoarginine and ATP in dialysed squid axons. *J Physiol* **507 (Pt 3)**, 737-47.

Droge W. (2002) Aging-related changes in the thiol/disulfide redox state: implications for the use of thiol antioxidants. *Exp Gerontol* **37**, 1333-45.

Droge W. (2005) Oxidative stress and ageing: is ageing a cysteine deficiency syndrome? *Philos Trans R Soc Lond B Biol Sci* **360**, 2355-72.

Droge W., Roth S., Altmann A. and Mihm S. (1987) Regulation of T-cell functions by L-lactate. *Cell Immunol* **108**, 405-16.

Erickson R. W., Malawista S. E., Garrett M. C., Van Blaricom G., Leto T. L. and Curnutte J. T. (1992) Identification of a thermolabile component of the human neutrophil NADPH oxidase. A model for chronic granulomatous disease caused by deficiency of the p67-phox cytosolic component. *J Clin Invest* **89**, 1587-95.

Erler I., Hirnet D., Wissenbach U., Flockerzi V. and Niemeyer B. A. (2004) Ca2+-selective transient receptor potential V channel architecture and function require a specific ankyrin repeat. *J Biol Chem* **279**, 34456-63.

Feissner R. F., Skalska J., Gaum W. E. and Sheu S. S. (2009) Crosstalk signaling between mitochondrial Ca2+ and ROS. *Front Biosci* **14**, 1197-218.

Feng X., Zhang J., Barak L. S., Meyer T., Caron M. G. and Hannun Y. A. (1998) Visualization of dynamic trafficking of a protein kinase C betaII/green fluorescent protein conjugate reveals differences in G protein-coupled receptor activation and desensitization. *J Biol Chem* **273**, 10755-62.

Feske S. (2007) Calcium signalling in lymphocyte activation and disease. *Nat Rev Immunol* **7**, 690-702.

Feske S., Gwack Y., Prakriya M., Srikanth S., Puppel S. H., Tanasa B., Hogan P. G., Lewis R. S., Daly M. and Rao A. (2006) A mutation in Orai1 causes immune deficiency by abrogating CRAC channel function. *Nature* **441**, 179-85.

Fixemer T., Wissenbach U., Flockerzi V. and Bonkhoff H. (2003) Expression of the Ca2+-selective cation channel TRPV6 in human prostate cancer: a novel prognostic marker for tumor progression. *Oncogene* **22**, 7858-61.

Forman H. J., Fukuto J. M. and Torres M. (2004) Redox signaling: thiol chemistry defines which reactive oxygen and nitrogen species can act as second messengers. *Am J Physiol Cell Physiol* **287**, C246-56.

Forman H. J. and Torres M. (2001) Signaling by the respiratory burst in macrophages. *IUBMB Life* **51**, 365-71.

Fukao M., Mason H. S., Britton F. C., Kenyon J. L., Horowitz B. and Keef K. D. (1999) Cyclic GMP-dependent protein kinase activates cloned BKCa channels expressed in mammalian cells by direct phosphorylation at serine 1072. *J Biol Chem* **274**, 10927-35.

Gajewski C. D., Yang L., Schon E. A. and Manfredi G. (2003) New insights into the bioenergetics of mitochondrial disorders using intracellular ATP reporters. *Mol Biol Cell* **14**, 3628-35.

Gaudet R. (2008) A primer on ankyrin repeat function in TRP channels and beyond. *Mol Biosyst* **4**, 372-9.

Gkika D., Mahieu F., Nilius B., Hoenderop J. G. and Bindels R. J. (2004) 80K-H as a new Ca2+ sensor regulating the activity of the epithelial Ca2+ channel transient receptor potential cation channel V5 (TRPV5). *J Biol Chem* **279**, 26351-7.

Goerke A., Sakai N., Gutjahr E., Schlapkohl W. A., Mushinski J. F., Haller H., Kolch W., Saito N. and Mischak H. (2002) Induction of apoptosis by protein kinase C delta is independent of its kinase activity. *J Biol Chem* **277**, 32054-62.

Golenhofen N., Doctor R. B., Bacallao R. and Mandel L. J. (1995) Actin and villin compartmentation during ATP depletion and recovery in renal cultured cells. *Kidney Int* **48**, 1837-45.

Gong Z., Son W., Chung Y. D., Kim J., Shin D. W., McClung C. A., Lee Y., Lee H. W., Chang D. J., Kaang B. K., Cho H., Oh U., Hirsh J., Kernan M. J. and Kim C. (2004) Two interdependent TRPV channel subunits, inactive and Nanchung, mediate hearing in Drosophila. *J Neurosci* **24**, 9059-66.

Gottesman M. M., Pastan I. and Ambudkar S. V. (1996) P-glycoprotein and multidrug resistance. *Curr Opin Genet Dev* **6**, 610-7.

Grubbs R. D. and Maguire M. E. (1987) Magnesium as a regulatory cation: criteria and evaluation. *Magnesium* **6**, 113-27.

Grynkiewicz G., Poenie M. and Tsien R. Y. (1985) A new generation of Ca2+ indicators with greatly improved fluorescence properties. *J Biol Chem* **260**, 3440-50.

Gschwendt M., Dieterich S., Rennecke J., Kittstein W., Mueller H. J. and Johannes F. J. (1996) Inhibition of protein kinase C mu by various inhibitors. Differentiation from protein kinase c isoenzymes. *FEBS Lett* **392**, 77-80.

Guerini D. (1998) The significance of the isoforms of plasma membrane calcium ATPase. *Cell Tissue Res* **292**, 191-7.

Guinamard R., Chatelier A., Lenfant J. and Bois P. (2004) Activation of the Ca(2+)-activated nonselective cation channel by diacylglycerol analogues in rat cardiomyocytes. *J Cardiovasc Electrophysiol* **15**, 342-8.

Gwanyanya A., Sipido K. R., Vereecke J. and Mubagwa K. (2006) ATP and PIP2 dependence of the magnesium-inhibited, TRPM7-like cation channel in cardiac myocytes. *Am J Physiol Cell Physiol* **291**, C627-35.

Hannun Y. A., Loomis C. R. and Bell R. M. (1985) Activation of protein kinase C by Triton X-100 mixed micelles containing diacylglycerol and phosphatidylserine. *J Biol Chem* **260**, 10039-43.

Hara Y., Wakamori M., Ishii M., Maeno E., Nishida M., Yoshida T., Yamada H., Shimizu S., Mori E., Kudoh J., Shimizu N., Kurose H., Okada Y., Imoto K. and Mori Y. (2002) LTRPC2 Ca2+-permeable channel activated by changes in redox status confers susceptibility to cell death. *Mol Cell* **9**, 163-73.

Hardie R. C. and Minke B. (1992) The trp gene is essential for a light-activated Ca2+ channel in Drosophila photoreceptors. *Neuron* **8**, 643-51.

Hildeman D. A., Mitchell T., Kappler J. and Marrack P. (2003) T cell apoptosis and reactive oxygen species. *J Clin Invest* **111**, 575-81.

Hilgemann D. W. (1997) Cytoplasmic ATP-dependent regulation of ion transporters and channels: mechanisms and messengers. *Annu Rev Physiol* **59**, 193-220.

Hilgemann D. W. and Ball R. (1996) Regulation of cardiac Na+,Ca2+ exchange and KATP potassium channels by PIP2. *Science* **273**, 956-9.

Hirnet D., Olausson J., Fecher-Trost C., Bodding M., Nastainczyk W., Wissenbach U., Flockerzi V. and Freichel M. (2003) The TRPV6 gene, cDNA and protein. *Cell Calcium* **33**, 509-18.

Hisatsune C., Kuroda Y., Nakamura K., Inoue T., Nakamura T., Michikawa T., Mizutani A. and Mikoshiba K. (2004) Regulation of TRPC6 channel activity by tyrosine phosphorylation. *J Biol Chem* **279**, 18887-94.

Hoenderop J. G., Nilius B. and Bindels R. J. (2003) Epithelial calcium channels: from identification to function and regulation. *Pflugers Arch* **27**, 27.

Hoenderop J. G., Vennekens R., Muller D., Prenen J., Droogmans G., Bindels R. J. and Nilius B. (2001) Function and expression of the epithelial Ca(2+) channel family: comparison of mammalian ECaC1 and 2. *J Physiol* **537**, 747-61.

Hollenstein K., Frei D. C. and Locher K. P. (2007) Structure of an ABC transporter in complex with its binding protein. *Nature* **446**, 213-6.

Hoth M. and Penner R. (1992) Depletion of intracellular calcium stores activates a calcium current in mast cells. *Nature* **355**, 353-6.

Hoth M. and Penner R. (1993) Calcium release-activated calcium current in rat mast cells. *J Physiol* **465**, 359-86.

Howard J. and Bechstedt S. (2004) Hypothesis: a helix of ankyrin repeats of the NOMPC-TRP ion channel is the gating spring of mechanoreceptors. *Curr Biol* **14**, R224-6.

Huang C. L. (2007) Complex roles of PIP2 in the regulation of ion channels and transporters. *Am J Physiol Renal Physiol* **293**, F1761-5.

Huang K., Zhang Z., Liu N., Zhang Y., Zhang G. and Yang K. (1992) Functional implication of disulfide bond, Cys250 -Cys283, in bovine chymosin. *Biochem Biophys Res Commun* **187**, 692-6.

Hughes D. A., Tang K., Strotmann R., Schoneberg T., Prenen J., Nilius B. and Stoneking M. (2008) Parallel selection on TRPV6 in human populations. *PLoS ONE* **3**, e1686.

Hulo N., Bairoch A., Bulliard V., Cerutti L., Cuche B. A., de Castro E., Lachaize C., Langendijk-Genevaux P. S. and Sigrist C. J. (2008) The 20 years of PROSITE. *Nucleic Acids Res* **36**, D245-9.

Hultqvist M., Olofsson P., Holmberg J., Backstrom B. T., Tordsson J. and Holmdahl R. (2004) Enhanced autoimmunity, arthritis, and encephalomyelitis in mice with a reduced oxidative burst due to a mutation in the Ncf1 gene. *Proc Natl Acad Sci U S A* **101**, 12646-51.

Imai Y., Kuba K., Neely G. G., Yaghubian-Malhami R., Perkmann T., van Loo G., Ermolaeva M., Veldhuizen R., Leung Y. H. C., Wang H. L., Liu H. L., Sun Y., Pasparakis M., Kopf M., Mech C., Bavari S., Peiris J. S. M., Slutsky A. S., Akira S., Hultqvist M., Holmdahl R., Nicholls J., Jiang C. Y., Binder C. J. and Penninger J. M. (2008) Identification of oxidative stress and toll-like receptor 4 signaling as a key pathway of acute lung injury. *Cell* **133**, 235-249.

Jakubowski W. and Bartosz G. (2000) 2,7-dichlorofluorescin oxidation and reactive oxygen species: what does it measure? *Cell Biol Int* **24**, 757-60.

Jamme I., Petit E., Divoux D., Gerbi A., Maixent J. M. and Nouvelot A. (1995) Modulation of mouse cerebral Na+,K(+)-ATPase activity by oxygen free radicals. *Neuroreport* **7**, 333-7.

Jin X., Touhey J. and Gaudet R. (2006) Structure of the N-terminal ankyrin repeat domain of the TRPV2 ion channel. *J Biol Chem*.

Jung J., Shin J. S., Lee S. Y., Hwang S. W., Koo J., Cho H. and Oh U. (2004) Phosphorylation of vanilloid receptor 1 by Ca2+/calmodulin-dependent kinase II regulates its vanilloid binding. *J Biol Chem* **279**, 7048-54.

Kaibuchi K., Takai Y. and Nishizuka Y. (1981) Cooperative roles of various membrane phospholipids in the activation of calcium-activated, phospholipid-dependent protein kinase. *J Biol Chem* **256**, 7146-9.

Kako K., Kato M., Matsuoka T. and Mustapha A. (1988) Depression of membrane-bound Na+-K+-ATPase activity induced by free radicals and by ischemia of kidney. *Am J Physiol* **254**, C330-7.

Karashima Y., Prenen J., Meseguer V., Owsianik G., Voets T. and Nilius B. (2008) Modulation of the transient receptor potential channel TRPA1 by phosphatidylinositol 4,5-biphosphate manipulators. *Pflugers Arch* **457**, 77-89.

Katz A. M. and Lorell B. H. (2000) Regulation of cardiac contraction and relaxation. *Circulation* **102**, IV69-74.

Kim J., Chung Y. D., Park D. Y., Choi S., Shin D. W., Soh H., Lee H. W., Son W., Yim J., Park C. S., Kernan M. J. and Kim C. (2003) A TRPV family ion channel required for hearing in Drosophila. *Nature* **424**, 81-4.

Kottgen M., Benzing T., Simmen T., Tauber R., Buchholz B., Feliciangeli S., Huber T. B., Schermer B., Kramer-Zucker A., Hopker K., Simmen K. C., Tschucke C. C., Sandford R., Kim E., Thomas G. and Walz G. (2005) Trafficking of TRPP2 by PACS proteins represents a novel mechanism of ion channel regulation. *Embo J* **24**, 705-16.

Kourie J. I. (1998) Interaction of reactive oxygen species with ion transport mechanisms. *Am J Physiol* **275**, C1-24.

Kuro O. M. (2009) Klotho and aging. *Biochim Biophys Acta*.

Lambers T. T., Weidema A. F., Nilius B., Hoenderop J. G. and Bindels R. J. (2004) Regulation of the mouse epithelial Ca2(+) channel TRPV6 by the Ca(2+)-sensor calmodulin. *J Biol Chem* **279**, 28855-61.

Lauritzen E. and Pluskal M. (1988) Improved HIV antiglycoprotein antibody detection by immunoblotting on a hydrophobic membrane. *J Acquir Immune Defic Syndr* **1**, 333-9.

Lee M. H. and Bell R. M. (1989) Phospholipid functional groups involved in protein kinase C activation, phorbol ester binding, and binding to mixed micelles. *J Biol Chem* **264**, 14797-805.

Lee N., Chen J., Sun L., Wu S., Gray K. R., Rich A., Huang M., Lin J. H., Feder J. N., Janovitz E. B., Levesque P. C. and Blanar M. A. (2003) Expression and characterization of human transient receptor potential melastatin 3 (hTRPM3). *J Biol Chem* **278**, 20890-7.

Lewis R. S. (2001) Calcium signaling mechanisms in T lymphocytes. *Annu Rev Immunol* **19**, 497-521.

Lewis R. S. and Cahalan M. D. (1989) Mitogen-induced oscillations of cytosolic Ca2+ and transmembrane Ca2+ current in human leukemic T cells. *Cell Regul* **1**, 99-112.

Liedtke W. and Kim C. (2005) Functionality of the TRPV subfamily of TRP ion channels: add mechano-TRP and osmo-TRP to the lexicon! *Cell Mol Life Sci* **62**, 2985-3001.

Liou J., Fivaz M., Inoue T. and Meyer T. (2007) Live-cell imaging reveals sequential oligomerization and local plasma membrane targeting of stromal interaction molecule 1 after Ca2+ store depletion. *Proc Natl Acad Sci U S A* **104**, 9301-6.

Liou J., Kim M. L., Heo W. D., Jones J. T., Myers J. W., Ferrell J. E., Jr. and Meyer T. (2005) STIM is a Ca2+ sensor essential for Ca2+-store-depletion-triggered Ca2+ influx. *Curr Biol* **15**, 1235-41.

Lioudyno M. I., Kozak J. A., Penna A., Safrina O., Zhang S. L., Sen D., Roos J., Stauderman K. A. and Cahalan M. D. (2008) Orai1 and STIM1 move to the immunological synapse and are up-regulated during T cell activation. *Proc Natl Acad Sci U S A* **105**, 2011-6.

Lishko P. V., Procko E., Jin X., Phelps C. B. and Gaudet R. (2007) The ankyrin repeats of TRPV1 bind multiple ligands and modulate channel sensitivity. *Neuron* **54**, 905-18.

Loo T. W. and Clarke D. M. (1995) Covalent modification of human P-glycoprotein mutants containing a single cysteine in either nucleotide-binding fold abolishes drug-stimulated ATPase activity. *J Biol Chem* **270**, 22957-61.

Lopshire J. C. and Nicol G. D. (1998) The cAMP transduction cascade mediates the prostaglandin E2 enhancement of the capsaicin-elicited current in rat sensory neurons: whole-cell and single-channel studies. *J Neurosci* **18**, 6081-92.

Miller B. A. (2006) The role of TRP channels in oxidative stress-induced cell death. *J Membr Biol* **209**, 31-41.

Minke B. and Selinger Z. (1992) The inositol-lipid pathway is necessary for light excitation in fly photoreceptors. *Soc Gen Physiol Ser* **47**, 201-17.

Missiaen L., De Smedt H., Droogmans G., Declerck I., Plessers L. and Casteels R. (1991) Uptake characteristics of the InsP3-sensitive and -insensitive Ca2+ pools in porcine aortic smooth-muscle cells: different Ca2+ sensitivity of the Ca2(+)-uptake mechanism. *Biochem Biophys Res Commun* **174**, 1183-8.

Mohapatra D. P. and Nau C. (2003) Desensitization of capsaicin-activated currents in the vanilloid receptor TRPV1 is decreased by the cyclic AMP-dependent protein kinase pathway. *J Biol Chem* **278**, 50080-90.

Mohapatra D. P. and Nau C. (2005) Regulation of Ca2+-dependent desensitization in the vanilloid receptor TRPV1 by calcineurin and cAMP-dependent protein kinase. *J Biol Chem* **280**, 13424-32.

Montell C. (2005) The TRP superfamily of cation channels. *Sci STKE* **2005**, re3.

Montell C. and Rubin G. M. (1989) Molecular characterization of the Drosophila trp locus: a putative integral membrane protein required for phototransduction. *Neuron* **2**, 1313-23.

Montero M., Alonso M. T., Albillos A., Garcia-Sancho J. and Alvarez J. (2001) Mitochondrial Ca(2+)-induced Ca(2+) release mediated by the Ca(2+) uniporter. *Mol Biol Cell* **12**, 63-71.

Mosavi L. K., Cammett T. J., Desrosiers D. C. and Peng Z. Y. (2004) The ankyrin repeat as molecular architecture for protein recognition. *Protein Sci* **13**, 1435-48.

Muller D., Hoenderop J. G., Meij I. C., van den Heuvel L. P., Knoers N. V., den Hollander A. I., Eggert P., Garcia-Nieto V., Claverie-Martin F. and Bindels R. J. (2000) Molecular cloning, tissue distribution, and chromosomal mapping of the human epithelial Ca2+ channel (ECAC1). *Genomics* **67**, 48-53.

Negulescu P. A., Shastri N. and Cahalan M. D. (1994) Intracellular calcium dependence of gene expression in single T lymphocytes. *Proc Natl Acad Sci U S A* **91**, 2873-7.

Niemeyer B. A., Bergs C., Wissenbach U., Flockerzi V. and Trost C. (2001) Competitive regulation of CaT-like-mediated Ca2+ entry by protein kinase C and calmodulin. *Proc Natl Acad Sci U S A* **98**, 3600-5.

Niemeyer B. A., Suzuki E., Scott K., Jalink K. and Zuker C. S. (1996) The Drosophila light-activated conductance is composed of the two channels TRP and TRPL. *Cell* **85**, 651-9.

Niethammer P., Grabher C., Look A. T. and Mitchison T. J. (2009) A tissue-scale gradient of hydrogen peroxide mediates rapid wound detection in zebrafish. *Nature* **459**, 996-9.

Nilius B., Vennekens R., Prenen J., Hoenderop J. G., Droogmans G. and Bindels R. J. (2001) The single pore residue Asp542 determines Ca2+ permeation and Mg2+ block of the epithelial Ca2+ channel. *J Biol Chem* **276**, 1020-5.

Numazaki M., Tominaga T., Toyooka H. and Tominaga M. (2002) Direct phosphorylation of capsaicin receptor VR1 by protein kinase Cepsilon and identification of two target serine residues. *J Biol Chem* **277**, 13375-8.

Oritani K. and Kincade P. W. (1996) Identification of stromal cell products that interact with pre-B cells. *J Cell Biol* **134**, 771-82.

Pan H. Z., Zhang L., Guo M. Y., Sui H., Li H., Wu W. H., Qu N. Q., Liang M. H. and Chang D. (2009) The oxidative stress status in diabetes mellitus and diabetic nephropathy. *Acta Diabetol*.

Park C. Y., Hoover P. J., Mullins F. M., Bachhawat P., Covington E. D., Raunser S., Walz T., Garcia K. C., Dolmetsch R. E. and Lewis R. S. (2009) STIM1 clusters and activates CRAC channels via direct binding of a cytosolic domain to Orai1. *Cell* **136**, 876-90.

Pedersen S. F., Owsianik G. and Nilius B. (2005) TRP channels: an overview. *Cell Calcium* **38**, 233-52.

Peng J. B., Chen X. Z., Berger U. V., Vassilev P. M., Tsukaguchi H., Brown E. M. and Hediger M. A. (1999) Molecular cloning and characterization of a channel-like transporter mediating intestinal calcium absorption. *J Biol Chem* **274**, 22739-46.

Peng J. B., Chen X. Z., Berger U. V., Weremowicz S., Morton C. C., Vassilev P. M., Brown E. M. and Hediger M. A. (2000) Human calcium transport protein CaT1. *Biochem Biophys Res Commun* **278**, 326-32.

Penner R. and Fleig A. (2007) The Mg2+ and Mg(2+)-nucleotide-regulated channel-kinase TRPM7. *Handb Exp Pharmacol*, 313-28.

Perez A. V., Picotto G., Carpentieri A. R., Rivoira M. A., Peralta Lopez M. E. and Tolosa de Talamoni N. G. (2008) Minireview on regulation of intestinal calcium absorption. Emphasis on molecular mechanisms of transcellular pathway. *Digestion* **77**, 22-34.

Phelps C. B., Huang R. J., Lishko P. V., Wang R. R. and Gaudet R. (2008) Structural analyses of the ankyrin repeat domain of TRPV6 and related TRPV ion channels. *Biochemistry* **47**, 2476-84.

Phillips A. M., Bull A. and Kelly L. E. (1992) Identification of a Drosophila gene encoding a calmodulin-binding protein with homology to the trp phototransduction gene. *Neuron* **8**, 631-42.

Premkumar L. S. and Ahern G. P. (2000) Induction of vanilloid receptor channel activity by protein kinase C. *Nature* **408**, 985-90.

Putney J. W., Jr. (1986) A model for receptor-regulated calcium entry. *Cell Calcium* **7**, 1-12.

Putney J. W., Jr. and Bird G. S. (1993) The inositol phosphate-calcium signaling system in nonexcitable cells. *Endocr Rev* **14**, 610-31.

Qiu A. and Hogstrand C. (2004) Functional characterisation and genomic analysis of an epithelial calcium channel (ECaC) from pufferfish, Fugu rubripes. *Gene* **342**, 113-23.

Quintana A., Griesemer D., Schwarz E. C. and Hoth M. (2005) Calcium-dependent activation of T-lymphocytes. *Pflugers Arch* **450**, 1-12.

Ramsey I. S., Delling M. and Clapham D. E. (2006) An introduction to TRP channels. *Annu Rev Physiol* **68**, 619-47.

Rathee P. K., Distler C., Obreja O., Neuhuber W., Wang G. K., Wang S. Y., Nau C. and Kress M. (2002) PKA/AKAP/VR-1 module: A common link of Gs-mediated signaling to thermal hyperalgesia. *J Neurosci* **22**, 4740-5.

Renard-Rooney D. C., Joseph S. K., Seitz M. B. and Thomas A. P. (1995) Effect of oxidized glutathione and temperature on inositol 1,4,5-trisphosphate binding in permeabilized hepatocytes. *Biochem J* **310 (Pt 1)**, 185-92.

Reth M. (2002) Hydrogen peroxide as second messenger in lymphocyte activation. *Nat Immunol* **3**, 1129-34.

Ringer S. (1883) A third contribution regarding the Influence of the Inorganic Constituents of the Blood on the Ventricular Contraction. *J Physiol* **4**, 222-5.

Rohacs T., Lopes C. M., Michailidis I. and Logothetis D. E. (2005) PI(4,5)P2 regulates the activation and desensitization of TRPM8 channels through the TRP domain. *Nat Neurosci* **8**, 626-34.

Rohacs T., Thyagarajan B. and Lukacs V. (2008) Phospholipase C Mediated Modulation of TRPV1 Channels. *Mol Neurobiol* **37**, 153-63.

Roitbak T., Ward C. J., Harris P. C., Bacallao R., Ness S. A. and Wandinger-Ness A. (2004) A polycystin-1 multiprotein complex is disrupted in polycystic kidney disease cells. *Mol Biol Cell* **15**, 1334-46.

Romani A. and Scarpa A. (1992) Regulation of cell magnesium. *Arch Biochem Biophys* **298**, 1-12.

Romani A. M. and Scarpa A. (2000) Regulation of cellular magnesium. *Front Biosci* **5**, D720-34.

Rooney T. A. and Thomas A. P. (1991) Organization of intracellular calcium signals generated by inositol lipid-dependent hormones. *Pharmacol Ther* **49**, 223-37.

Roos J., DiGregorio P. J., Yeromin A. V., Ohlsen K., Lioudyno M., Zhang S., Safrina O., Kozak J. A., Wagner S. L., Cahalan M. D., Velicelebi G. and Stauderman K. A. (2005) STIM1, an essential and conserved component of store-operated Ca2+ channel function. *J Cell Biol* **169**, 435-45.

Salter M. W. and Kalia L. V. (2004) Src kinases: a hub for NMDA receptor regulation. *Nat Rev Neurosci* **5**, 317-28.

Sanger F., Nicklen S. and Coulson A. R. (1977) DNA sequencing with chain-terminating inhibitors. *Proc Natl Acad Sci U S A* **74**, 5463-7.

Scamps F. and Vassort G. (1990) Mechanism of extracellular ATP-induced depolarization in rat isolated ventricular cardiomyocytes. *Pflugers Arch* **417**, 309-16.

Schafer F. Q. and Buettner G. R. (2001) Redox environment of the cell as viewed through the redox state of the glutathione disulfide/glutathione couple. *Free Radic Biol Med* **30**, 1191-212.

Schwarz E. C., Kummerow C., Wenning A. S., Wagner K., Sappok A., Waggershauser K., Griesemer D., Strauss B., Wolfs M. J., Quintana A. and Hoth M. (2007) Calcium dependence of T cell proliferation following focal stimulation. *Eur J Immunol* **37**, 2723-33.

Schwarz E. C., Wissenbach U., Niemeyer B. A., Strauss B., Philipp S. E., Flockerzi V. and Hoth M. (2006) TRPV6 potentiates calcium-dependent cell proliferation. *Cell Calcium* **39**, 163-73.

Schwoebel E. D., Ho T. H. and Moore M. S. (2002) The mechanism of inhibition of Ran-dependent nuclear transport by cellular ATP depletion. *J Cell Biol* **157**, 963-74.

Semenova S. B., Vassilieva I. O., Fomina A. F., Runov A. L. and Negulyaev Y. A. (2009) Endogenous expression of TRPV5 and TRPV6 calcium channels in human leukemia K562 cells. *Am J Physiol Cell Physiol* **296**, C1098-104.

Shi J., Mori E., Mori Y., Mori M., Li J., Ito Y. and Inoue R. (2004) Multiple regulation by calcium of murine homologues of transient receptor potential proteins TRPC6 and TRPC7 expressed in HEK293 cells. *J Physiol* **561**, 415-32.

Shirai Y. and Saito N. (2002) Activation mechanisms of protein kinase C: maturation, catalytic activation, and targeting. *J Biochem* **132**, 663-8.

Soboloff J., Spassova M. A., Dziadek M. A. and Gill D. L. (2006) Calcium signals mediated by STIM and Orai proteins--a new paradigm in inter-organelle communication. *Biochim Biophys Acta* **1763**, 1161-8.

Sokal I., Li N., Surgucheva I., Warren M. J., Payne A. M., Bhattacharya S. S., Baehr W. and Palczewski K. (1998) GCAP1 (Y99C) mutant is constitutively active in autosomal dominant cone dystrophy. *Mol Cell* **2**, 129-33.

Stokes A. J., Shimoda L. M., Koblan-Huberson M., Adra C. N. and Turner H. (2004) A TRPV2-PKA signaling module for transduction of physical stimuli in mast cells. *J Exp Med* **200**, 137-47.

Stoyanovsky D., Murphy T., Anno P. R., Kim Y. M. and Salama G. (1997) Nitric oxide activates skeletal and cardiac ryanodine receptors. *Cell Calcium* **21**, 19-29.

Suzuki Y., Landowski C. P. and Hediger M. A. (2008a) Mechanisms and regulation of epithelial Ca2+ absorption in health and disease. *Annu Rev Physiol* **70**, 257-71.

Suzuki Y., Pasch A., Bonny O., Mohaupt M. G., Hediger M. A. and Frey F. J. (2008b) Gain-of-function haplotype in the epithelial calcium channel TRPV6 is a risk factor for renal calcium stone formation. *Hum Mol Genet* **17**, 1613-8.

Thyagarajan B., Lukacs V. and Rohacs T. (2008) Hydrolysis of phosphatidylinositol 4,5-bisphosphate mediates calcium-induced inactivation of TRPV6 channels. *J Biol Chem* **283**, 14980-7.

Tominaga M., Wada M. and Masu M. (2001) Potentiation of capsaicin receptor activity by metabotropic ATP receptors as a possible mechanism for ATP-evoked pain and hyperalgesia. *Proc Natl Acad Sci U S A* **98**, 6951-6.

Topala C. N., Schoeber J. P., Searchfield L. E., Riccardi D., Hoenderop J. G. and Bindels R. J. (2009) Activation of the Ca2+-sensing receptor stimulates the activity of the epithelial Ca2+ channel TRPV5. *Cell Calcium* **45**, 331-9.

Toullec D., Pianetti P., Coste H., Bellevergue P., Grand-Perret T., Ajakane M., Baudet V., Boissin P., Boursier E., Loriolle F. and et al. (1991) The bisindolylmaleimide GF 109203X is a potent and selective inhibitor of protein kinase C. *J Biol Chem* **266**, 15771-81.

Tsuruda P. R., Julius D. and Minor D. L., Jr. (2006) Coiled coils direct assembly of a cold-activated TRP channel. *Neuron* **51**, 201-12.

van de Graaf S. F., Chang Q., Mensenkamp A. R., Hoenderop J. G. and Bindels R. J. (2006) Direct interaction with Rab11a targets the epithelial Ca2+ channels TRPV5 and TRPV6 to the plasma membrane. *Mol Cell Biol* **26**, 303-12.

van de Graaf S. F., Hoenderop J. G., Gkika D., Lamers D., Prenen J., Rescher U., Gerke V., Staub O., Nilius B. and Bindels R. J. (2003) Functional expression of the epithelial Ca(2+) channels (TRPV5 and TRPV6) requires association of the S100A10-annexin 2 complex. *Embo J* **22**, 1478-87.

van de Graaf S. F., Rescher U., Hoenderop J. G., Verkaart S., Bindels R. J. and Gerke V. (2008) TRPV5 is internalized via clathrin-dependent endocytosis to enter a Ca2+-controlled recycling pathway. *J Biol Chem* **283**, 4077-86.

Vassilev P. M., Peng J. B., Hediger M. A. and Brown E. M. (2001) Single-Channel Activities of the Human Epithelial Ca2+ Transport Proteins CaT1 and CaT2. *J Membr Biol* **184**, 113-120.

Vazquez G., Wedel B. J., Kawasaki B. T., Bird G. S. and Putney J. W., Jr. (2004) Obligatory role of Src kinase in the signaling mechanism for TRPC3 cation channels. *J Biol Chem* **279**, 40521-8.

Vellani V., Mapplebeck S., Moriondo A., Davis J. B. and McNaughton P. A. (2001) Protein kinase C activation potentiates gating of the vanilloid receptor VR1 by capsaicin, protons, heat and anandamide. *J Physiol* **534**, 813-25.

Venkatachalam K. and Montell C. (2007) TRP channels. *Annu Rev Biochem* **76**, 387-417.

Venkatachalam K., Zheng F. and Gill D. L. (2003) Regulation of canonical transient receptor potential (TRPC) channel function by diacylglycerol and protein kinase C. *J Biol Chem* **278**, 29031-40.

Vennekens R., Hoenderop J. G., Prenen J., Stuiver M., Willems P. H., Droogmans G., Nilius B. and Bindels R. J. (2000) Permeation and gating properties of the novel epithelial Ca(2+) channel. *J Biol Chem* **275**, 3963-9.

Vennekens R., Owsianik G. and Nilius B. (2008) Vanilloid transient receptor potential cation channels: an overview. *Curr Pharm Des* **14**, 18-31.

Vig M., Beck A., Billingsley J. M., Lis A., Parvez S., Peinelt C., Koomoa D. L., Soboloff J., Gill D. L., Fleig A., Kinet J. P. and Penner R. (2006a) CRACM1 multimers form the ion-selective pore of the CRAC channel. *Curr Biol* **16**, 2073-9.

Vig M., Peinelt C., Beck A., Koomoa D. L., Rabah D., Koblan-Huberson M., Kraft S., Turner H., Fleig A., Penner R. and Kinet J. P. (2006b) CRACM1 is a plasma membrane protein essential for store-operated Ca2+ entry. *Science* **312**, 1220-3.

Voets T., Janssens A., Droogmans G. and Nilius B. (2004) Outer pore architecture of a Ca2+-selective TRP channel. *J Biol Chem* **279**, 15223-30.

Voets T., Janssens A., Prenen J., Droogmans G. and Nilius B. (2003) Mg(2+)-dependent Gating and Strong Inward Rectification of the Cation Channel TRPV6. *J Gen Physiol* **121**, 245-60.

Voets T. and Nilius B. (2003) The pore of TRP channels: trivial or neglected? *Cell Calcium* **33**, 299-302.

Voets T. and Nilius B. (2007) Modulation of TRPs by PIPs. *J Physiol* **582**, 939-44.

Voets T., Prenen J., Fleig A., Vennekens R., Watanabe H., Hoenderop J. G., Bindels R. J., Droogmans G., Penner R. and Nilius B. (2001) CaT1 and the calcium-release activated calcium channel manifest distinct pore properties. *J Biol Chem* **30**, 30.

Voss P. and Siems W. (2006) Clinical oxidation parameters of aging. *Free Radic Res* **40**, 1339-49.

Wilkinson S. E., Parker P. J. and Nixon J. S. (1993) Isoenzyme specificity of bisindolylmaleimides, selective inhibitors of protein kinase C. *Biochem J* **294 (Pt 2)**, 335-7.

Wissenbach U. and Niemeyer B. A. (2007) Trpv6. *Handb Exp Pharmacol*, 221-34.

Wissenbach U., Niemeyer B. A., Fixemer T., Schneidewind A., Trost C., Cavalie A., Reus K., Meese E., Bonkhoff H. and Flockerzi V. (2001) Expression of CaT-like, a novel calcium-selective channel, correlates with the malignancy of prostate cancer. *J Biol Chem* **276**, 19461-8.

Xu H., Zhao H., Tian W., Yoshida K., Roullet J. B. and Cohen D. M. (2003) Regulation of a transient receptor potential (TRP) channel by tyrosine phosphorylation. SRC family kinase-dependent tyrosine phosphorylation of TRPV4 on TYR-253 mediates its response to hypotonic stress. *J Biol Chem* **278**, 11520-7.

Xu L., Eu J. P., Meissner G. and Stamler J. S. (1998) Activation of the cardiac calcium release channel (ryanodine receptor) by poly-S-nitrosylation. *Science* **279**, 234-7.

Xu X. Z., Chien F., Butler A., Salkoff L. and Montell C. (2000) TRPgamma, a drosophila TRP-related subunit, forms a regulated cation channel with TRPL. *Neuron* **26**, 647-57.

Xu Z. P., Gao W. C., Wang H. P. and Wang X. H. (2009) [Expression of transient receptor potential subfamily mRNAs in rat testes]. *Nan Fang Yi Ke Da Xue Xue Bao* **29**, 519-20.

Yamamoto S., Shimizu S., Kiyonaka S., Takahashi N., Wajima T., Hara Y., Negoro T., Hiroi T., Kiuchi Y., Okada T., Kaneko S., Lange I., Fleig A., Penner R., Nishi M., Takeshima H. and Mori Y. (2008) TRPM2-mediated Ca2+influx induces chemokine production in monocytes that aggravates inflammatory neutrophil infiltration. *Nat Med* **14**, 738-47.

Yazawa K., Kameyama A., Yasui K., Li J. M. and Kameyama M. (1997) ATP regulates cardiac Ca2+ channel activity via a mechanism independent of protein phosphorylation. *Pflugers Arch* **433**, 557-62.

Yoshida T., Inoue R., Morii T., Takahashi N., Yamamoto S., Hara Y., Tominaga M., Shimizu S., Sato Y. and Mori Y. (2006) Nitric oxide activates TRP channels by cysteine S-nitrosylation. *Nat Chem Biol* **2**, 596-607.

Yu R. and Hinkle P. M. (2000) Rapid turnover of calcium in the endoplasmic reticulum during signaling. Studies with cameleon calcium indicators. *J Biol Chem* **275**, 23648-53.

Yuan J. P., Zeng W., Dorwart M. R., Choi Y. J., Worley P. F. and Muallem S. (2009) SOAR and the polybasic STIM1 domains gate and regulate Orai channels. *Nat Cell Biol* **11**, 337-43.

Yue L., Peng J. B., Hediger M. A. and Clapham D. E. (2001) CaT1 manifests the pore properties of the calcium-release-activated calcium channel. *Nature* **410**, 705-9.

Zhang L. and Saffen D. (2001) Muscarinic acetylcholine receptor regulation of TRP6 Ca2+ channel isoforms. Molecular structures and functional characterization. *J Biol Chem* **276**, 13331-9.

Zhang S. L., Kozak J. A., Jiang W., Yeromin A. V., Chen J., Yu Y., Penna A., Shen W., Chi V. and Cahalan M. D. (2008) Store-dependent and -independent modes regulating Ca2+ release-activated Ca2+ channel activity of human Orai1 and Orai3. *J Biol Chem* **283**, 17662-71.

Zhang S. L., Yeromin A. V., Zhang X. H., Yu Y., Safrina O., Penna A., Roos J., Stauderman K. A. and Cahalan M. D. (2006) Genome-wide RNAi screen of Ca(2+) influx identifies genes that regulate Ca(2+) release-activated Ca(2+) channel activity. *Proc Natl Acad Sci U S A* **103**, 9357-62.

Zhang X., Huang J. and McNaughton P. A. (2005) NGF rapidly increases membrane expression of TRPV1 heat-gated ion channels. *Embo J* **24**, 4211-23.

Zima A. V. and Blatter L. A. (2006) Redox regulation of cardiac calcium channels and transporters. *Cardiovasc Res* **71**, 310-21.

Zima A. V., Copello J. A. and Blatter L. A. (2004) Effects of cytosolic NADH/NAD(+) levels on sarcoplasmic reticulum Ca(2+) release in permeabilized rat ventricular myocytes. *J Physiol* **555**, 727-41.

Zitt C., Strauss B., Schwarz E. C., Spaeth N., Rast G., Hatzelmann A. and Hoth M. (2004) Potent inhibition of Ca2+ release-activated Ca2+ channels and T-lymphocyte activation by the pyrazole derivative BTP2. *J Biol Chem* **279**, 12427-37.

Zweifach A. and Lewis R. S. (1993) Mitogen-regulated Ca2+ current of T lymphocytes is activated by depletion of intracellular Ca2+ stores. *Proc Natl Acad Sci U S A* **90**, 6295-9.

11   Curriculum Vitae

Personal data:

Name   Dalia Mohamed Moselhi Al-Ansary

Date of birth   27.10.1976. Cairo-Egypt

E-mail address   ptdaan@uks.eu

Education

2006-present   PhD student in the Graduate School Calcium-Signaling and Cellular Nanodomains (GK 1326), at the University of Saarland, Germany.

2005   Master of science in Pharmacology and Toxicology, Cairo University, Egypt.

1999   Bachelor of Pharmacy, Cairo University, Egypt.

Honours and Invitations

Poster titled "PKCßII regulation counteracts ATP effects on TRPV6 calcium currents and points to functional difference between TRPV6 polymorphic alleles" was selected for an oral Platform presentation at the Biophysical Society 53rd Annual Meeting, held February 28 - March 4, 2009, in Boston, MA. Also, a student award travel was granted.

Publications

Erler I., Al-Ansary D. M., Wissenbach U., Wagner T. F., Flockerzi V. and Niemeyer B. A. (2006) Trafficking and assembly of the cold-sensitive TRPM8 channel. *J Biol Chem* **281**, 38396-404.

Al-Ansary D., Bogeski I., Disteldorf B. M., Becherer U. and Niemeyer B. A. (2009) ATP modulates Ca2+ uptake by TRPV6 and is counteracted by isoform-specific phosphorylation. *Faseb J*. (in press)

Bogeski I., Kummerow C.*, Al-Ansary D.*, Koehler R., Schwarz E. C., Kozai D., Takahashi N., Peinelt C., Griesemer D., Bozem M., Mori Y., Hoth M. & Niemeyer B. A. Differential redox regulation of ORAI channels: a mechanism to tune T-cell responses (Submitted).* Equal Contribution

Quintana A. *, Pasche M. *, Al-Ansary D., Junker C., Nuñez L, Villalobos C., Niemeyer B.A., Becherer U., Rettig J. & Hoth M. Calcium microdomains at the immunological synapse: how ORAI channels, mitochondria and calcium pumps generate local calcium signals for T-cell activation (Manuscript in preparation). * Equal Contribution